ADA040444

BRL CR 337

BRL

12

NW

AD

CONTRACT REPORT NO. 337

SHAPED CHARGE JET BREAKUP STUDIES USING RADIOGRAPH MEASUREMENT AND SURFACE INSTABILITY CALCULATIONS

Prepared by

Dyna East Corporation
Wynnewood, PA 19096

April 1977

Approved for public release; distribution unlimited.

USA ARMAMENT RESEARCH AND DEVELOPMENT COMMAND
USA BALLISTIC RESEARCH LABORATORY
ABERDEEN PROVING GROUND, MARYLAND

Destroy this report when it is no longer needed.
Do not return it to the originator.

Secondary distribution of this report by originating or sponsoring activity is prohibited.

Additional copies of this report may be obtained from the National Technical Information Service, U.S. Department of Commerce, Springfield, Virginia 22151.

The findings in this report are not to be construed as an official Department of the Army position, unless so designated by other authorized documents.

UNCLASSIFIED

SECURITY CLASSIFICATION OF THIS PAGE (When Data Entered)

REPORT DOCUMENTATION PAGE		READ INSTRUCTIONS BEFORE COMPLETING FORM
1. REPORT NUMBER BRL CONTRACT REPORT NO. 337	2. GOVT ACCESSION NO.	3. RECIPIENT'S CATALOG NUMBER BRL-CR-337
4. TITLE (and Subtitle) SHAPED CHARGE JET BREAKUP STUDIES USING RADIOGRAPH MEASUREMENT AND SURFACE INSTABILITY CALCULATIONS.		5. TYPE OF REPORT & PERIOD COVERED Final
		6. PERFORMING ORG. REPORT NUMBER DE-TR-76-1
7. AUTHOR(s) P. C. Chou C. A. Tanzio J. Carleone R. D. Cicarelli		8. CONTRACT OR GRANT NUMBER(s) DAAD05-75-C-0753
9. PERFORMING ORGANIZATION NAME AND ADDRESS Dyna East Corporation Wynnewood, PA 19096		10. PROGRAM ELEMENT, PROJECT, TASK AREA & WORK UNIT NUMBERS 61102A 1L161102AH43 00 001AJ
11. CONTROLLING OFFICE NAME AND ADDRESS US Army Ballistic Research Laboratory Aberdeen Proving Ground, MD 21005		12. REPORT DATE APRIL 1977
		13. NUMBER OF PAGES 91
14. MONITORING AGENCY NAME & ADDRESS(if different from Controlling Office) US Army Materiel Development & Readiness Command 5001 Eisenhower Avenue Alexandria, VA 22333		15. SECURITY CLASS. (of this report) UNCLASSIFIED
		15a. DECLASSIFICATION/DOWNGRADING SCHEDULE

16. DISTRIBUTION STATEMENT (of this Report)

Approved for public release; distribution unlimited.

17. DISTRIBUTION STATEMENT (of the abstract entered in Block 20, if different from Report)

18. SUPPLEMENTARY NOTES

This work was supported by the US Army Ballistic Research Laboratory under Contract No. DAAD05-75-C-0753 and this report comprises the final report of this contract.

19. KEY WORDS (Continue on reverse side if necessary and identify by block number)

Shaped Charge
Jet
Warhead
Explosive
Surface Instability

20. ABSTRACT (Continue on reverse side if necessary and identify by block number)

A study of the shaped charge jet breakup phenomenon is undertaken by two approaches. In the first approach, jet velocity, jet breakup time, and jet radius distributions are measured using timed flash radiographs of broken jets from eleven different shaped charge designs. Experimental results are correlated to theoretical predictions and a semi-empirical jet breakup time vs. jet radius curve is presented for copper lined charges. The second approach applied the concepts of hydrodynamic instability to shaped charge jets. A

(continued)

Item 20 (Cont'd)

cont. numerical study of the effects of yield strength, inertia forces, surface disturbance wavelength, and irregular or "random" surface disturbances is presented. Results indicato that high yield strength and low density jet materials will both cause earlier breakup. A critical range of disturbance wave-lengths exists in shaped charge jets; if a random surface disturbance is imposed, a critical wavelength will prevail and eventually cause the jet to breakup into segments with lengths approximately equal to experimentally measured values.

Table of Contents

List of Illustrations

List of Tables

Acknowledgment

The authors would like to express appreciation to Robert Karpp, Robert Jameson, Julius Simon and John Majerus of BRL for supplying the many jet radiographs used in the present study, and also for the many helpful discussions and suggestions during the course of this work. We would also like to thank Michael Khalil for his help with the many radiograph measurements, computer calculations and data reduction contained here.

I. INTRODUCTION

In recent years, tremendous advances have been made in the basic understanding of shaped charge mechanics. These include the processes of liner collapse, jet formation, and formulas for jet radius and strain. Both two-dimensional computer codes and one-dimensional modeling have been used successfully for the analysis of shaped charges. One important area, however, has not been well understood and cannot be simulated easily by computer methods. This area is the breakup of the shaped charge jet. This breakup, or segmentation, occurs in all jets that have a large velocity gradient with higher speeds at the tip and lower speeds near the tail. This process can be seen in Fig. 1 which shows flash radiographs of a typical shaped charge jet at three successive times, displayed in the proper position-time coordinates. At the earliest time the jet segmentation has begun near the tip; most of the jet is still continuous. The later times show the completely segmented jet.

In [1] and [2], we have presented initial studies on the jet breakup phenomenon. Let us now briefly review the results of these initial studies. Formulas for the strain and radius of shaped charge jets based on a one-dimensional model are presented in [1]. Further, in [1] and [2], a method to determine the jet breakup time distribution from timed flash jet radiographs was developed. This method was then applied to jets from a series of identical BRL 81.3mm standard 42° copper-lined charges and an unconfined 105mm 42° copper lined charge in [1]. Despite the scatter in the results, the breakup time does show a definite "trend" as is indicated in [1]. In fact, for the particular charge studied, the trend indicates that the jet breaks first near the tip with a progressively increasing breakup time towards the tail. Thus, shaped charge jets do not necessarily break simultaneously along their length, as assumed previously by some investigators. The resulting jet breakup time distribution was then contrasted to the one-dimensional theoretical jet strain and radius distributions. This is presented in [1] and [2] where it is concluded that, for copper liners, the breakup time distribution is related to the jet radius distribution. No other correlation was indicated in [1] or [2].

The present study addresses the problem of jet breakup through the use of two approaches: (1) triple-flash radiographs of various jets to determine jet velocity, breakup time, etc., and (2) surface instability as a cause of breakup.

The first approach is actually an extension or continuation of the work we have presented in [1]. The method of [1] to measure breakup time, jet velocity, etc. from timed flash radiographs is applied here to many jets from various shaped charges having different cone angles, different liner wall thicknesses, liners with tapered walls, different liner materials, and light or heavy confinement. This approach has enabled us to obtain many characteristics of jets from a large cross-section of shaped charges. The data from all of these charges are

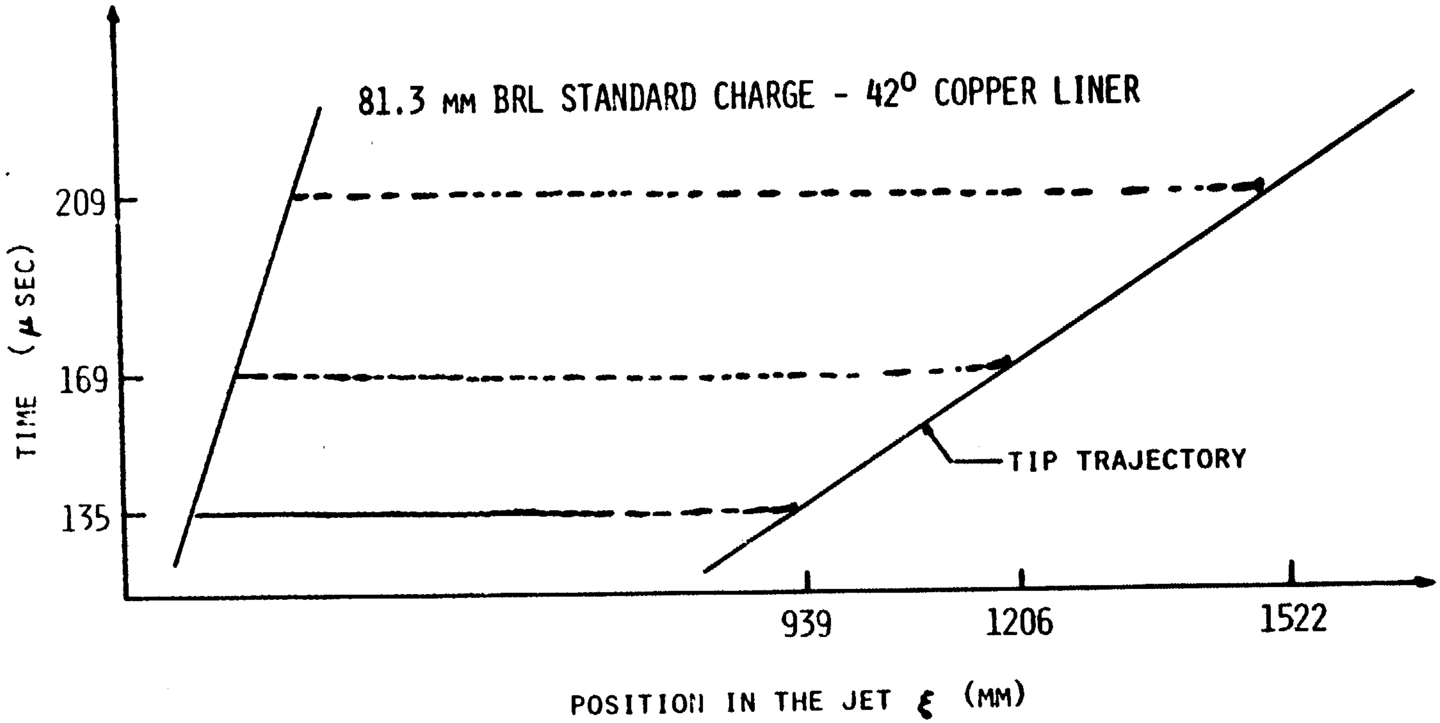

FIGURE 1. Radiographs showing the jet breakup phenomenon.
(Radiographs courtesy of R. Jameson, BRL)

conveniently tabulated and graphically displayed in this report. The geometry of the charges studied are given in Appendix A. The measured jet velocity, breakup time and jet radius are plotted graphically in Appendix B. Appendix C contains a tabular list of this data and in addition includes the aspect ratio of the jet segments and difference in velocity between neighboring particles. All of this data has been analyzed to obtain trends in the breakup phenomenon. The breakup trends have been contrasted with the one-dimensional strain and radius predictions using the formulas of [1]. Within an individual jet no general correlation has been observed between breakup time and one-dimensional parameters. The results of the breakup time measurements of all copper jets studied, however, do exhibit a definite trend. This trend yields a semi-empirical design curve for breakup time which can be used in conjunction with a one-dimensional shaped charge model to predict breakup time for copper jets. This first approach is presented in Section II.

The second approach involves the study of the instability caused by various disturbances in the jet with the goal of determining whether or not this instability may cause the jet to breakup. We know from classical hydrodynamics that a continuous liquid jet will break into small segments because of surface instability. The breakup of a shaped charge jet resembles this very much, and our study shows that the shaped charge jet is indeed subject to surface instability. In principle, there are three forces which may cause this instability: surface tension, aerodynamic force, and material strength (elastic-plastic force) in the jet. Both analytical studies and two-dimensional finite-difference numerical calculations were made, and the results indicate that material strength is the main cause for shaped charge jet instability and breakup. In addition, the effect of strain-rate, time of disturbance initiation, and inertia were considered. The results of this stability study are discussed in Section III. Finally, general conclusions are stated in Section IV.

We would like to note that the results presented in this report summarize the work conducted during the entire contract period. Some of these results were presented previously in quarterly progress reports.

II. JET RADIOGRAPH DATA

The results which we presented in [1] indicate that the measurement of jet radiographs provides an efficient and useful procedure to obtain breakup data. Also breakup trends are indicated in [1] which warrant further investigation. In this study, we have therefore continued using this approach to study jets from a large number of charges having different geometries and liner materials.

A. General Approach

The detailed development and equations for the computation of breakup time, jet velocity, etc. from the radiograph measurements are given in [1]. Here, we will give only a brief description of this method. Figure 2 shows the position-time plot of two typical neighboring jet segments labeled as K and K+1. Suppose we have radiographs of these two segments at times t_1 and t_2 as indicated in Figure 2. (Note: in the actual case, we have analyzed three timed flash radiographs, as supplied by BRL). We may then compute the velocity of each segment by measuring how far the segments have traveled during the time t_2-t_1. In the two radiographs the segments are separated by a gap as shown. Under the assumption that the segments remain at constant length and constant velocity after breakup (which is a good approximation after the jet is completely broken as evidenced by the radiographs), it is a simple matter to trace back the front of segment (K+1) and the rear of segment K until they meet, i.e. the gap becomes zero. The time of this meeting t_b is the breakup time of segment K from segment (K+1). This procedure may be applied successively to each pair of particles, i.e. K and (K+1), (K+1) and (K+2), etc., until the complete breakup time distribution is obtained. There is a certain degree of approximation to this procedure. Since the particles do not break successively from one end of the jet to the other, we sometimes have the situation where a larger segment breaks from the main jet, continues to stretch, and then finally breaks into smaller, constant velocity, constant length segments. However, the time between the initial break and the succeeding breaks is small, therefore the procedure may still be applied approximately to this breakup situation. The resulting breakup times have been found to be within the accuracy of the experimental procedures.

This method of determining the breakup time was then applied to jet radiographs from many various shaped charges. These radiographs were obtained from BRL through the courtesy of R. Jameson, R. Karpp, J. Simon and J. Majerus. For convenience, the different charges are listed in Table I; the detailed geometry and drawings of each are given in Appendix A. It can be seen from this table that we have studied the effects of cone angle, wall thickness, wall taper, and liner material on the breakup mechanism.

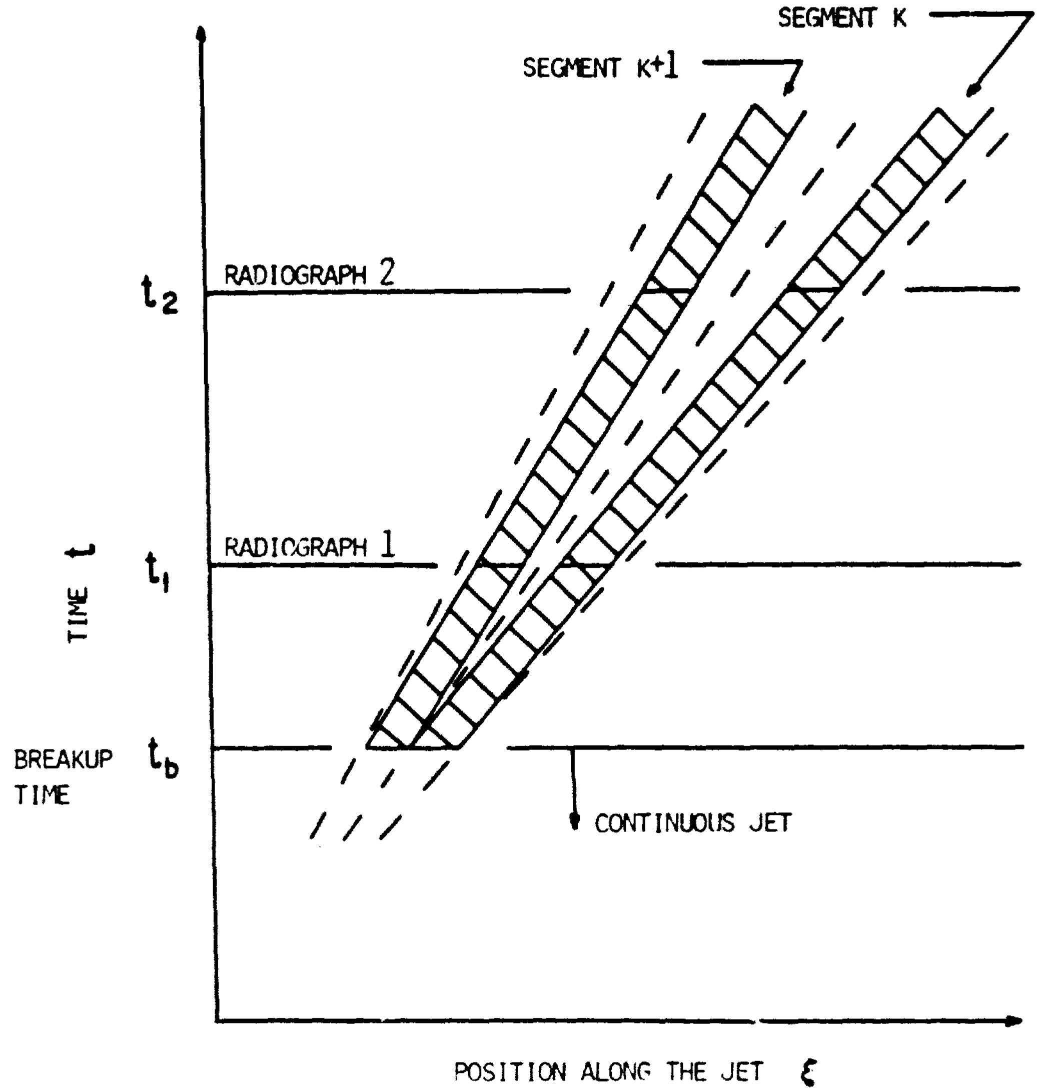

FIGURE 2. Position-time plot of two typical jet segments showing the method of determining the breakup time from jet radiograph measurements.

Table I

List of Charges Examined*

Copper Lined

Charge No.	Cone Angle	Diameter mm	Wall Thickness mm
1	20°	38.1	1.168
2	40°	38.1	1.168
3	60°	38.1	1.168
4	90°	38.1	1.168
5	42°	50.8	0.762
6	42°	50.8	1.524
7	42°	50.8	2.540
8	42°**	81.3	tapered wall

Aluminum Lined

Charge No.	Cone Angle	Diameter mm	Wall Thickness mm
9	40°	38.1	1.626
10	60°	38.1	1.626
11	90°	38.1	1.626

* Note that we have also performed a breakup study of jets from the BRL Standard 81.3mm charge and the 105mm unconfined charge in [1].

** Angle of inside wall

B. Results of Radiograph Measurements

From the measurements of the jet radiographs, we have determined the jet velocity, jet breakup time, and jet radius distributions for all of the charges listed in Table I. Plots of all of the data obtained are given in Appendix B. Figure B1 shows the jet velocity distribution along the length of the jet at a particular time for the series of 31.8mm copper lined charges having cone angles of 20°, 40°, 60° and 90° (Charge Nos. 1-4). Test results of these charges were first reported in [3], where the average breakup time of the complete jet was given. The time base used in all of the present studies is given as $t = 0$ when the detonation wave reaches the apex of the cone.* From Fig. B1 we see that, for a given liner material, the tip velocity of the jet decreases as the cone angle increases. It should be noted that, for the 20° copper cone, the resulting jet possessed a bifurcated region at the tip portion. We therefore made our radiograph measurements starting from the first fully coherent particle of the jet, which has a velocity of 8.4mm/μsec, much smaller than 9.9mm/μsec reported in [3]. We should further note that it has been determined that this bifurcated region is caused by supersonic flow in the jet formation region (See [4] for details). None of the other charges examined under this study possessed this bifurcated region.

The jet velocity distributions for the remaining charges are shown in Figures B2-B6. It is interesting to note that Fig. B6 indicates that the 81.3mm tapered wall charge studied here has a higher jet velocity (8.3 km/sec at the tip) than the 81.3mm standard charge with constant wall thickness studied in [1] (7.9 km/sec at the tip). This somewhat surprising result has a fairly simple explanation. Because of the wall taper (thicker at the cone apex tapering linearly toward the cone base), as we proceed from the apex toward the base the liner elements reach higher collapse velocity than corresponding elements of the charge with a constant wall thickness. This effect provides the tapered wall liner with an overall decrease in the collapse angle (i.e. the angle of the collapsing liner with the charge axis, denoted as β in [1]). From the basic one-dimensional jet formation theory [5] a decrease in collapse angle, in general, produces a higher jet velocity. Finally, from Figs. B1-B6 we also observe that the velocity distribution for each of the charges studied is approximately a straight line.

Plots of the breakup time of the jet particles versus their position in the jet at a particular time for the eleven charges examined are given in Figs. B7-B17. The scatter in the results is to be expected because of the nature of the breakup mechanism. In all cases a definite trend in breakup time exists. To demonstrate this trend, a straight line was passed through the data using the method of least squares. This line is also shown in Figs. B7-B17. All of the jets studied exhibit trends which indicate that the tip portion breaks earlier than the rear portion except for the 38.1mm, 40° copper charge (Charge No.2) and the 81.3mm, 42° copper tapered wall

---

* Except for the data which is tabulated in Appendix C: The data there is based on the initiation time of the main explosive charge. See Appendix C for details.

charge (Charge No.8). Breakup trends for these two charges show that these jets breakup almost simultaneously. Note that since only part of the jet for each charge appeared in the radiographs, these conclusions are only valid for the portion of the jets measured.

Next, the measured jet radius distributions for the eleven charges studied are given in Figures B18-B28. We see from Figs. B18-B21 that for copper lined charges of a given diameter and wall thickness the average jet radius increases with increasing cone angle. This effect is not so pronounced in the case of the aluminum lined charges as can be seen from Figs. B22-B24. Further, we note from Figs. B25-B27 that, all else being equal, relatively large increases in wall thickness give only small increases in jet radius.

Finally, all of the data resulting from the radiograph measurements are tabulated in Appendix C. In addition to the jet velocity, breakup time, and jet radius, which were graphically displayed in Appendix B, we have also tabulated the aspect ratio (length to diameter, ℓ/d) of each segment and the jet velocity difference between neighboring segments ΔV_j. The average ℓ/d and average ΔV_j are summarized in Tables II and III. In these tables, we have also summarized this data for the BRL Standard 81.3mm and 105mm unconfined charges which were studied in [1]. Since there was a certain amount of scatter in these quantities, the coefficient of variation (standard deviation divided by the mean) in each case was also computed. From Table II we see that the average ℓ/d varies between 4 and 6 for copper lined conical charges of constant wall thickness. The tapered wall cone has an ℓ/d ratio of 3.3 which may indicate that, even though this charge has a higher tip velocity than the corresponding constant wall charge, its penetration performance at longer standoffs may be poorer because of the small segment size and early breakup time. The aluminum lined charges studied have average ℓ/d ratios of 3.89, 4.92, and 8.39.

From Table III we observe that the overall average velocity difference between neighboring segments for the copper lined charges is approximately 110m/sec. Recently, Held [6] has published that the average ΔV_j for the copper lined German charges he studied was approximately 100m/sec. For the aluminum lined charges studied here, we found an overall average ΔV_j of 145m/sec. Finally, we obtained radiographs of a copper lined French charge, the ISL "S2T", from Perez [7] and found the average ℓ/d to be 5.62 and the average ΔV_j to be 137m/sec. Data of this nature is useful in obtaining rough estimates of the number of jet segments in newly designed charges.

C. Comparison of Data with Theory

In [1] and [8] an improved one-dimensional theoretical shaped charge model was developed. This improved model is based on the classical Pugh-Eichelberger-Rostoker [5] theory but uses a semi-empirical collapse formula to describe the explosive-metal interaction process. Further, formulas for jet strain and jet radius were

Table II

Average Aspect Ratio (ℓ/d) of Jet Segments

Copper Lined

Charge No.	Geometry (Dia., Cone Angle, Wall Thk.)	ℓ/d (Average)	Coeff. of Variation
1	38.1 mm, 20°, 1.168 mm	4.69	.520
2	38.1 mm, 40°, 1.168 mm	5.95	.411
3	38.1 mm, 60°, 1.168 mm	5.91	.447
4	38.1 mm, 90°, 1.168 mm	4.49	.301
5	50.8 mm, 42°, 0.762 mm	4.18	.412
6	50.8 mm, 42°, 1.524 mm	4.48	.361
7	50.8 mm, 42°, 2.540 mm	4.48	.336
8	81.3 mm, 42°, tapered	3.31	.417
*	81.3 mm, 42°, 1.905 mm	5.93	.375
*	86.4 mm, 42°, 2.921 mm	5.21	.324
	Average ℓ/d for all copper jets	4.86	
	C.V.	.180	

Aluminum Lined

Charge No.	Geometry (Dia., Cone Angle, Wall Thk.)	ℓ/d	Coeff. of Variation
9	38.1 mm, 40°, 1.626 mm	3.89	.454
10	38.1 mm, 60°, 1.626 mm	4.92	.420
11	38.1 mm, 90°, 1.626 mm	8.39	.426
	Average ℓ/d for all Aℓ jets	5.73	
	C.V.	.411	

* These charges were studied in [1] and this data is included here for completeness

Table III

Average Jet Velocity Difference Between Neighboring Segments (ΔV_j)

Copper Lined

Charge No.	Geometry (Dia., Cone Angle, Wall Thk.)	ΔV_j (m/sec)	Coeff. of Variation
1	38.1 mm, 20°, 1.168 mm	106	.474
2	38.1 mm, 40°, 1.168 mm	111	.367
3	38.1 mm, 60°, 1.168 mm	135	.335
4	38.1 mm, 90°, 1.168 mm	109	.344
5	50.8 mm, 42°, 0.762 mm	110	.497
6	50.8 mm, 42°, 1.524 mm	115	.522
7	50.8 mm, 42°, 2.540 mm	119	.449
8	81.3 mm, 42°, tapered	108	.519
*	81.3 mm, 42°, 1.905 mm	96	.557
*	86.4 mm, 42°, 2.921 mm	113	.445
	Average ΔV_j for all copper jets	112	
	C.V.	.090	

Aluminum Lined

Charge No.	Geometry (Dia., Cone Angle, Wall Thk.)	ΔV_j (m/sec)	Coeff. of Variation
9	38.1 mm, 40°, 1.626 mm	143	.362
10	38.1 mm, 60°, 1.626 mm	130	.528
11	38.1 mm, 90°, 1.626 mm	162	.154
	Average ΔV_j for all Aℓ jets	145	
	C.V.	.111	

* These charges were studied in [1] and this data is included here for completeness.

developed for this model. Since the publication of [1] and [8], we have improved this model further by incorporating the effect of liner acceleration during collapse. This enables the prediction of the inverse jet velocity gradient region during formation.

This improved one-dimensional model was applied to the eleven charges studied here. In Figs. B1-B6 the theoretical jet velocity distribution of each charge is shown in contrast to the experimental data. We see that excellent agreement is obtained between theory and experiment. Note that in Fig. B4 and B5 there is some discrepancy between the experimental tip velocity and the tip velocity predicted by the theory for Charge Nos. 6 and 7. This prediction could be improved by using a different value for the acceleration. At present, the acceleration values used in all the cases are given by a simple empirical formula which depends only on liner density and thickness. For these two particular charges the liner thickness to liner diameter ratio is much higher than the other charges studied and therefore this simple acceleration formula may be inaccurate for these two charges. Theoretical jet radius distributions were also computed from the one-dimensional model at the breakup times t_b. The t_b lines in Figs. B7-B17 were used. As shown in Figs. B18-B28, the theoretical radius distributions compare reasonably well with experimental values.

We next compared the breakup time distribution with the theoretical distribution of other jet properties. The goal here was to find some correlation among these distributions which would indicate controlling parameters in the breakup mechanism. We compared trends in the following properties to the breakup trend: jet strain η, jet radius r_j, and jet strain rate $\dot{\eta}$. The quantities η and r_j are defined in [1], and $\dot{\eta}$ is simply the first time derivative of η defined there. We also contrasted these properties to the amount of time elapsed from the formation of an element until it breaks up. This quantity is the absolute breakup time minus the absolute time when the element is first formed, and is denoted t_b-t_f. The quantity t_b is from the experimental least squares line and the quantity t_f is computed from the one-dimensional model.

Since the quantities jet strain, jet radius, and jet strain rate before breakup are continuously changing with time, it is appropriate to compare the breakup time of each segment with these quantities at the time when each segment breaks up. To do this, we first trace back each segment in the radiograph to its original position in the cone, x, using the one-dimensional model. We are then able to compute η, r_j, and $\dot{\eta}$ of the segment at its own particular breakup time from the least squares experimental trend. Figure 3 shows a plot of η, r_j, $\dot{\eta}$, t_b and t_b-t_f versus x/h for the 38.1mm, 60° copper charge (Charge No.3). Note that x denotes the original liner position and h denotes the original height of the cone. Also plotted in Fig. 3 is r_j at t = 55 μsec which is a time before any breakup has occurred.

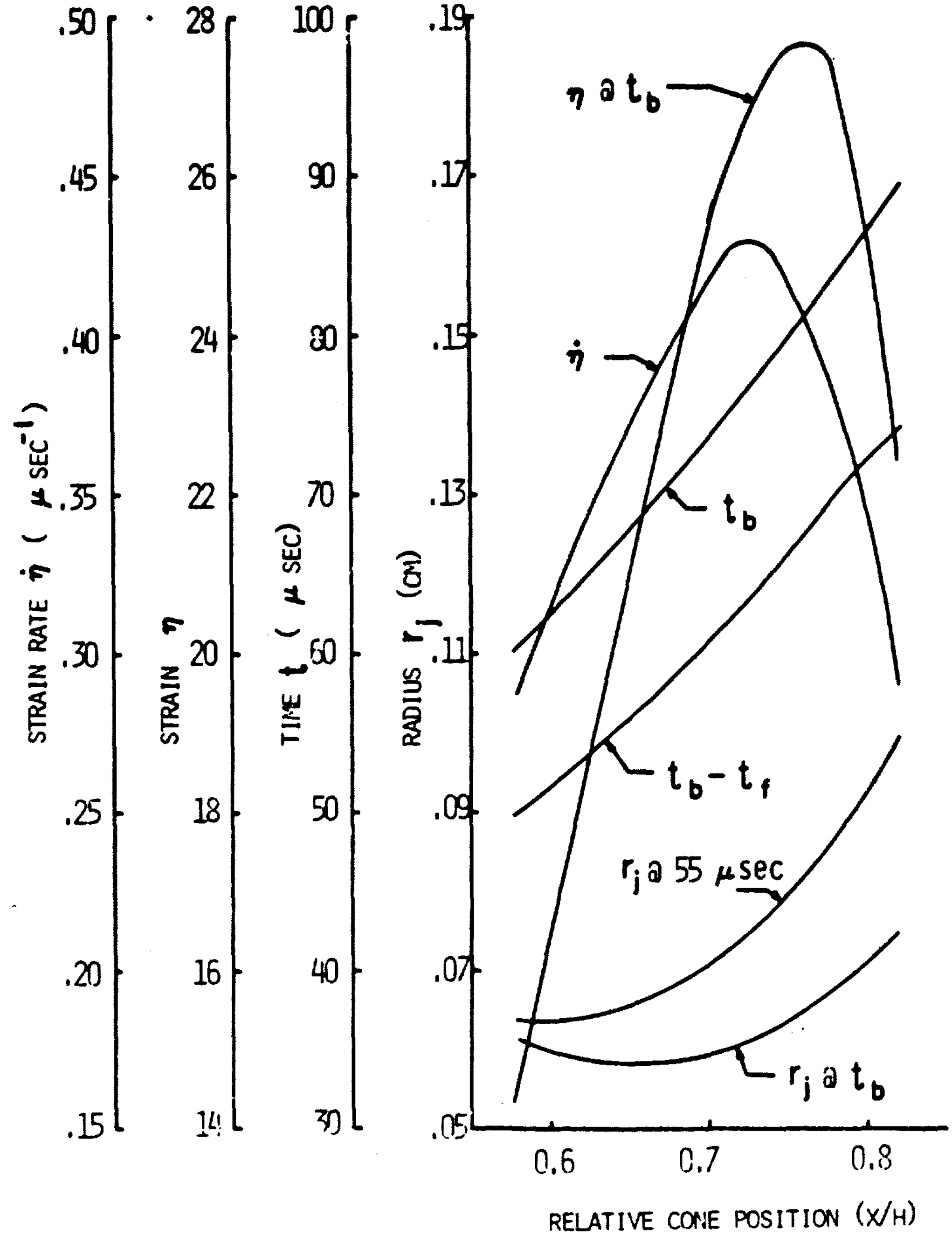

FIGURE 3. Theoretical jet strain-rate, strain, radius and experimental breakup time vs. relative cone position for the 38.1mm, 60° Cu charge. (Charge No. 3)

Figure 3 indicates that there is no reasonable correlation between the breakup time distribution and η at t_b or $\dot{\eta}$ at t_b. Both the r_j at t_b and r_j at 55 μsec appear to follow the general trend of the breakup time. Plots similar to Figure 3 for the remaining 10 charges were also plotted but are not presented here in the interest of space*. However, the results indicate that within one jet even r_j at t_b and r_j at a time before breakup may not follow the trend of breakup time. Results do indicate that for copper lined charges r_j at a time before breakup seems to increase as the breakup time increases but no general conclusion may be drawn.

We next looked at the breakup data from all the copper lined charges together rather than just throughout a single jet. In Fig. 4 we have made a plot of $t_b - t_f$ vs. r_j at t_b for all of the copper lined charges studied here (Charge Nos. 1-8). Also, in Fig. 4, we have plotted the data for the 81.3mm BRL Standard Charge and the 105mm unconfined charge studied in [1]. Three data points were selected from each jet. With the exception of one charge, the 38.1mm, 90° copper (Charge No.4), all of the data points for $t_b - t_f$ fall within a narrow region monotonically increasing with increasing r_j. We may speculate that the 90° charge does not fall in this region because the low collapse velocities in a charge with a large cone angle results in lower pressures and velocities at the stagnation point during formation. Therefore, the properties of this jet may be different from those of smaller angle cones. Figure 4 indicates a correlation between the two quantities for the other charges however. In fact, if we draw a line through these points, we obtain a useful breakup time vs. radius curve, which can be used for design purposes. For example, suppose we design a new copper lined charge and wish to obtain its breakup time distribution. We can compute the radius of the elements of the jet as functions of time. If we then plot the radius vs. time curve of a particular jet element on the breakup time vs. radius coordinates, we find that this curve will intersect the breakup curve. This intersection gives the breakup time of that element. We then repeat this procedure for a series of jet elements. This then yields a breakup time distribution for the new charge. This breakup time information may then be used together with other information on a penetration analysis to evaluate the final performance of the new design.

* These plots for the remaining 10 charges may be found in [9] and [10].

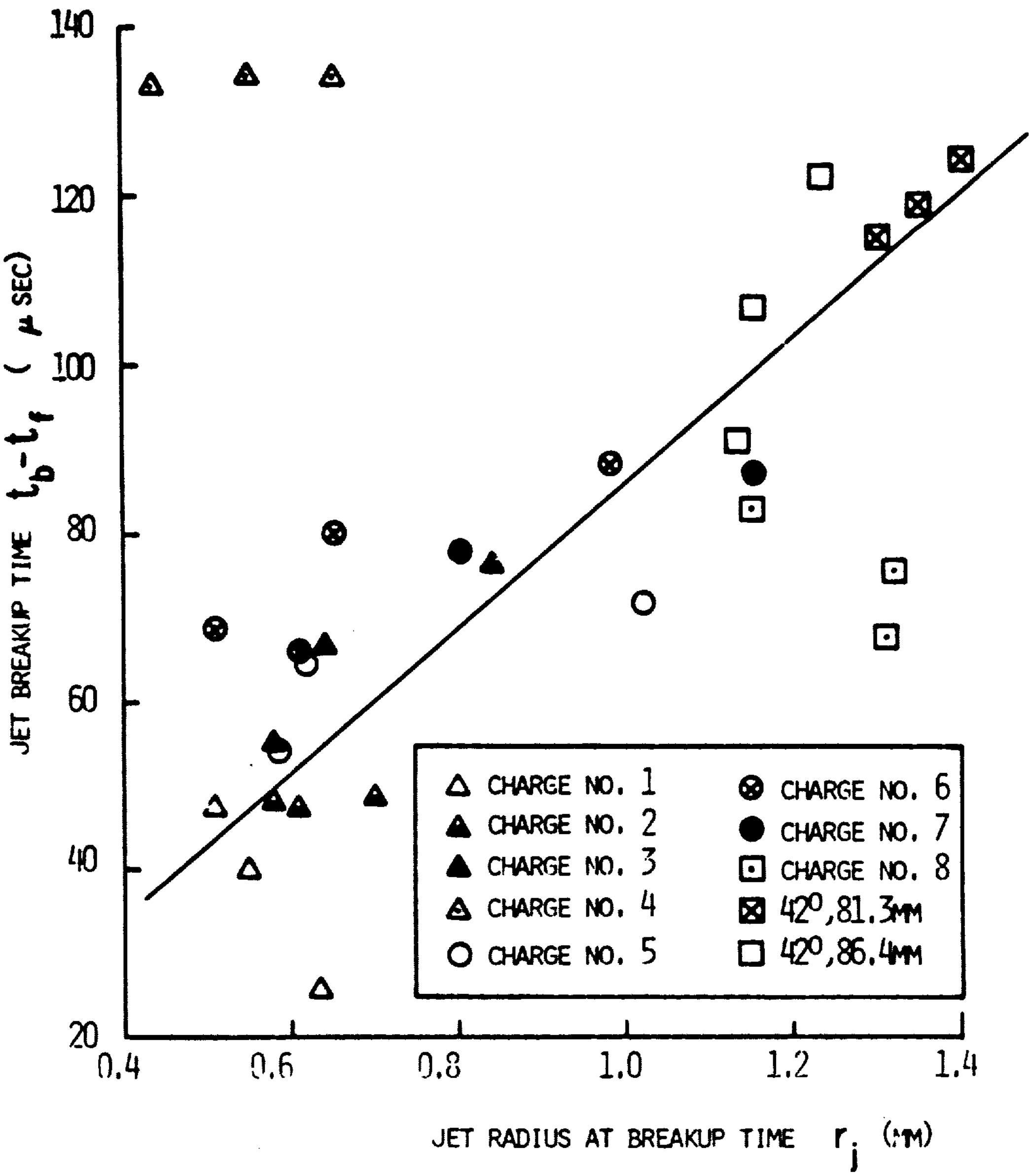

Figure 4. Breakup time vs. jet segment radius for various charges. Ten charges are included. Three data points selected from each charge.

III. STABILITY OF SHAPED CHARGE JETS AS A CAUSE FOR BREAKUP

A. Background

The concept of liquid jet stability in classical hydrodynamics has been studied by many authors (e.g. [11]-[14]). The idea of applying a stability approach to shaped charge jets was motivated by the remarkable resemblance of the breakup of shaped charge jets to that of liquid jets. This resemblance is shown in Fig. 5 where the breakup of a glycerine-water jet [15] is contrasted with a typical shaped charge jet. Further, we note that the average ℓ/d ratio for all of the copper jet segments studied, 4.86 (see Table II), is very close to the value of the critical $\lambda/2r_0$ ratio of 4.5 predicted by classical stability analyses of liquid jets, where λ is the wavelength of the surface disturbance, and r_0 is the radius of the undisturbed jet. These facts suggest that the shaped charge breakup phenomenon may be caused by surface instability.

The first stability analysis of a liquid jet was published in 1879 by Lord Rayleigh [11]. He considered an inviscid fluid jet moving at a constant uniform axial velocity subjected to surface disturbances about the equilibrium position. He obtained the most unstable wavelength and the perturbation growth rate using energy considerations. His values of wavelength and growth rate have been verified by experiments, and his work is still considered the foundation for the study of jet stability.

Weber [12] extended Rayleigh's work to include viscous Newtonian fluids. The wavelength of the most unstable surface disturbance for a viscous fluid does not deviate too much from the ideal fluid case of $(\lambda/2r_0) = 4.5$. He also found that Newtonian viscosity tends to dampen the instability. Anno [16,17] gave a more general derivation of the analyses by Rayleigh and Weber.

Goldin, et al [15] studied the breakup of non-Newtonian viscous fluid jets. They used essentially the same approach as Levich [13] and obtained results on critical wavelength, growth rate, and breakup time for fluids possessing general viscoelastic stress-strain relations. In [15], it is shown that the Newtonian fluid is the most stable one among viscous fluids. Experimental evidence for different types of fluids seems to verify their results.

In our initial work, we have determined that three effects may cause jet breakup: surface tension, aerodynamic forces, and strength of the jet material. We have applied all the essential results of the classical analyses to the conditions of a typical shaped charge jet. We have also examined many experimental breakup records in the light of stability considerations. These results have ruled out the importance of the surface tension and aerodynamic effects in the stability of a shaped charge jet. This leaves the effect of jet strength. Since strength effects are not readily amenable to analytical treatment, we have turned to numerical approaches to study the

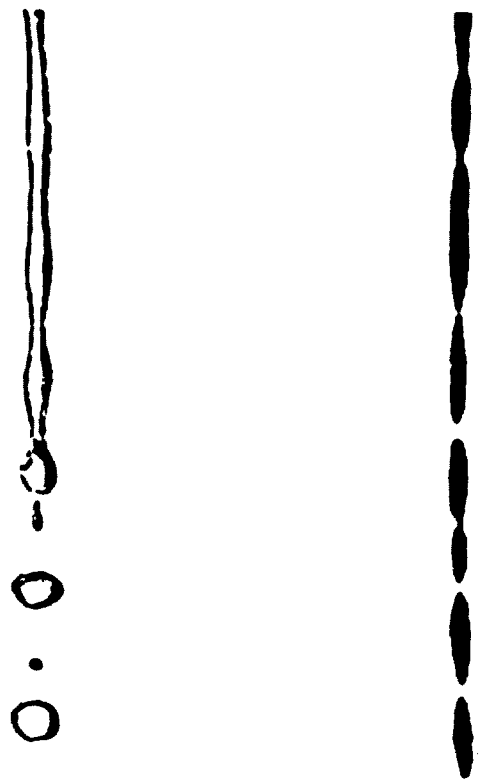

FIGURE 5. The resemblance between the breakup of a liquid jet and a shaped charge jet.

effects of jet strength.

In the next section of this report, we will first present results of a preliminary analytical study. Then more detailed results on the numerical study will be presented, including the study of various surface disturbances, time of disturbance initiation, strain rate, and inertia effects in jets with strength.

B. Preliminary Analytical Stability Study of Shaped Charge Jets

The results and formulas developed in the classical analyses of liquid jet stability were applied to the case of a typical shaped charge copper jet. Analyses for non-stretching and stretching jets were used. The results of this study are summarized in Table IV and will be briefly discussed below.

1. Non-stretching Jets

(a) Surface Tension. In our initial analysis, we have applied the classical formulas of Rayleigh [11] and Weber [12] to the conditions of a typical copper shaped charge jet. Rayleigh's work governs the case of an ideal fluid under the effect of surface tension and Weber's results are applicable to a viscous fluid under the effect of surface tension. The growth rate of disturbances on the surface of the jet as predicted from these formulas is quite small as compared to that observed in radiographs of shaped charge jets. In fact, according to these formulas the amplitude of the initial disturbance only grows 8% in 100 μsec, whereas it is observed from experiments that the shaped charge jet used for this analysis breaks up at approximately 100 μsec. The value of surface tension for copper used was 1.0 N/m.

(b) Aerodynamic Force. We have applied the formulas of Levich [13] to the problem of air passing over a shaped charge jet. A very large disturbance growth rate was predicted by this analysis. We feel, however, that the analysis is not too realistic for the present problem since Levich only considers linear incompressible aerodynamics and the present case is actually in the hypersonic regime. We would also like to indicate two experimental observations which demonstrate that aerodynamic effects are not important in the breakup of shaped charge jets. Vitali [18] has pointed out that superplastic jets do not breakup along their length in the typical manner of a copper jet, yet both jets are subject to the same aerodynamic force. Also, Frey [19] has studied photographs of copper jets in a vacuum, and found the typical surface disturbance growing within 100 μsec, similar to those found in jets traveling through air.

2. Stretching Jets

Mikami, et al [14] has developed an analytical approach to study the growth of disturbances on the surface of a stretching viscous thread surrounded by another viscous medium. We have modified this analysis to make it applicable to the case of a shaped charge jet. As shown in Table IV, appreciable growth rates and reasonable $\lambda/2r$ ratios

Table IV

Analytical Approaches to Shaped Charge Jet Stability

Approach	Stretching	Medium	Surface Forces	Most Unstable $\lambda/2r$	Disturbance Growth Rage	Other Comments
Rayleigh	no	both ideal and viscous fluids	Surface tension	4.5	8% in 100 μsec	
Levich	no	viscous (Newtonian)	Aerodynamic force	4	1000% in 22 μsec	used incompressible aerodynamics, not realistic for present case.
Present study	yes	viscous (Newtonian)	None	8.9 after 64 μsec (broad range)	100% in 64 μsec	inertia force neglected in governing equations
Present study	yes	viscous (Newtonian)	Surface tension	5.2 after 16 μsec (broad range)	100% in 16 μsec	" "

were predicted by this analysis at times in the regime of typical breakup times: (Note that in the stretching jet case $\lambda/2r$ changes with time thus making the comparison more complicated.) However, the approach of [14] has neglected inertia forces to make the governing equations analytically tractable. Because of the high strain rates present in the shaped charge problem inertia effects will be important. This importance of inertia effects will be verified by numerical calculations in the next sub-section. Thus, we feel that the results of this analytical method of [14] as applied to the shaped charge problem are not conclusive.

C. Numerical Study of Shaped Charge Jet Stability

In the previous sub-section we have studied surface tension and aerodynamic effects on jet stability by relatively simple analytical techniques. Since effects such as material strength are, at present, not readily amenable to analytical treatment, we have used numerical techniques to study this and other effects. One advantage of numerical studies over analytical studies is that in the numerical treatment all of the pertinent effects may be included at the outset, whereas analytical treatments necessitate the use of certain simplifying assumptions.

1. General Approach

The numerical study of jet stability was undertaken through the use of the two-dimensional code HEMP [20,21]. The HEMP code is a general purpose code which solves the conservation equations of two-dimensional elastic-plastic flow in plane coordinates or in axisymmetric coordinates. The solution is by the method of finite differences and uses the Lagrangian formulation. The code has the capability of handling many various boundary and initial conditions.

Karpp [22] first applied HEMP code calculations to the problem of a stretching elastic-plastic jet with the surface slightly disturbed. After calculating various wavelengths of the surface disturbance, he found a broad range of most unstable wavelengths with reasonable growth rates. We have applied the same basic method to study the breakup problem in more detail. The boundary and initial conditions of this method will now be briefly described.

A stretching shaped charge jet is modelled by a prismatic circular bar fixed at one end, with the other end moving at a constant velocity. A linear velocity distribution in the axial direction is imposed as the initial condition, and the surface of the bar is initially perturbed in the shape of a cosine function, as shown in Fig. 6. The perturbed surfaces are free from any tractions and the end surfaces are free of any shear stresses. Let the axial velocity be $V(x,r,t)$, the radial velocity be $u(x,r,t)$, the stress vector on the lateral surface be $\underset{\sim}{\sigma}(x,r_s,t)$, and the shear stresses on the end surfaces be $\tau_{rx}(0,r,t)$, $\tau_{x\theta}(0,r,t)$, $\tau_{rx}(L,r,t)$, $\tau_{x\theta}(L,r,t)$, then the boundary conditions are

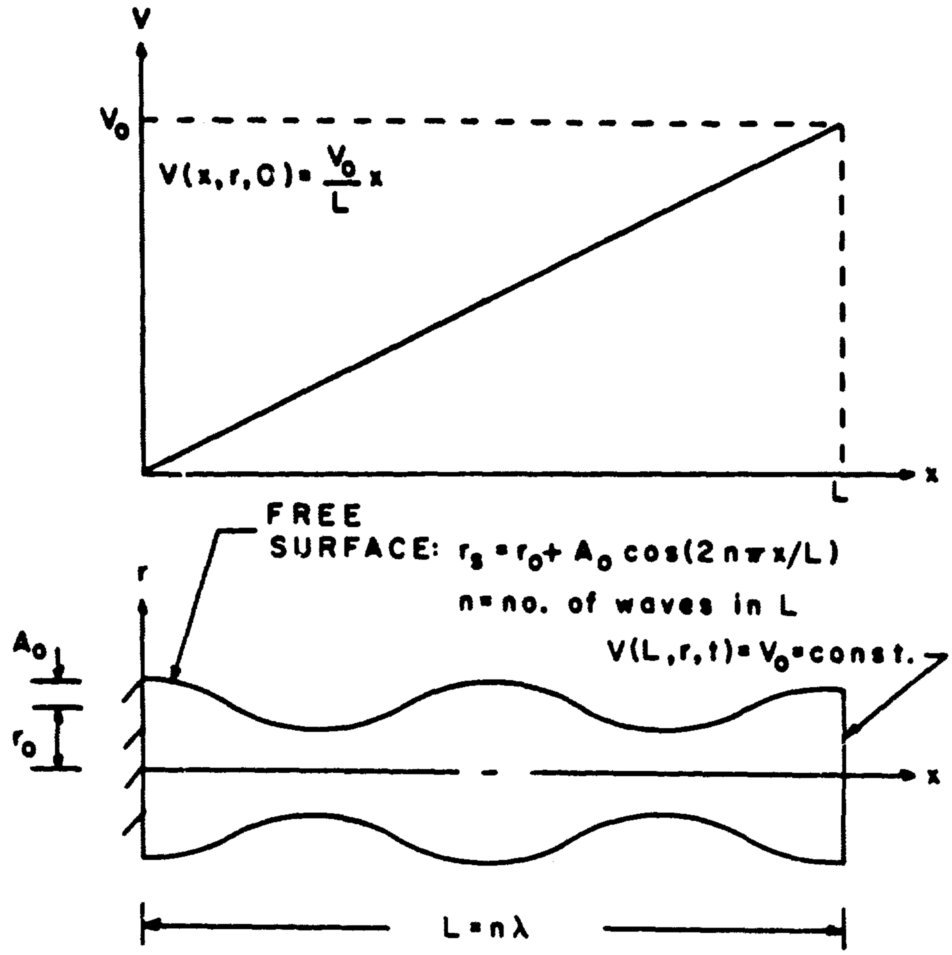

FIGURE 6. Initial and boundary conditions for the numerical jet stability computations.

$$
\begin{aligned}
V(0,r,t) &= 0 \\
V(L,r,t) &= V_0 \\
\underset{\sim}{g}(x,r_s,t) &= \underset{\sim}{0} \\
\tau_{rx}(0,r,t) = \tau_{x\theta}(0,r,t) &= \tau_{rx}(L,r,t) = \tau_{x\theta}(L,r,t) = 0
\end{aligned} \tag{1}
$$

and the initial conditions are

$$
\begin{aligned}
V(x,r,0) &= (V_0/L)x \\
u(x,r,0) &= 0
\end{aligned} \tag{2}
$$

The calculation may often be limited to only one cycle of the surface wave along the axial direction because of the symmetry of the problem.*

2. The Effect of Yield Strength

In the analytical studies discussed previously all of the jets were assumed to be fluid in nature and the driving forces for the instability were restricted to surface tensions, viscosity, and aerodynamic forces. Now we will study the effect of yield strength on the stability of an elastic-plastic jet.**

To study this, we computed four jet segments having different yield strengths but being otherwise identical. In these calculations we selected a copper jet segment with one cycle surface disturbance having an initial length of 7.5mm and an initial mean radius of 1.5mm. The initial amplitude of the wave was taken as 10% of the initial radius. The velocity difference between the two ends of the segment was 0.0625 mm/μsec. In a real jet this initial time corresponds typically to a time 50 μsec after the segment was formed or approximately 100 μsec after the detonation of a BRL 81.3mm charge. This initial configuration and calculation mesh is shown in Fig. 7. In all cases the copper equation of state as specified in HEMP was used. The value of density used was 8.9×10^3 kg/m^3 (8.9 g/cm^3) and the elastic shear modulus was taken as 4.56×10^{10} Pa (456 kbar). The first of the four segments has no strength, i.e. purely fluid; the next three have yield strengths of 2×10^7 Pa (.2 kbar), 2×10^8 Pa (2 kbar), and 2×10^9 Pa (20 kbar). The configuration after 32 μsec for each of these four cases is also shown in Fig. 7. To compare results we have computed a quantity Δ, the relative growth of amplitude, which is defined as the difference between the amplitude of the disturbance after stretching, A, and the initial amplitude, A_0, divided by the initial amplitude, i.e. $(A-A_0)/A_0$. This quantity is also given for each case in Fig. 7. We observe from these calculations that the disturbance grows faster for jets with larger values of yield strength.

* We are studying a typical element in the middle of the jet. This element is being stretched by the force of the forward part of the jet on one side and the rear part of the jet on the other. The details of how the momentum and energy is transferred from one portion of the jet to another are currently being studied.

** Note that Karpp and Simon [23] have recently studied the strength in shaped charge jets using the experimental results of rotating charges and also by using two-dimensional numerical calculations.

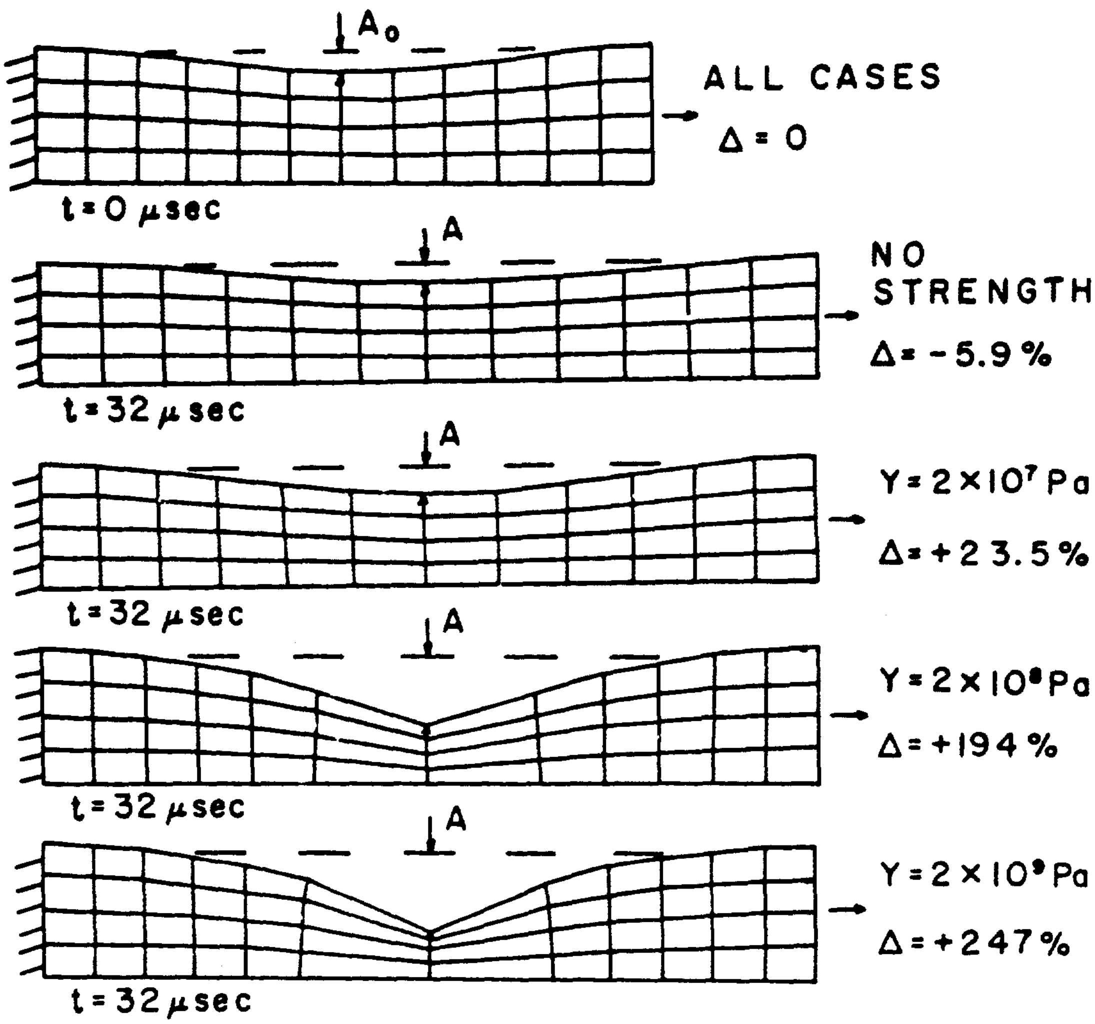

INITIAL LENGTH: 7.5MM

INITIAL MEAN RADIUS: 1.5MM

VELOCITY AT MOVING END: 0.0625MM/μSEC

Δ= RELATIVE GROWTH OF DISTURBANCE = $(A-A_0)/A_0$

Y = YIELD STRESS (ELASTIC-PERFECT PLASTIC)

FIGURE 7. Comparison of stretching jets with various yield strengths.

For static applications, we are used to the concept that, when comparing two materials, the one with higher strength will sustain larger stress, larger strain, and more stretching. Our present results indicate, however, that under dynamic conditions, the opposite case, which seems contrary to common sense, prevails. That is, under dynamic conditions of stretching, the material with higher yield stress is more unstable, will neck more, and break sooner.

3. The Effect of Disturbance Initiation Time

In this sub-section the effects of initiating the disturbance at various times in a realistic shaped charge jet are presented. Consider an element of a jet at several stages from the time when it is first formed until the time of its breakup as shown schematically in Fig. 8. This element of jet has an initial velocity difference of 0.13 mm/μsec between its two ends. The initial length and velocity gradient were selected such that, at the breakup time, the element will have a length equivalent to the average measured length of a typical jet segment from a 81.3mm BRL standard charge. We may therefore consider only one wavelength disturbance over this selected element. When this jet element is first formed one-dimensional calculations indicate its length whould be approximately 1.1mm and its radius should be approximately 3mm. The times chosen to introduce the disturbance, labelled t_1 through t_5 in Fig. 8, correspond to times 0 μsec, 7.92 μsec, 17.62 μsec, 25.69 μsec, and 45.71 μsec after the element was first formed, respectively. The overall dimensions of this element at these different times are summarized in Table V.

Table V

Dimensions of Jet Element Studied at Various Times After Its Formation

Run No.	Time after formation (μsec)	Element Length (mm)	Element radius (mm)	$\lambda/2r$	Amplitude of Imposed Disturbance (mm)	Strain Rate (μsec^{-1})
1	0	1.10	2.98	0.18	0.149	0.118
2	7.92	2.13	2.13	0.5	0.107	0.061
3	17.62	3.39	1.69	1.0	0.085	0.038
4	25.69	4.44	1.48	1.5	0.074	0.029
5	45.77	7.05	1.17	3.0	0.059	0.018

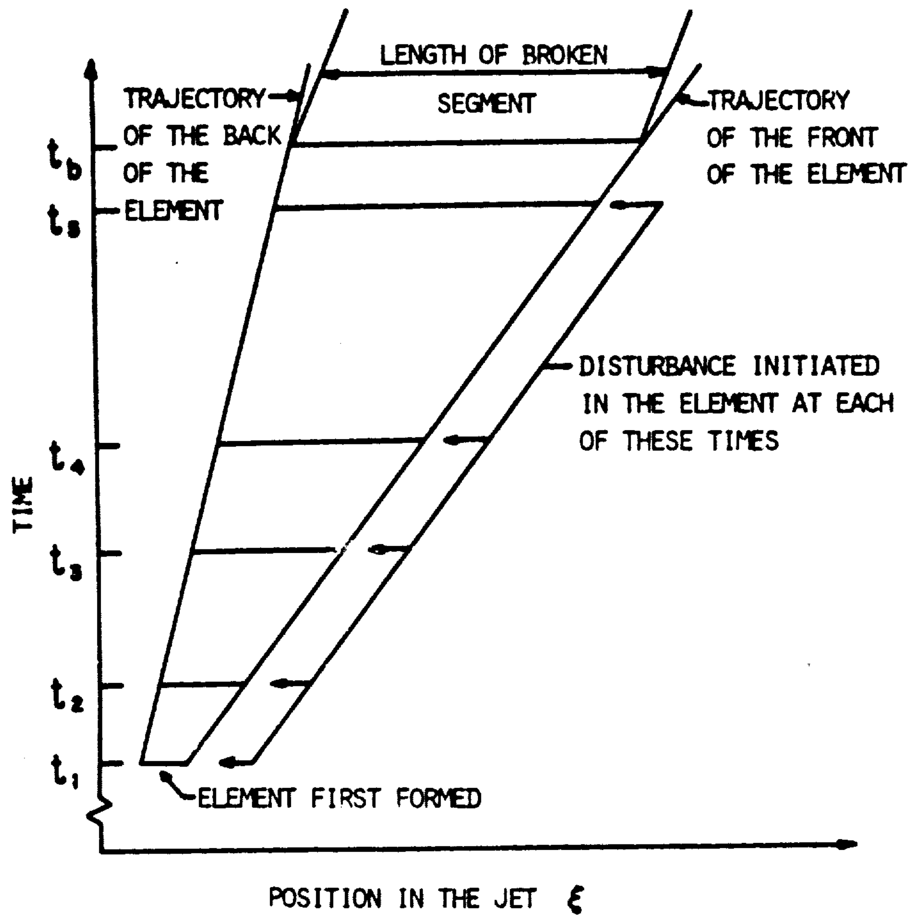

FIGURE 8. Schematic showing a position-time plot of a jet element which stretches to the typical breakup length. Disturbances are initiated seperately at each of the times indicated for independent HEMP calculations of the element.

The HEMP calculations were performed using each of these times as a separate starting point. The disturbance was introduced independently at each of these times and each was treated as a separate problem. The equation of state and other constants for copper stated in the previous problem were again used. The yield stress was 2×10^9 Pa (2 kbar). The amplitude of the imposed disturbance was taken at 5% of the radius in each instance and is also given in Table V.

The five HEMP calculations indicate that, during short times after the initiation of the disturbance, the amplitude of the surface disturbance in Run No.4 grows the largest amount. This can be seen in Fig. 9, where the relative growth, Δ, at a time 18 µsec after the disturbance initiation for each case is plotted versus the initial strain rate. This gives an indication of how soon each disturbance begins to grow. As time proceeds, however, and we continue the calculations, the earlier configurations (Run Nos. 1-3) eventually reach a configuration similar to Run No.4, and then the disturbance begins to grow quickly. This can be seen in Fig. 10 where the relative growth of Run Nos. 2,3, and 4 are plotted versus time. Examining Run No.2, we see that the disturbance is stable until a time of approximately 30-35 µsec after formation, then the growth rate drastically increases. Run Nos. 3 and 4, in which the disturbance is initiated at times later than Run No.2, also begin to grow more rapidly in the region 30-35 µsec. Thus we see that, no matter how early we initiate the disturbance, when a critical time is reached, the disturbance will begin to grow and eventually the same final breakup configuration will be obtained.

4. The Effect of Disturbance Wavelength

The effect of disturbance wavelength was studied by considering a jet of realistic radius and strain rate at a reasonably early time after formation and introducing surface disturbances of different wavelengths. A jet element having an initial radius of 2.13mm and an initial strain rate of 0.061 µsec^{-1} was used. The equation of state and material constants for copper stated in the previous problem were again used. Four separate surface disturbances having initial wavelengths of 1.065mm, 2.13mm, 4.26mm, and 8.52mm were introduced and HEMP calculations made for each case. Note that we have chosen this problem such that the case $\lambda = 2.13$mm will eventually grow to the observed segment length after the experimentally determined breakup time for a typical shaped charge jet. Let us denote this "correct" initial wavelength as $\lambda_0 = 2.13$mm. We can then denote the other cases as $\lambda = \lambda_0/2$, $\lambda = 2\lambda_0$ and $\lambda = 4\lambda_0$. The relative growth, as computed using the HEMP code for each of these cases, is plotted vs. time in Fig. 11. From this plot we see that the disturbances having initial wavelengths of $\lambda = \lambda_0/2$ and $\lambda = 4\lambda_0$ grow very slowly. The wavelength $\lambda = \lambda_0$, which will grow into the proper segment size, grows very quickly but not quite as fast as the case $\lambda = 2\lambda_0$.

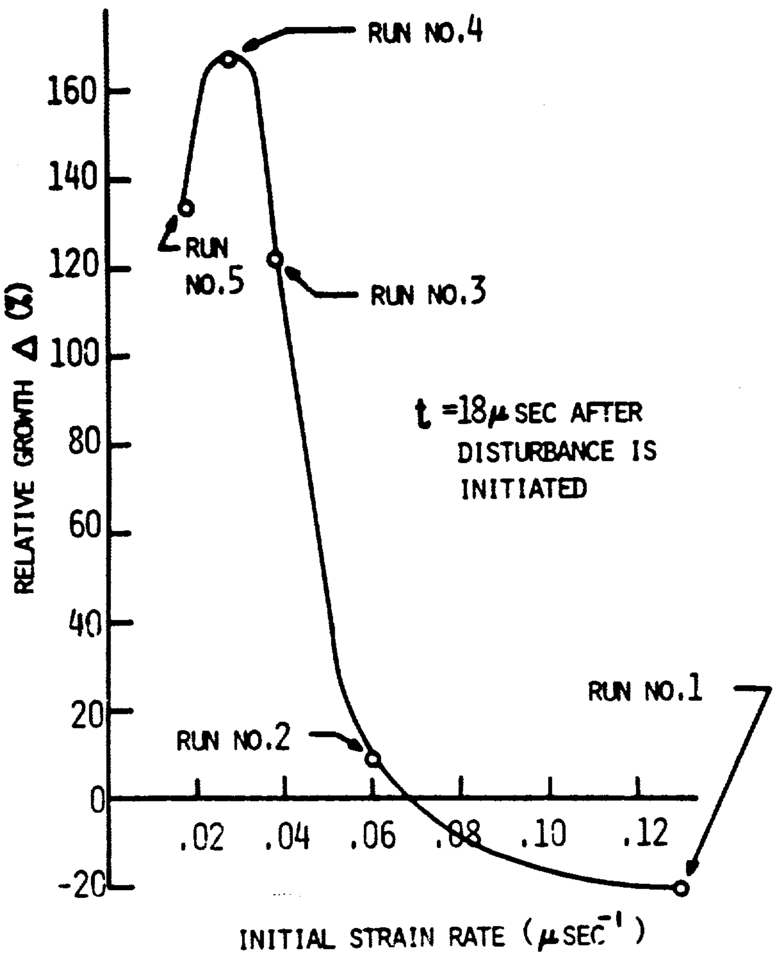

FIGURE 9. Relative growth vs. initial strain rate for five successive element configurations at 18μsec after disturbance initiation in each configuration.

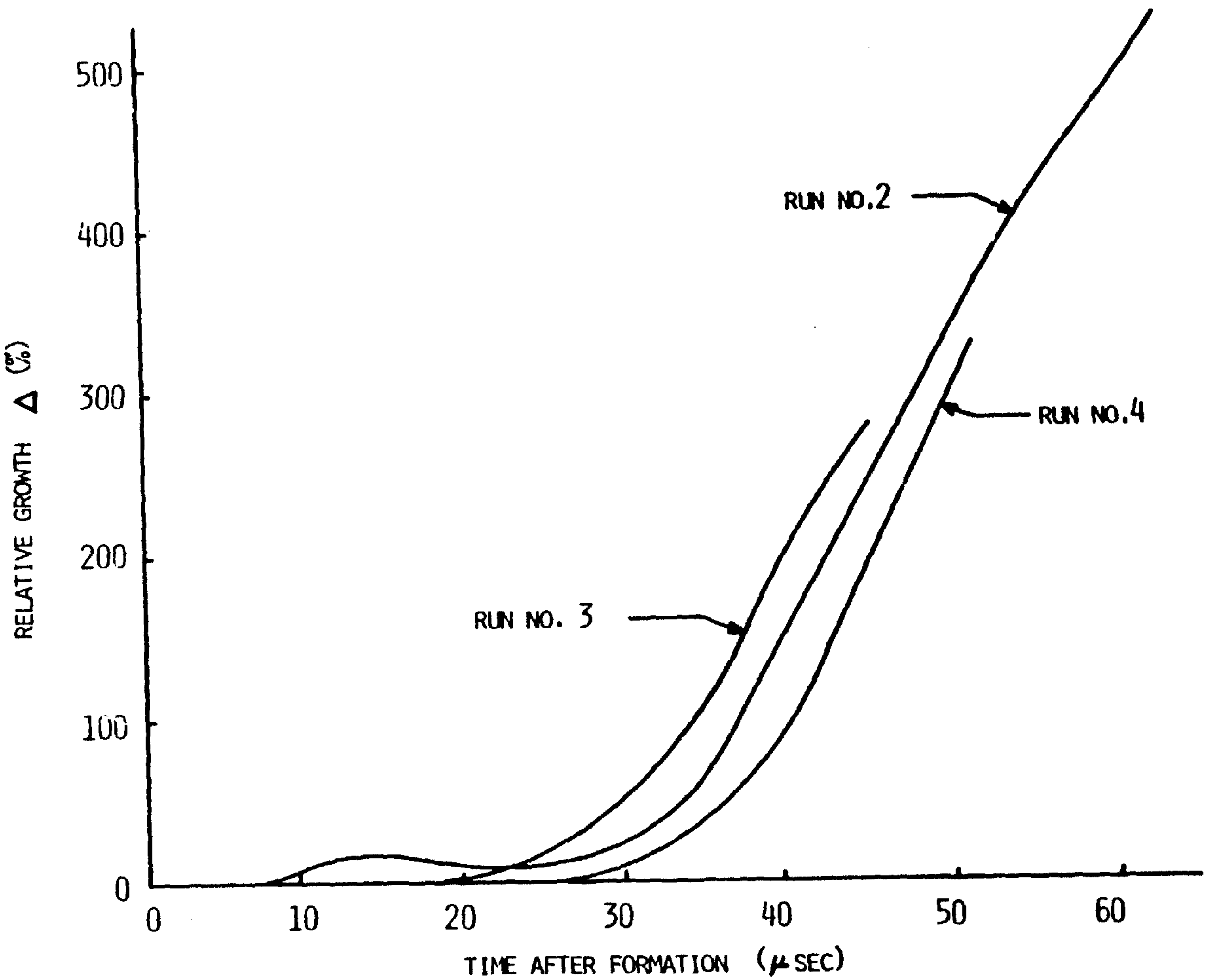

FIGURE 10. Relative growth vs. time for three different disturbance initiation times in a typical jet element.

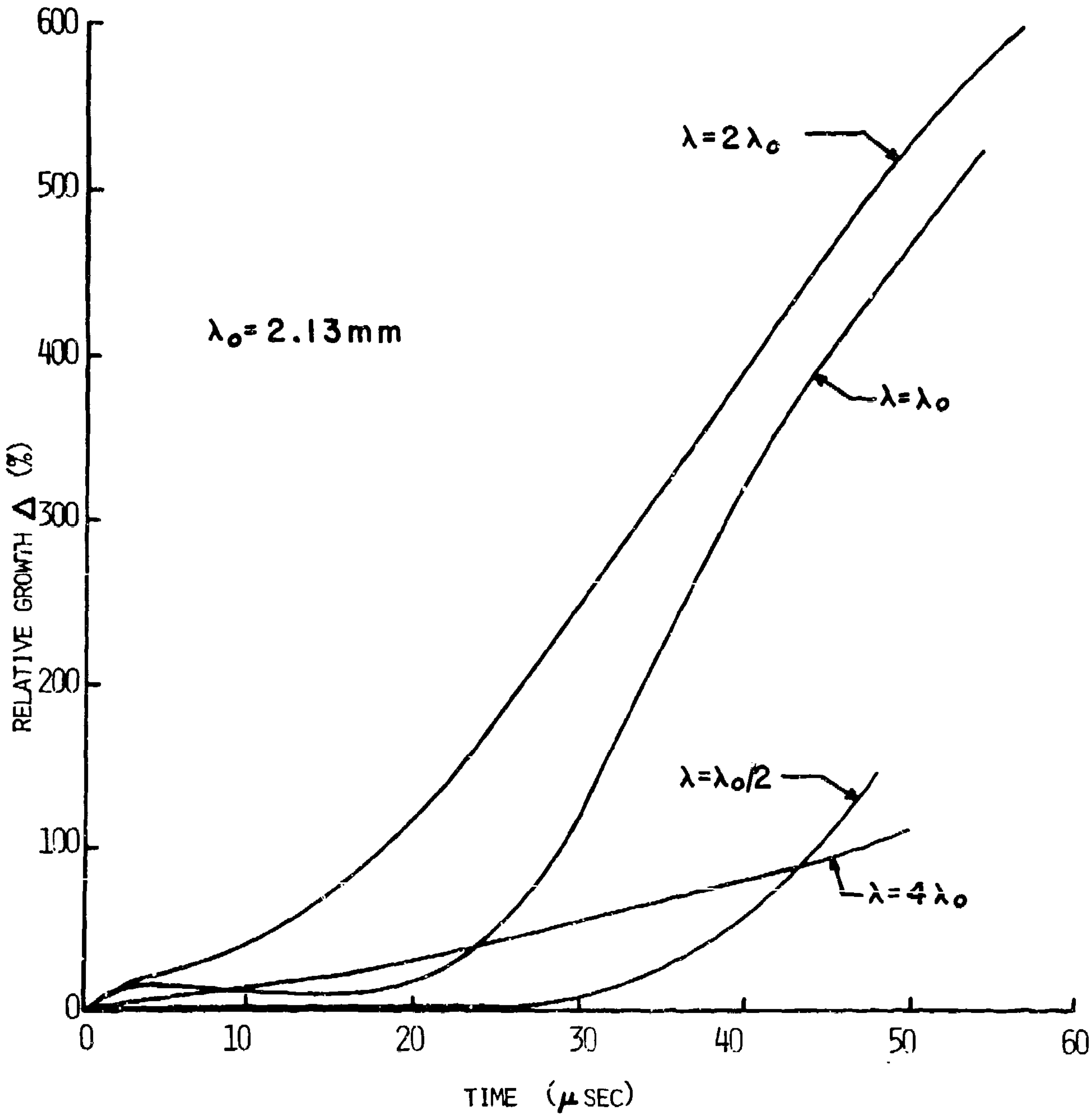

FIGURE 11. Relative growth vs. time for surface disturbances of four different wavelengths. In all cases, the jets initially have the same radius and strain rate.

5. Irregular Surface Disturbance

To examine these wavelength effects further, we have numerically studied jets having an irregular surface disturbance. In previous cases, we have considered jets having a surface of a single sinusoidal curve. Next, we have combined the four wavelengths of the previous study to obtain an irregular surface disturbance which is described by the following function:

$$r_s = r_0 + A_0 \sum_{i=1}^{4} \cos \frac{2\pi x}{k_i}$$

where $k_1 = \lambda_0/2$, $k_2 = \lambda_0$, $k_3 = 2\lambda_0$, $k_4 = 4\lambda_0$. We have taken numerical values to be $r_0 = 2.13$mm, $\lambda_0 = 2.13$mm, $A_0 = 0.026$mm, and the initial strain rate equal to 0.061 μsec^{-1}. We again used the material constants for copper described previously. The initial configuration which has a length of $2\lambda_0$ is shown in Fig. 12, together with the configuration after 52 μsec. We observe that the jet appears to neck in two places. This indicates that λ_0 is the dominant or fastest growing wavelength, which is in agreement with the experimentally obtained segment length. To demonstrate this more quantitatively, we have fit a Fourier series to the outer surface of the configuration after 52 μsec shown in Fig. 12 and have examined the coefficients of the terms of each wavelength. Denoting the length after 52 μsec as $2\lambda_1$, we observe that the largest of all the Fourier coefficients is that of the term containing the length $\lambda = \lambda_1$. A comparison of the coefficients of the four wavelengths of interest are also shown in Fig. 12. Thus, this result indicates that the component with an initial wavelength of $\lambda = \lambda_0$, which stretches into $\lambda = \lambda_1$ after 52 μsec is the most critical one.

In the case above, the initial disturbance consists of four waves of different wavelength, which are all "in phase". We performed yet another irregular surface disturbance calculation. In this calculation, a "random" disturbance was used which was comprised of five waves of different wavelength and phase angles, so that the waves would not be "in phase" at the ends. Thus, this new disturbance represents more closely a random one. The function used for the surface was

$$r_s = r_0 + A_0 \sum_{i=1}^{5} \cos \left(\frac{2\pi x}{k_i} - \phi_i \right)$$

where $k_1 = \lambda_0/2$, $k_2 = 3\lambda_0/4$, $k_3 = \lambda_0$, $k_4 = 3\lambda_0/2$, $k_5 = 2\lambda_0$, and $\phi_1 =$ [illegible]7°, $\phi_2 = 36°$, $\phi_3 =$ [illegible], $\phi_4 = 54°$, $\phi_5 =$ [illegible]3°. Numerical values were taken as $r_0 = 2.13$, $\lambda_0 = 2.13$mm, $A_0 = 0.053$mm, and the initial strain rate equal to 0.061 μsec^{-1}. The initial configuration and the configuration after 4[illegible] μsec of stretching as calculated by the HEMP code are shown in Fig. 13. We see the jet necking in two places which again indicates that the growth of the $\lambda = \lambda_0$ wave predominates and that the proper jet segment length will be attained at breakup.

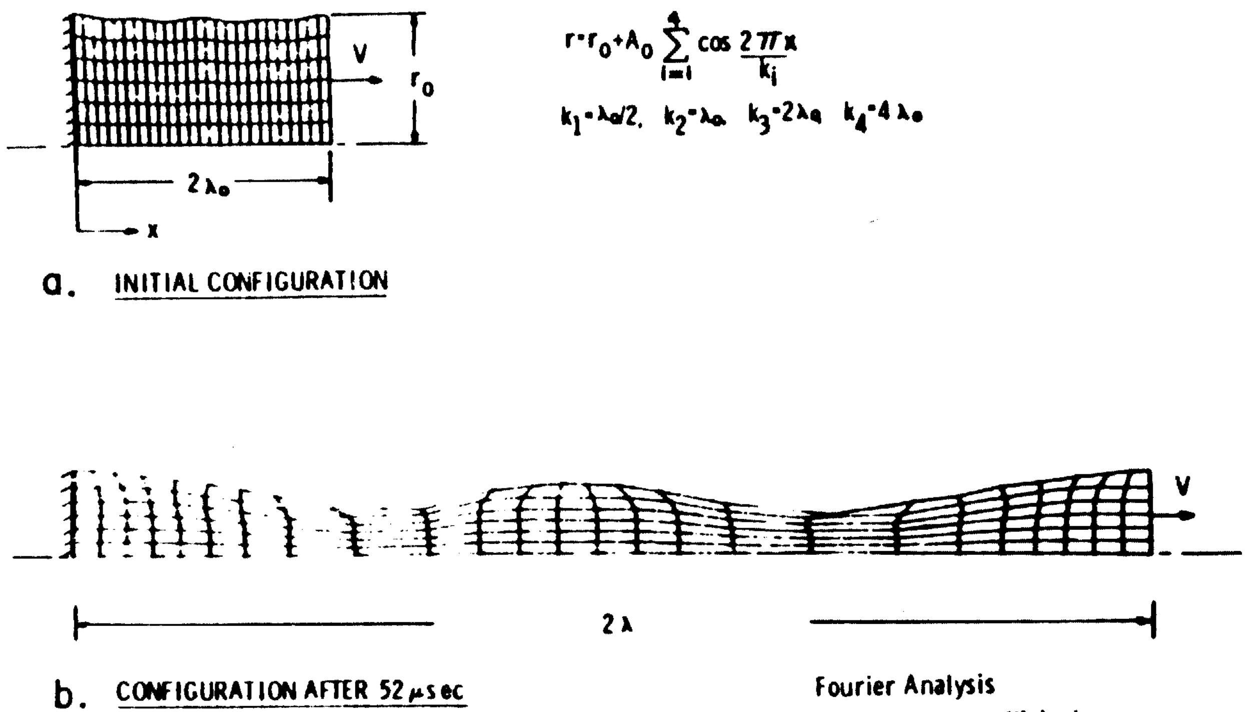

Fourier Analysis

wavelength	coefficient
$\lambda/2$	-.00003
λ	.0246
2λ	.0164
4λ	.0045

FIGURE 12. Results of HEMP calculations of a stretching jet with an irregular surface disturbance.

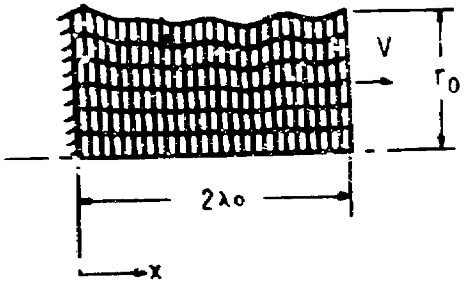

$$r = r_0 + A_0 \sum_{i=1}^{5} \cos\left[\frac{2\pi x}{k_i} - \phi_i\right]$$

$k_1 = \lambda_0/2,\ k_2 = 3\lambda_0/4,\ k_3 = \lambda_0,\ k_4 = 3\lambda_0/2,\ k_5 = 2\lambda_0$
$\phi_1 = 27^0,\ \phi_2 = 36^0,\ \phi_3 = 45^0,\ \phi_4 = 54^0,\ \phi_5 = 63^0$

a. INITIAL CONFIGURATION

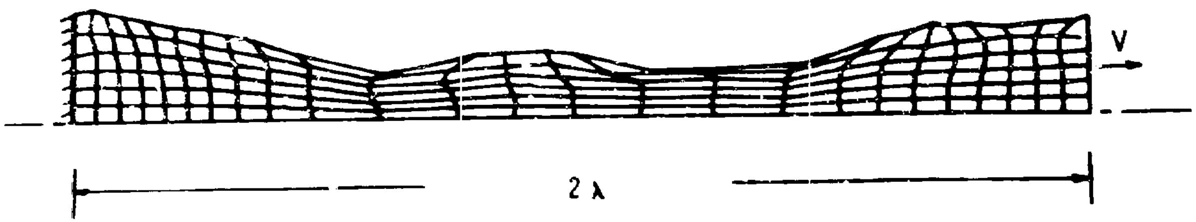

b. CONFIGURATION AFTER 48 μsec

FIGURE 13. Results of HEMP calculations of a stretching jet with "random" surface disturbances.

6. The Effect of Inertia

To study the importance of inertia effects on the growth of surface disturbances in stretching shaped charge jets, we have made HEMP code calculations of three jets. Each jet was identical in all respects except for the density of the material used in the calculations. The configuration used was the standard single wave surface disturbance depicted in Fig. 6 with $r_0 = 2.13$mm and wavelength equal to 2.13mm. The initial amplitude used was $A_0 = 0.107$mm and the initial strain rate equal to .061 μsec^{-1}. The equation of state and material constants described previously for copper were used except now three different values of density were used $\rho_0 = 1 \times 10^3$ kg/m^3, $\rho_0 = 8.9 \times 10^3$ kg/m^3, and $\rho_0 = 16.5 \times 10^3$ kg/m^3. The relative growth vs. time for each case is plotted in Fig. 14. We observe that increased density, i.e. increased inertia force, has a retarding effect on disturbance growth.

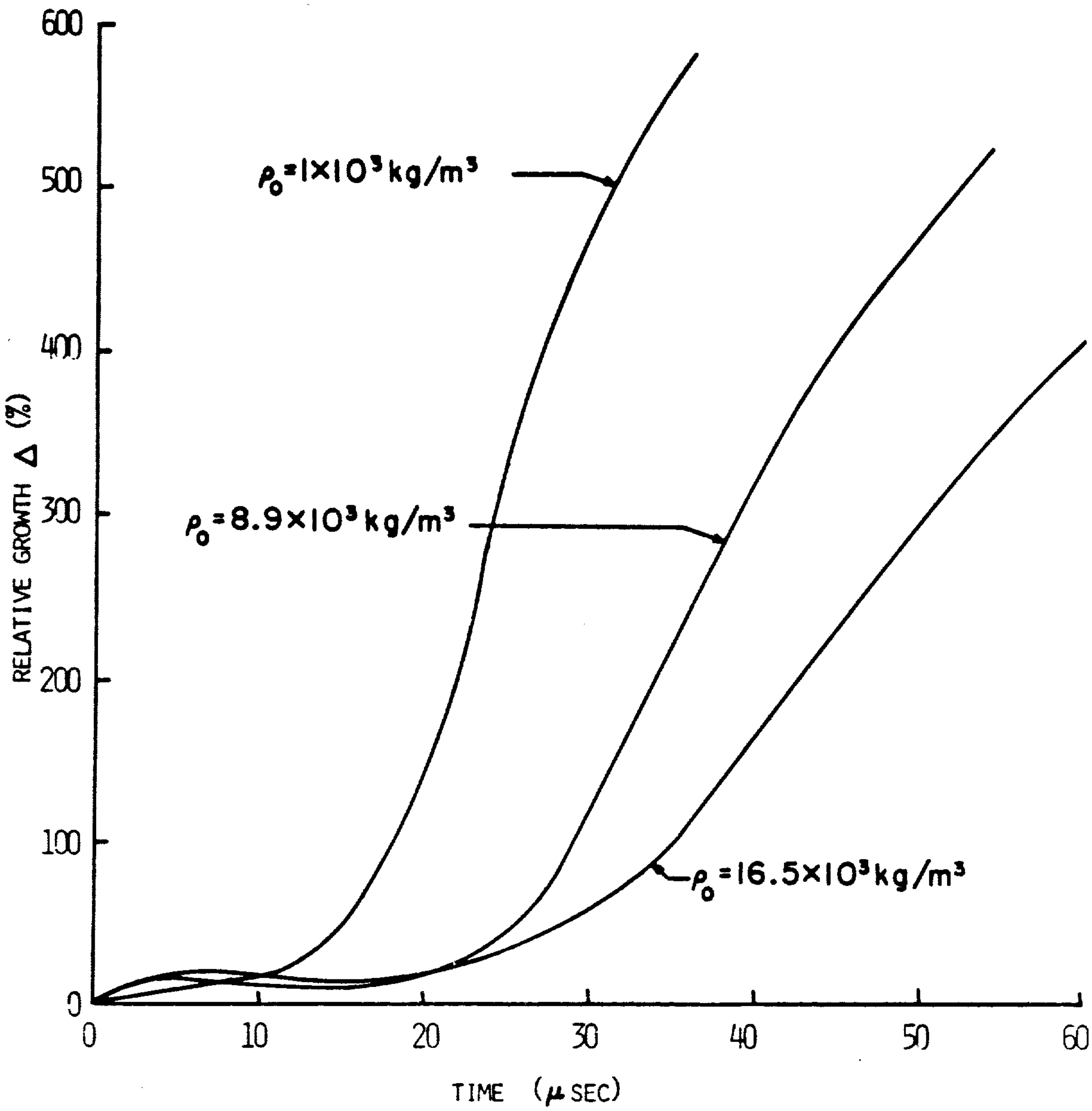

FIGURE 14. Relative growth vs. time for the stretching jets of different densities as predicted by HEMP.

IV. CONCLUSIONS

The major results and conclusions of the present research may be summarized as follows:

A. Measurement of Jet Radiographs

1. Data from jet radiographs, including jet velocity, breakup time, and segment size, for jets from eleven charges were compiled and plotted for easy reference.

2. These measured jet velocity and jet radius data agree closely with those calculated from a one-dimensional shaped charge model.

3. Analysis of this data together with using one-dimensional calculations resulted in a semi-empirical breakup time vs. jet radius curve for copper jets. This curve can be used to estimate an approximate breakup time for new charge designs.

B. Stability of Shaped Charge Jets

1. Simple stability analyses and experimental results indicate that surface tension and aerodynamic forces are not important in the breakup of shaped charge jets.

2. Numerical HEMP code calculations of stretching elastic-plastic jets subjected to surface disturbances were conducted. The effects of material yield strength, time of disturbance initiation, wavelength of the disturbance, irregular surface disturbances and jet density were examined. The following results were found:

a. Jets with higher yield strengths break sooner, all else being equal.

b. Jets with lower densities will break sooner, all else being equal.

c. For the shaped charge jet calculated, there is a critical time for the growth of the disturbance amplitude. Disturbances introduced early do not grow appreciably before this time, but grow rapidly after this critical time. Disturbances introduced after this time also grow rapidly.

d. A critical wavelength (or a range of wavelengths) exists; disturbances having this wavelength grow faster than all others. The length of the broken jet segment caused by this critical wave is in the range of measured jet segment lengths.

e. When irregular, or random, surface disturbances are introduced, the growth is again dominated by the disturbance component with the critical wavelength. The jet surface grows into a shape similar to that obtained if only the wave with the critical length were introduced.

3. Materials with high density and low yield strength are promising liner materials which will likely retard the breakup of the resulting jet.

V. REFERENCES

1. Chou, P.C. and Carleone, J., "Calculation of Shaped Charge Jet Strain, Radius, and Breakup Time," U.S. ..rmy Ballistic Research Laboratories (BRL) Contract Report No. 246, July 1975. (AL *B007240L)

2. Chou, P.C. and Carleone, J., "The Breakup of Shaped Charge Jets," Proceedings of the 2nd International Symposium on Ballistics, March 9-11, 1976, Daytona Beach, Florida, Sponsored by the American Defense Preparedness Association.

3. DiPersio, R., Jones, W.H., Merendino, A.B., and Simon, J., "Characteristics of Jets from Small Caliber Shaped Charges with Copper and Aluminum Liners," U.S. Army Ballistic Research Laboratories (BRL) Memorandum Rept. No. 1866, Sept. 1967. (AD #823839)

4. Chou, P.C., Carleone, J., and Karpp, R.R., "Criteria for Jet Formation from Impinging Shells and Plates," J. Applied Physics, Vol. 47, July 1976, pp. 2975-2981.

5. Pugh, E.M., Eichelberger, R.J., and Rostoker, N., "Theory of Jet Formation by Charges with Lined Conical Cavities," J. Applied Physics, Vol. 23, No. 5, May 1952, pp. 532-536.

6. Held, M., "Air Target Warheads," International Defense Review, No. 5, 1975.

7. Perez, E., private communication, French-German Institute of Saint Louis (ISL), 12 Rue de l'Industril, St. Louis 58 France.

8. Carleone, J. and Chou, P.C., "A One-Dimensional Theory to Predict the Strain and Radius of Shaped Charge Jets," Proceedings of the First International Symposium on Ballistics, Nov. 13-15, 1974, Orlando, Florida, sponsored by the American Defense Preparedness Association.

9. Chou, P.C. and Carleone, J., "Shaped Charge Jet Breakup Research," Quarterly Tech. Rept. for Contract No. DAAD05-75-C-0753 for the period June 12-Sept. 11, 1975.

10. Chou, P.C. and Carleone, J., "Shaped Charge Jet Breakup Research," Quarterly Tech. Rept. for Contract No. DAAD05-75-C-0753 for the period Sept. 12-Dec. 11, 1975.

11. Lord Rayleigh, The Theory of Sound, 2nd. ed., Vol. 2, Dover, New York, 1945, pp. 351-363.

12. Weber, C., "Zum Zerfall eines Flussigkeitsstrahles" (Disentegration of a Liquid Jet), Zeitschrift fur Angewandte Mathematik und Mechanik, Vol.11, No. 2, April 1931, pp. 136-153.

13. Levich, V.G., Physicochemical Hydrodynamics, Prentice-Hall 1962.

14. Mikami, T., Cox, R.G., and Mason, S.G., "Breakup of Extending Liquid Threads," Post-Graduate Research Laboratory Report, Pulp and Paper Research Institute of Canada, PGRL/72, October 1974.

15. Goldin, M., Yerushalmi, J., Pfeffer, R. and Shinnar, R., "Breakup of a Laminar Capillary Jet of a Viscoelastic Fluid," J. Fluid Mech., Vol. 38, part 4, 1969, pp. 689-711.

16. Anno, J.N. and Walowit, J.A., "Integral Form of the Derivation of Reyleigh's Criterion for the Instability of an Inviscid Cylindrical Jet," American Journal of Physics, Vol. 38, No. 10, Oct. 1970, pp. 1255-1256.

17. Anno, J.N., "Influence of Viscosity on the Stability of a Cylindrical Jet," AIAA Journal, Vol. 12, No. 8, Aug. 1974, pp. 1137-1138.

18. Vitali, R., private communication, U.S. Army Ballistic Research Laboratories.

19. Frey, R., private communication, U.S. Army Ballistic Research Laboratories.

20. Wilkins, M.L., "Calculation of Elastic-Plastic Flow," University of California, Lawrence Livermore Laboratory, Rept. UCRL-7322, Rev. 1, Jan. 24, 1969.

21. Giroux, E.D., "HEMP User's Manual," University of California, Lawrence Livermore Laboratory, Rept. UCRL-51079, June 24, 1971.

22. Karpp, R.R., private communication, U.S. Army Ballistic Research Laboratories.

23. Karpp, R.R. and Simon, J., "An Estimate of the Strength of a Copper Shaped Charge Jet and the Effect of Strength on the Breakup of a Stretching Jet," U.S. Army Ballistic Research Laboratories (BRL) Report No. 1893, June 1976. (AD #B012141)

24. Simon, J., "The Effect of Explosive Detonation Characteristics on Shaped Charge Performance," Army Science Conference, West Point, N.Y., June, 1974.

Appendix A

This appendix contains the specifications of the eleven charges studied in this report.

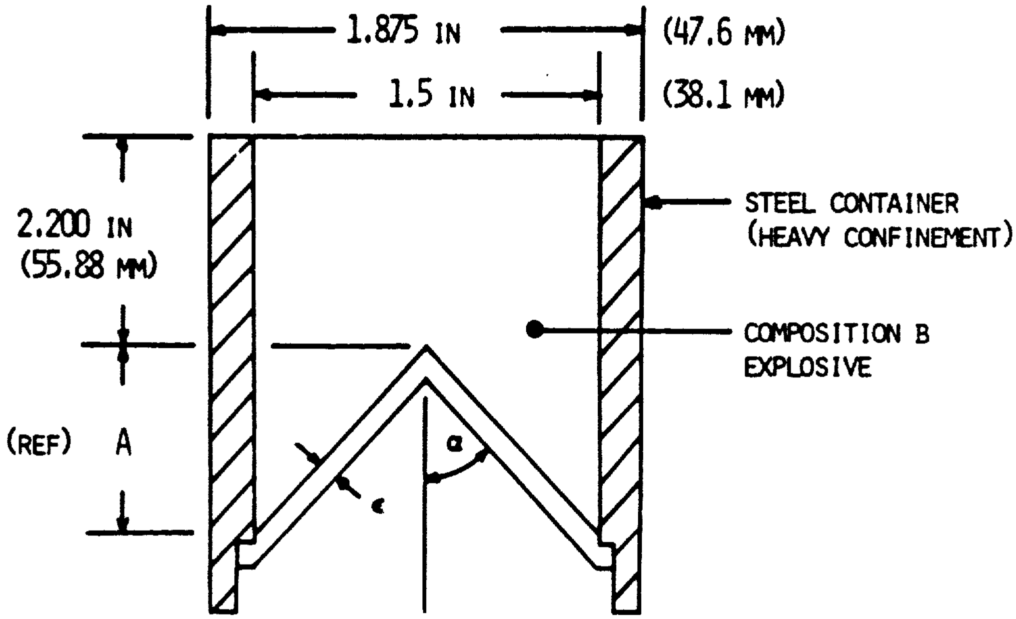

CHARGE NO.	LINER MAT'L	α	ε IN (MM)	A IN (MM)
1	Cu	10°	0.046 1.168	4.253 108.0
2	Cu	20°	0.046 1.168	2.061 52.35
3	Cu	30°	0.046 1.168	1.299 33.00
4	Cu	45°	0.046 1.168	0.750 19.05
9	AL	20°	0.064 1.626	2.061 52.35
10	AL	30°	0.064 1.626	1.299 33.00
11	AL	45°	0.064 1.626	0.750 19.05

FIGURE A1. Geometry of the 38.1 mm Copper and Aluminum lined charges with various cone angles. (Charge Nos. 1-4,9-11) (from Ref. 3)

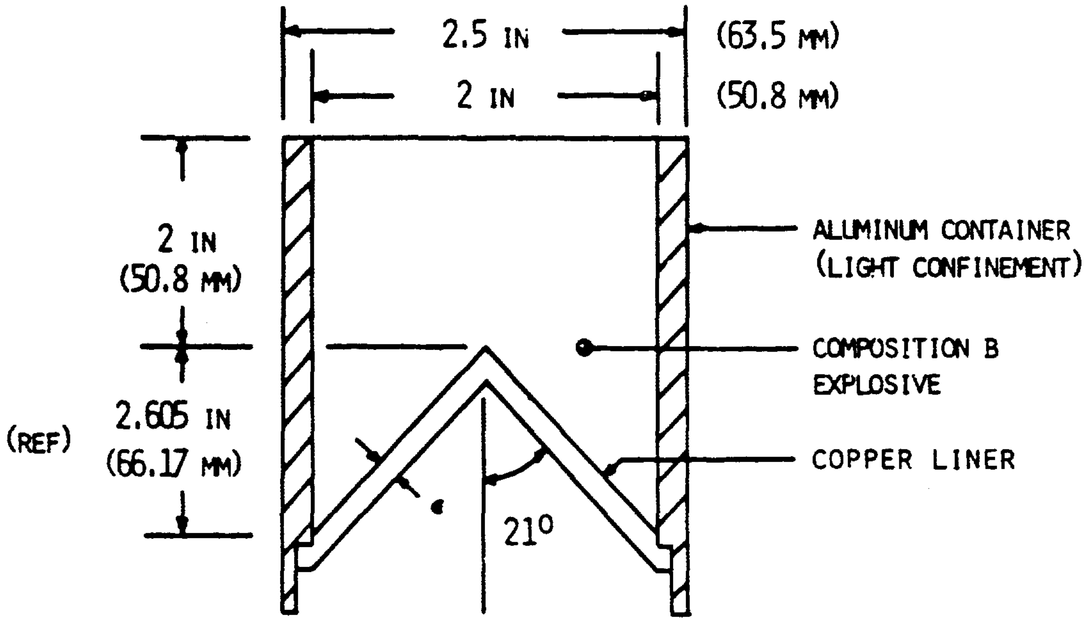

CHARGE NO.	ϵ IN (MM)
5	0.030 0.762
6	0.060 1.524
7	0.100 2.540

FIGURE A2. Geometry of the 50.8 mm, 42° Copper lined charges with different wall thicknesses. (Charge Nos. 5-7)
(Courtesy of R. Jameson)

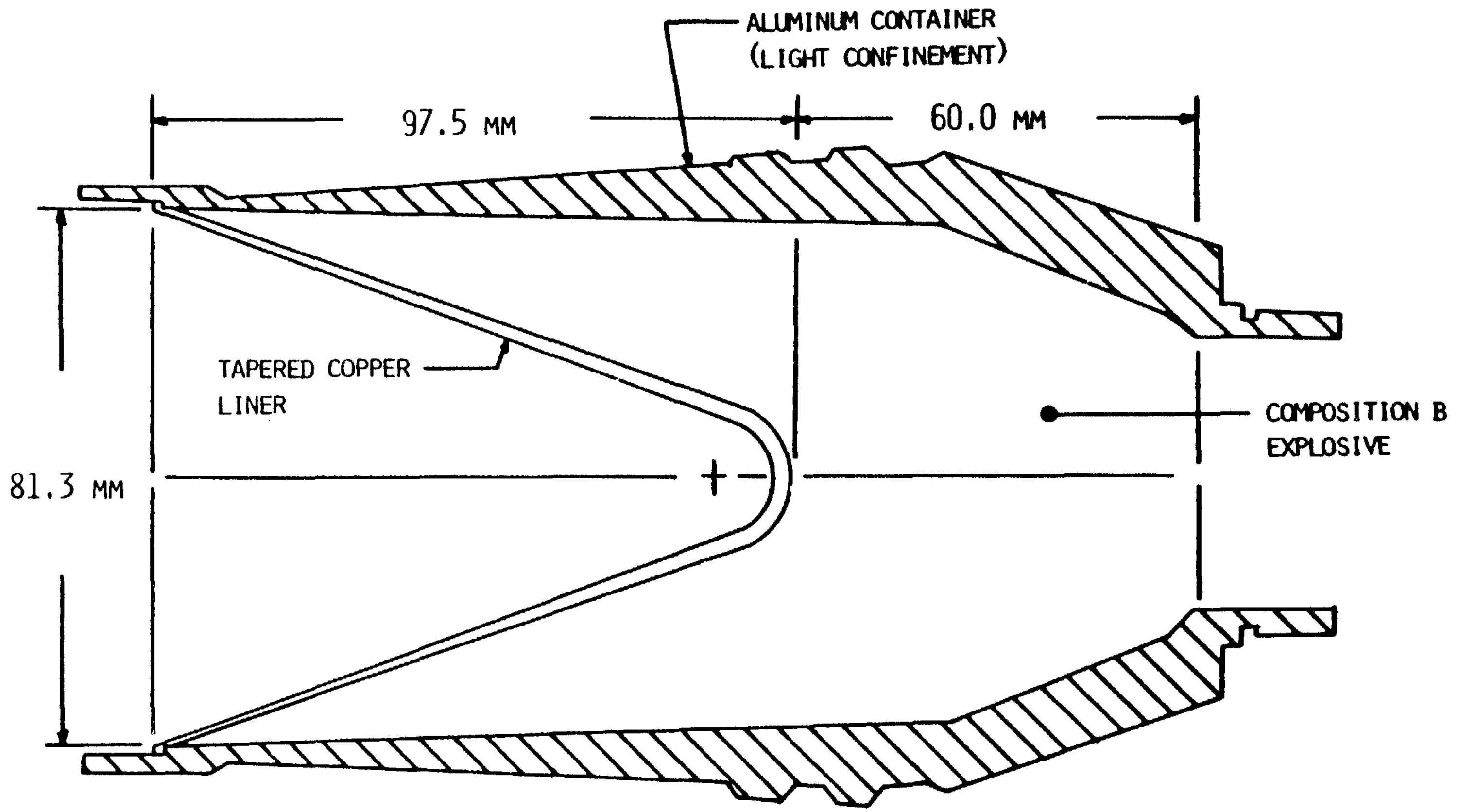

FIGURE A3. Overall dimensions of the 81.3 mm, 42^{o} tapered wall charge.
(Charge No. 8)
(Ref. 24, except liner)

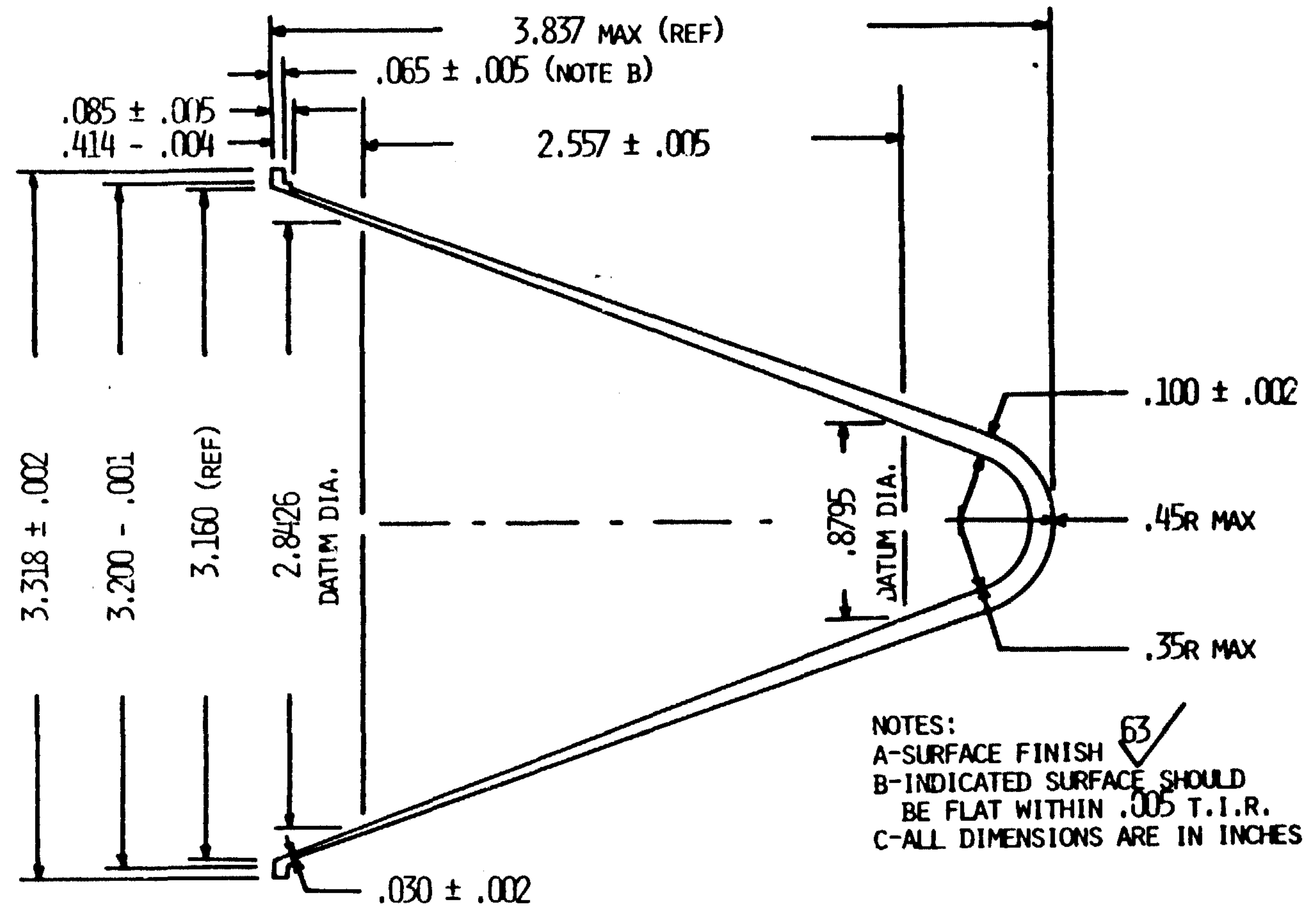

FIGURE A4. Details of the 81.3 mm, 42° tapered liner.
(Charge No. 8) (Liner was made at BRL.)
(Courtesy of R. Jameson)

Appendix B

This appendix contains a graphical display of jet velocity, jet breakup time, and jet radius data computed from the jet radiographs of the eleven charges studied in this report.

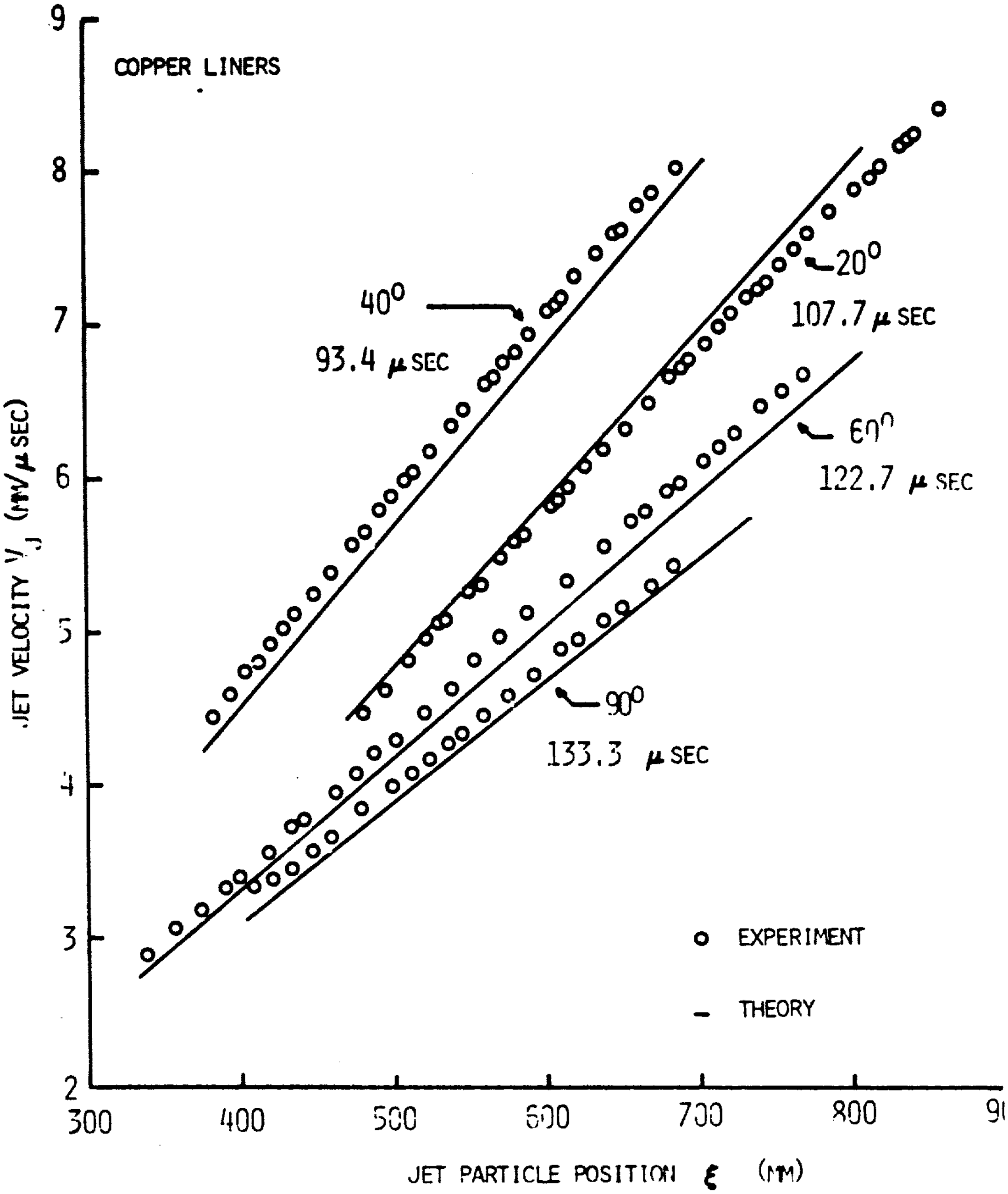

FIGURE B1. Theoretical and experimental jet velocity vs. jet particle position for the series of 38.1mm, 1.168mm wall, copper lined charges with various cone angles at various times after the arrival of the detonatic wave at the cone apex. (charge nos. 1-4).

PRECEDING PAGE BLANK-NOT FILMED

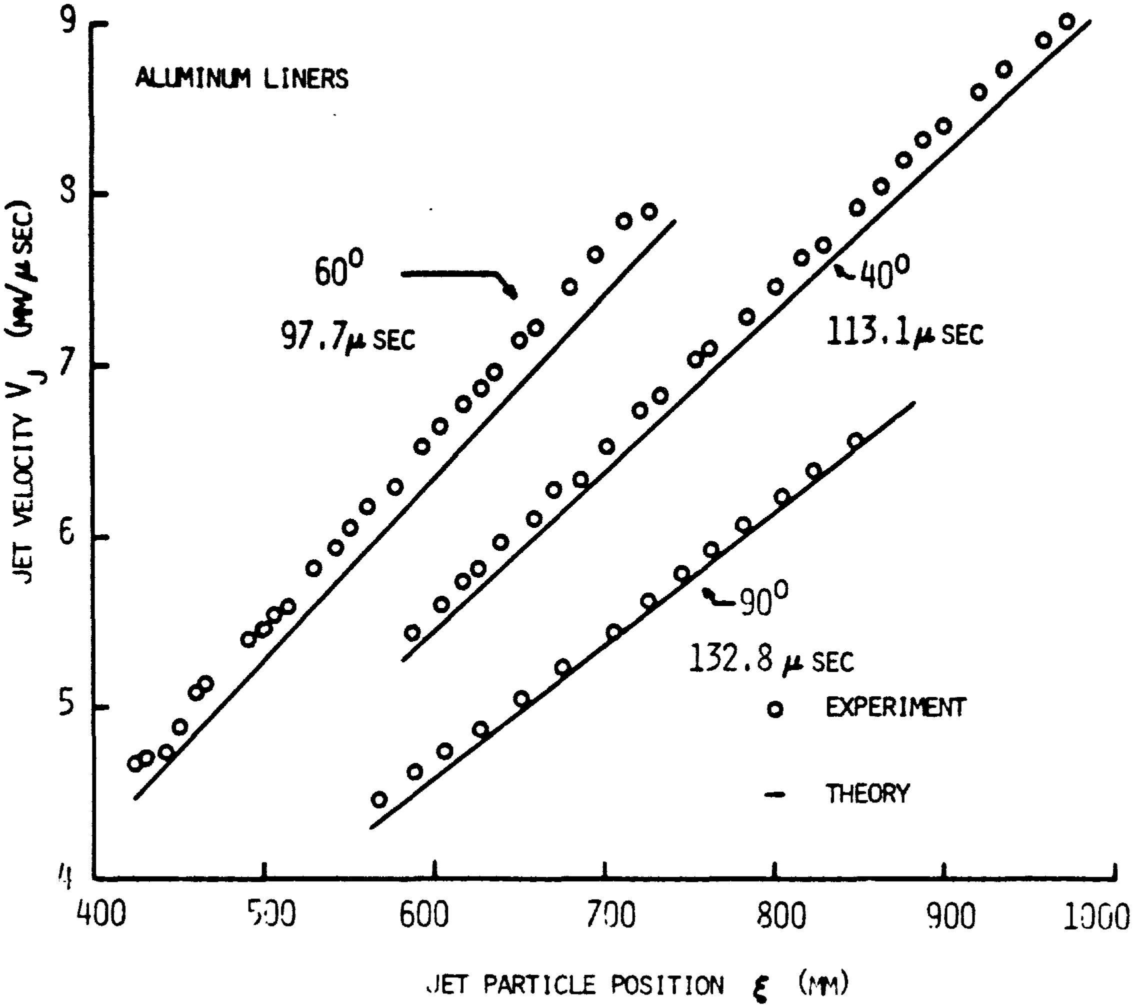

FIGURE B2. Theoretical and experimental jet velocity vs. jet particle position for the series of 38.1mm, 1.626mm wall, aluminum lined charges with various cone angles, at various times after the arrival of the detonation wave at the cone apex. (Charge Nos. 9-11)

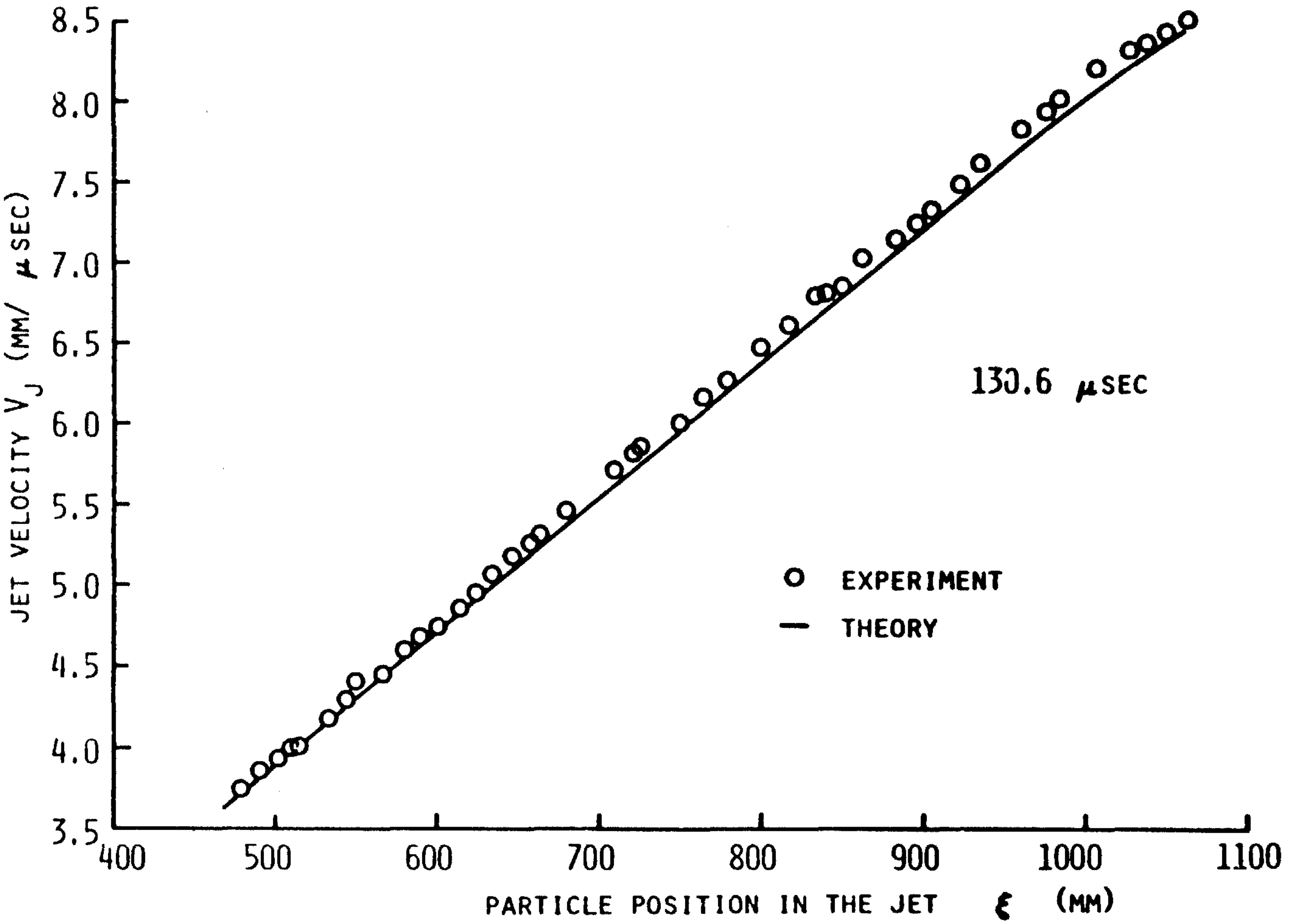

FIGURE B3. Theoretical and experimental jet velocity vs. jet particle position for the 50.8mm, 42°, 0.762mm wall copper lined charge at 130.6 usec after detonation wave arrival at cone apex. (charge No. 5)

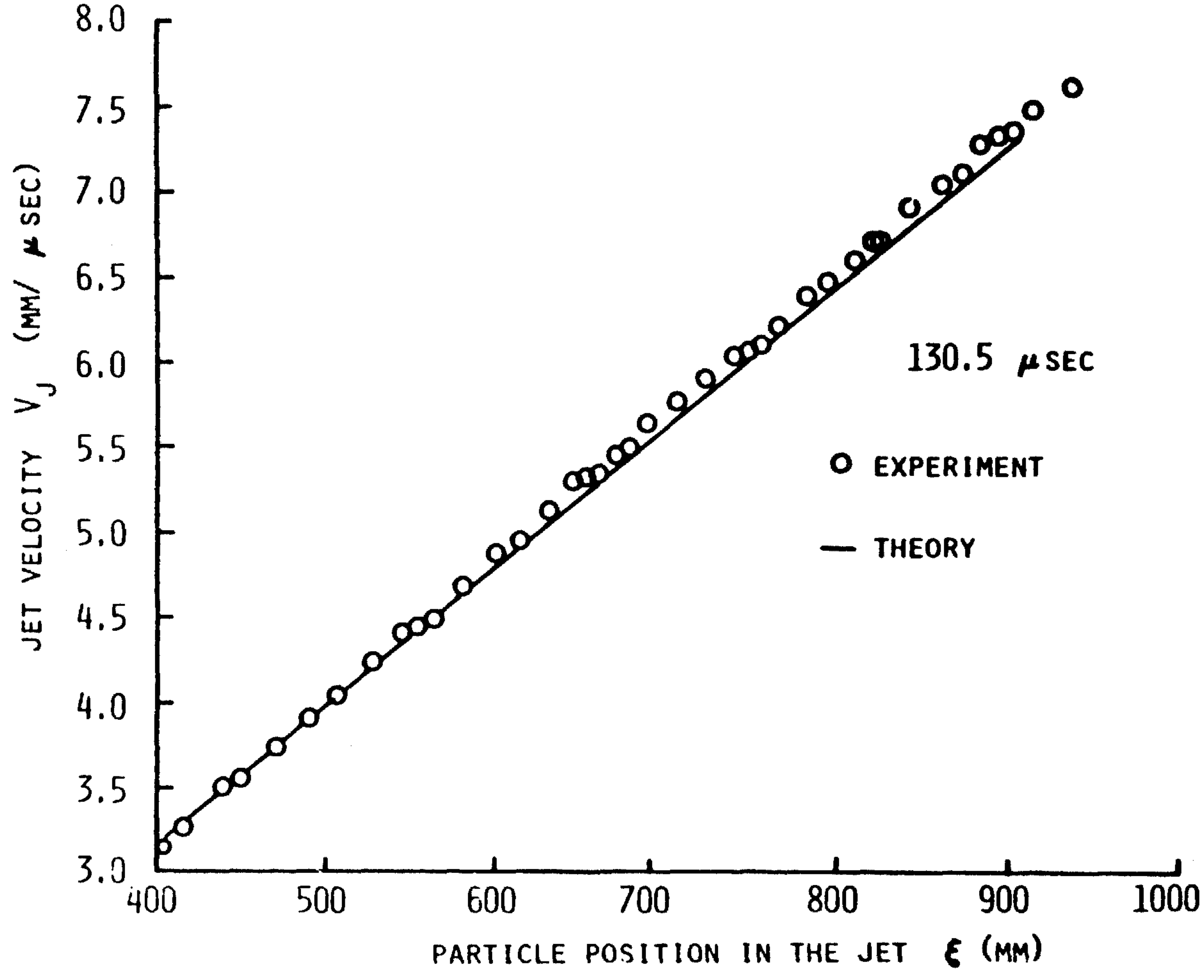

FIGURE B4. Theoretical and experimental jet velocity vs. jet particle position for the 50.8mm, 42°, 1.524mm wall, copper lined charge at 130.5 μsec after detonation wave arrival at cone apex. (Charge No. 6)

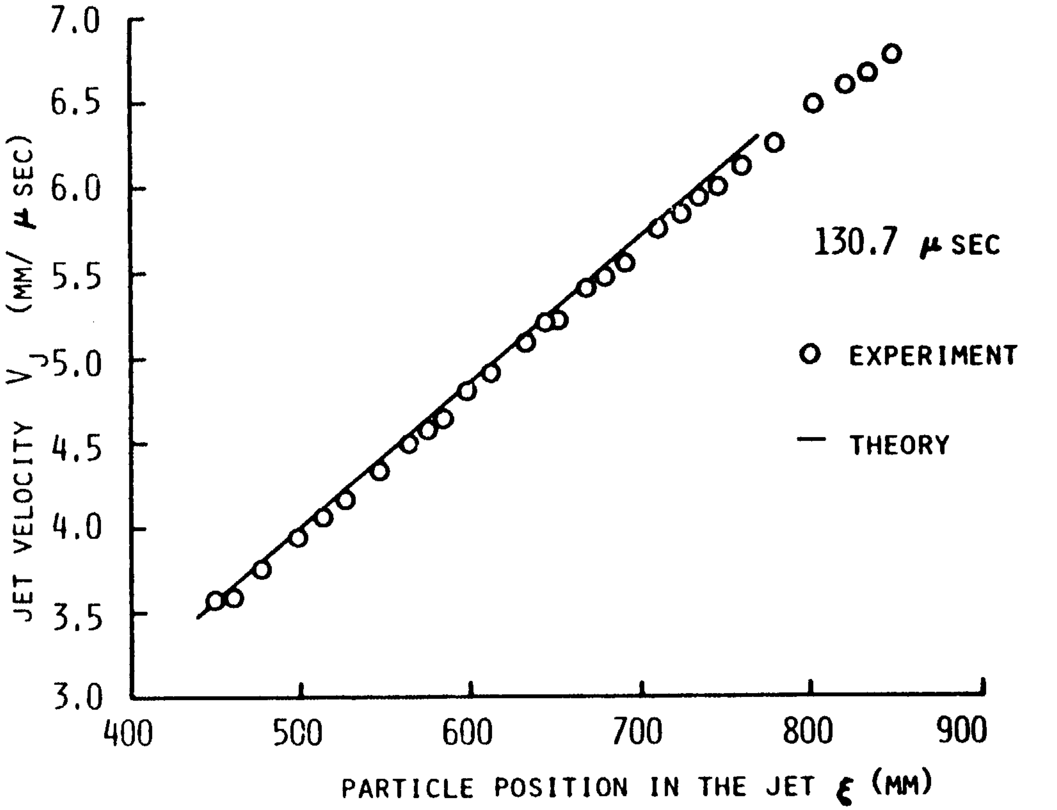

FIGURE B5. Theoretical and experimental jet velocity vs. jet particle position for the 50.8mm, 42°, 2.54mm wall, copper lined charge at 130.7 μsec after detonation wave arrival at cone apex. (charge No. 7)

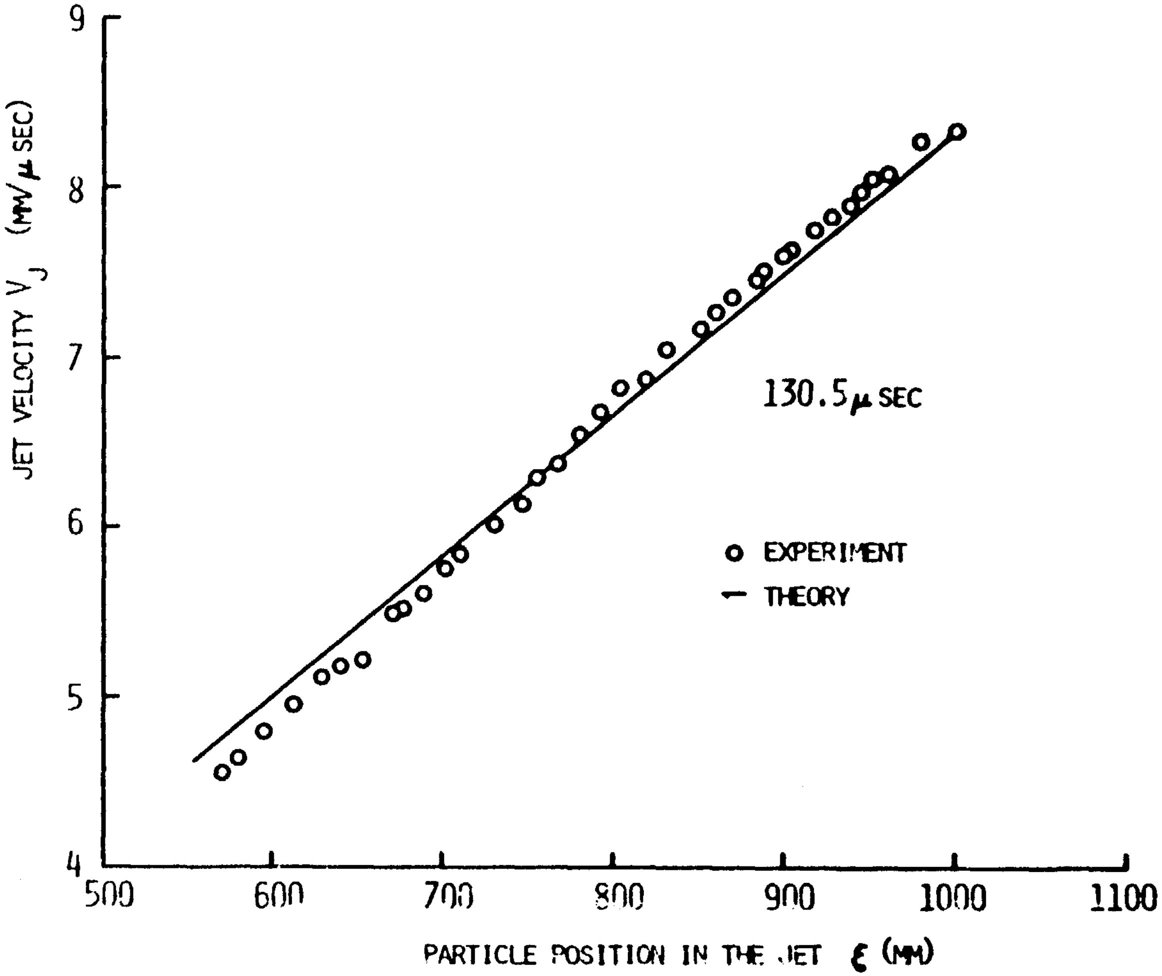

FIGURE B6. Theoretical and experimental jet velocity vs. jet particle position for the 81.3mm, 42°, tapered wall, Copper lined charge at 130.5 usec after detonation wave arrival at cone apex. (charge No. 8)

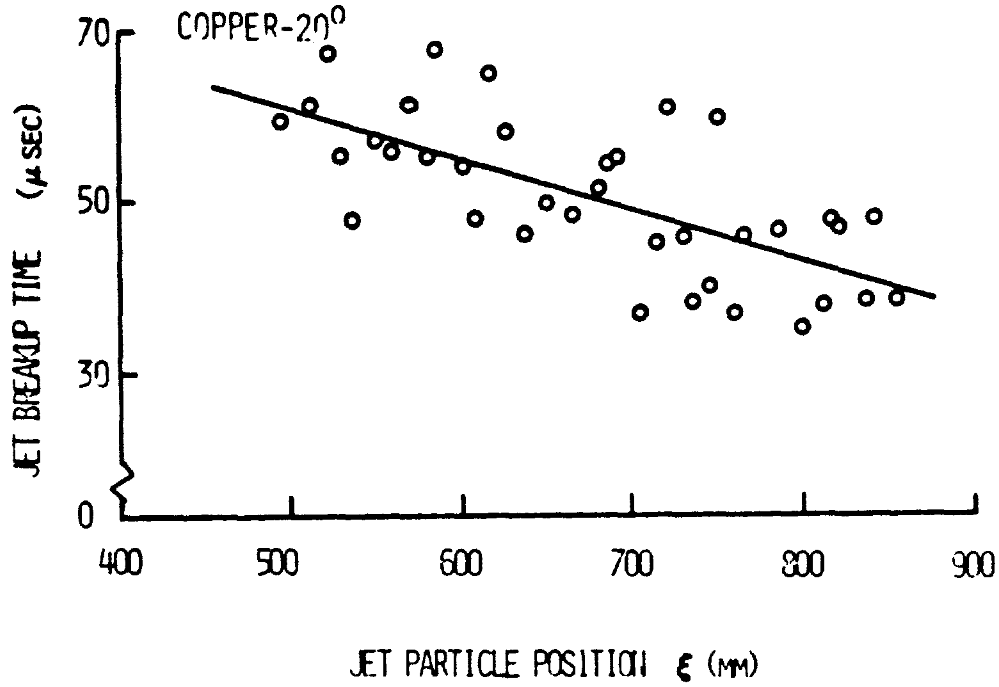

FIGURE B7. Jet breakup time vs. jet particle position at t=107.7 μsec for the 38.1 mm, 20°, 1.168 mm wall, copper lined charge (charge no. 1).

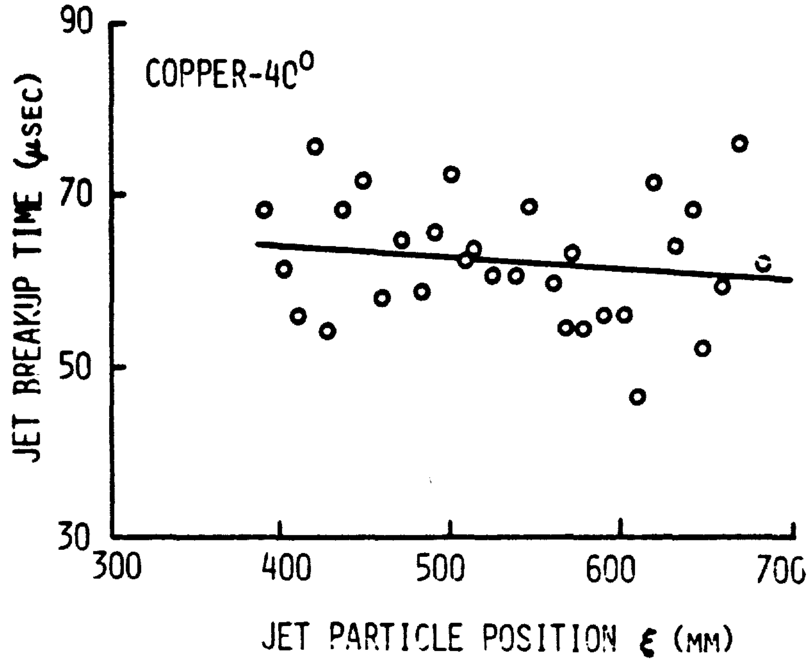

FIGURE B8. Jet breakup time vs. jet particle position at t=93.4 μsec for the 38.1mm, 40°, 1.168 mm wall copper lined charge. (Charge No.2)

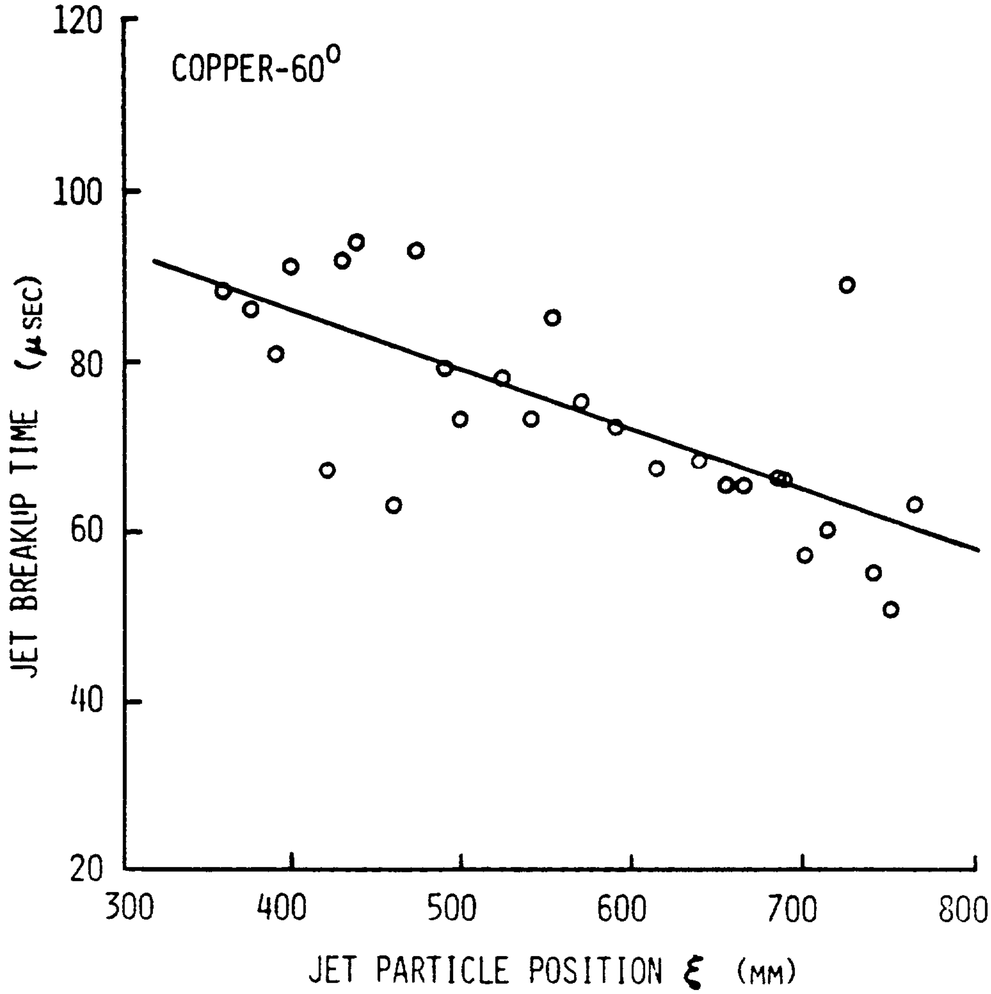

FIGURE B9. Jet breakup time vs. jet particle position at t=122.7 μsec for the 38.1mm, 60°, 1.168 mm wall Copper lined charge. (Charge No. 3)

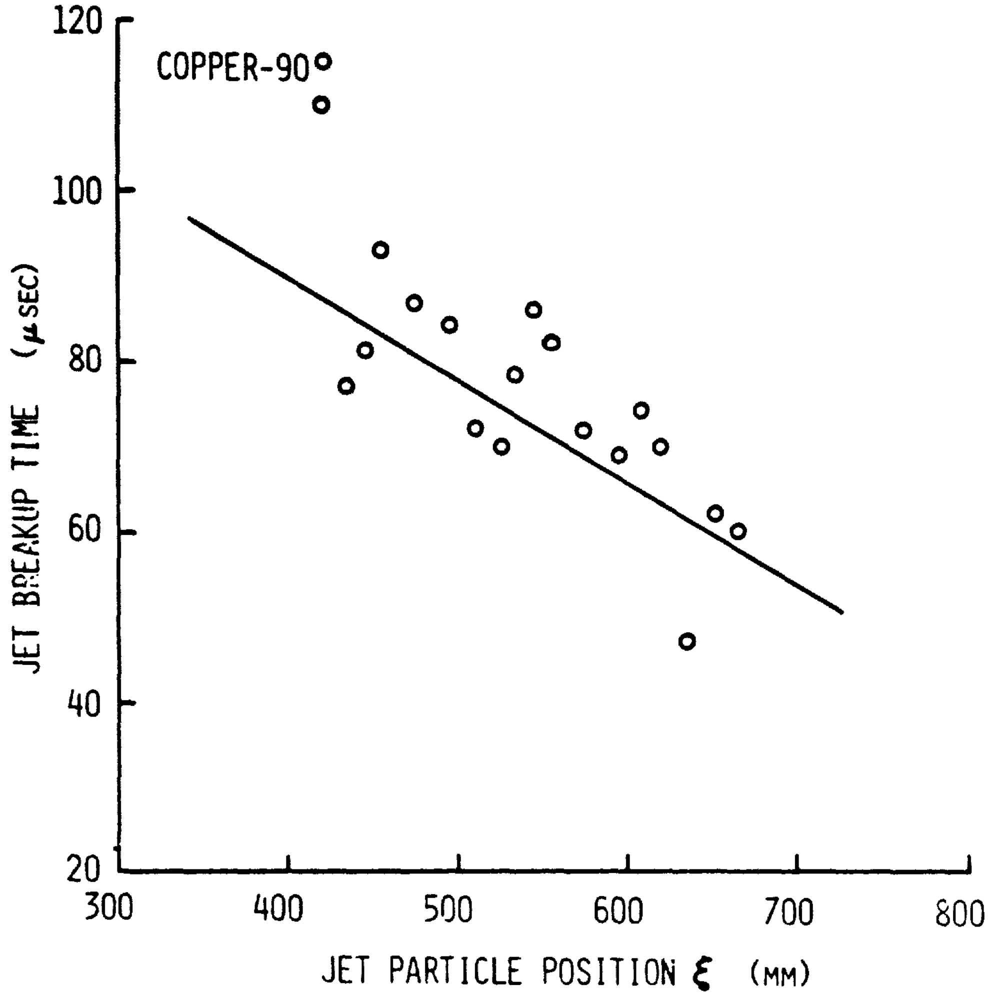

FIGURE B10. Jet breakup time vs. jet particle position at t=133.3 μsec for the 38.1mm, 90°, 1.168 mm wall copper lined charge. (Charge No. 4)

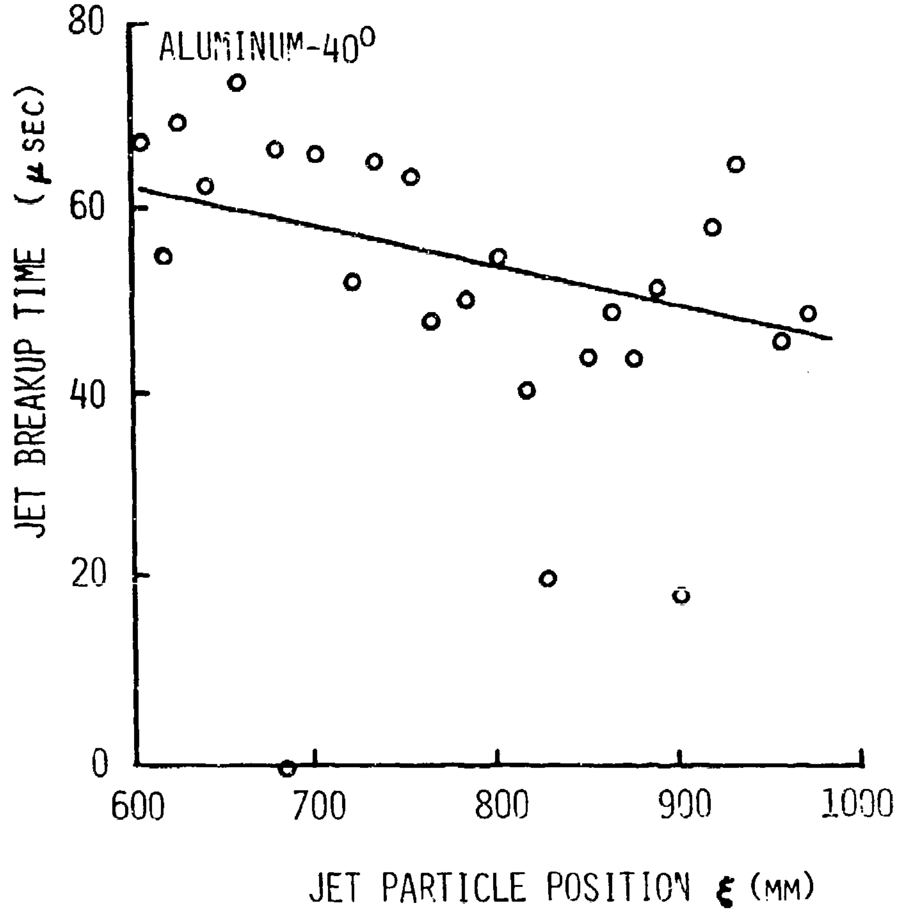

FIGURE B11. Jet breakup time vs. jet particle position at t=113.1 μsec for the 38.1mm, 40°, 1.626mm wall aluminum lined charge. (Charge No.9)

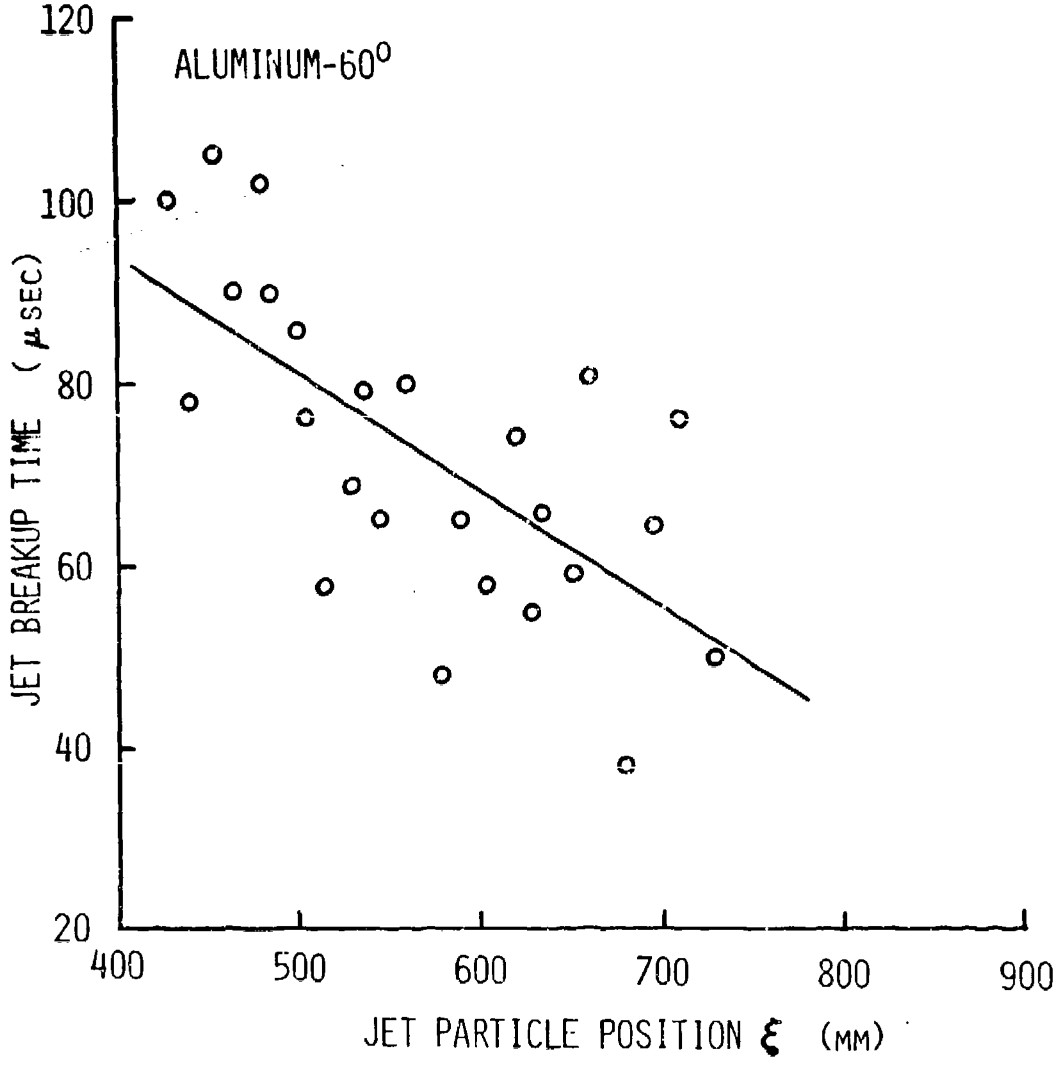

FIGURE B12. Jet breakup time vs. jet particle position at t=97.7 μsec for the 38.1mm, 60°, 1.626 mm wall aluminum lined charge. (Charge No. 10)

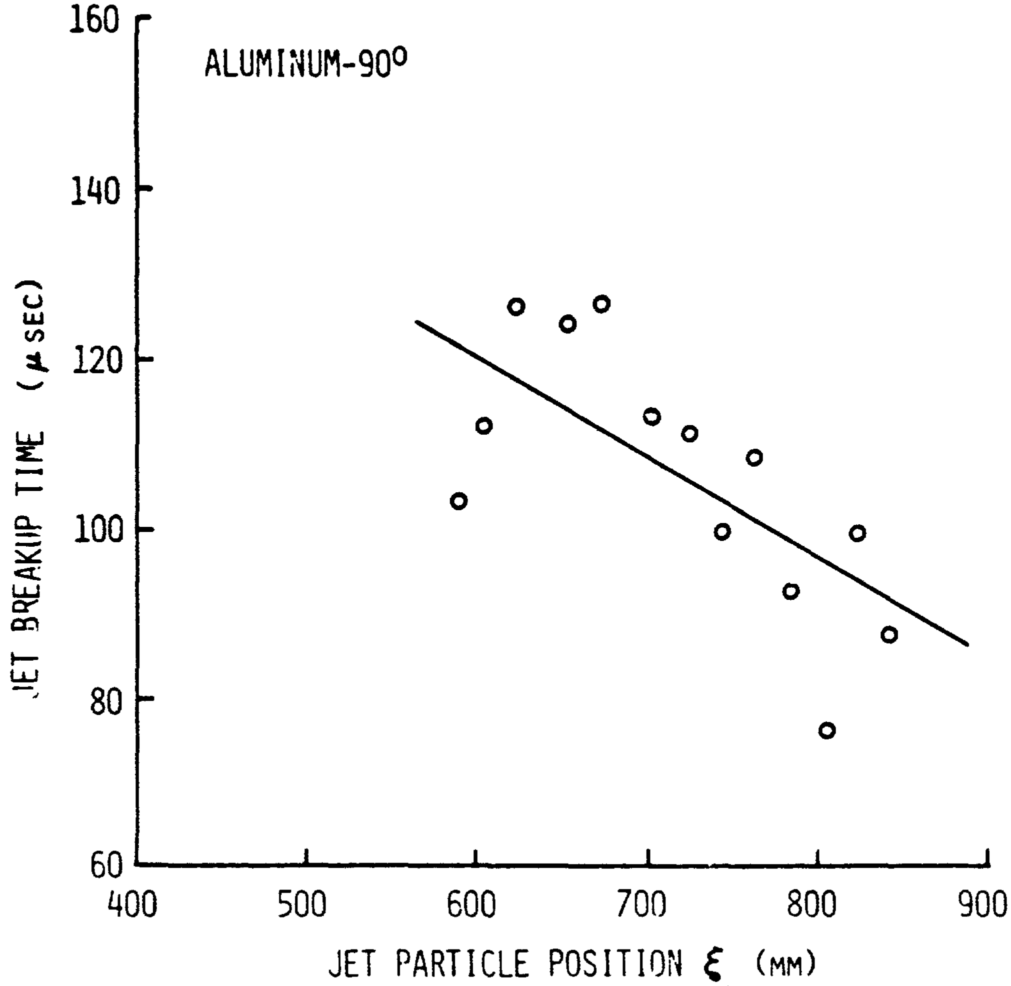

FIGURE B13. Jet breakup time vs. jet particle position at t=132.8 μsec for the 38.1mm, 90°, 1.626 mm wall aluminum lined charge. (charge No. 11)

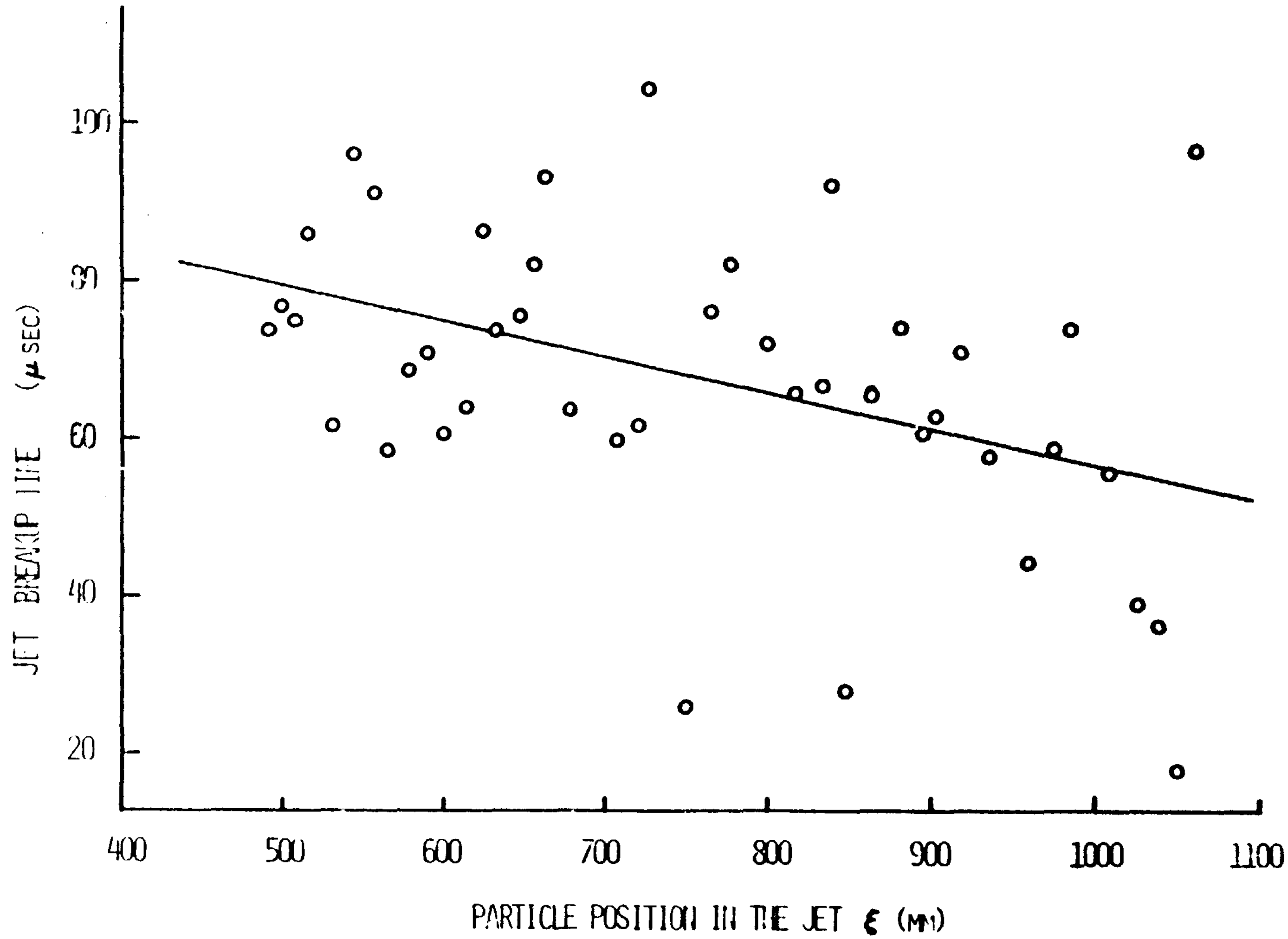

FIGURE B14. Jet breakup time vs. jet particle position at t=130.6 μsec for the 50.8 mm, 42°, 0.762 mm wall, copper lined charge (charge no. 5).

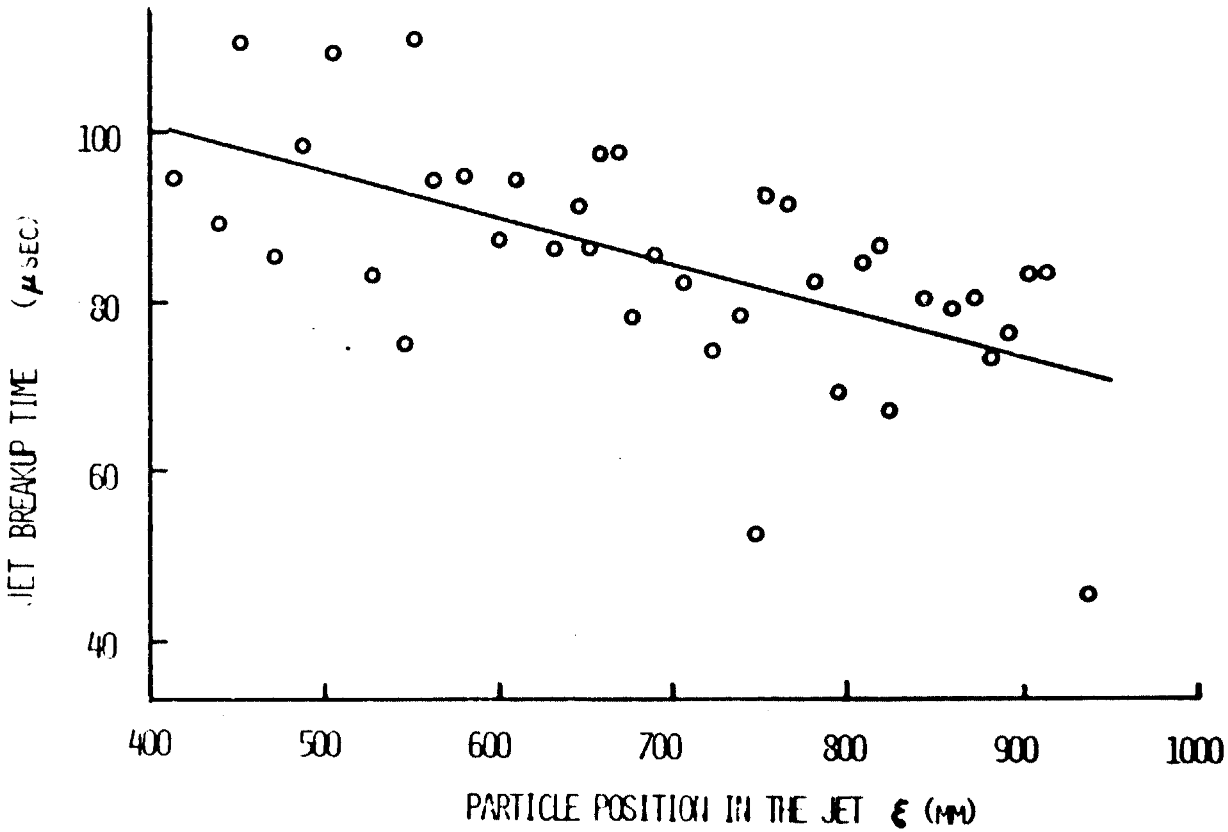

FIGURE B15. Jet breakup time vs. jet position at t=130.5 μsec for the 50.8 mm, 42°, 1.524 mm wall, copper lined charge (charge no. 6).

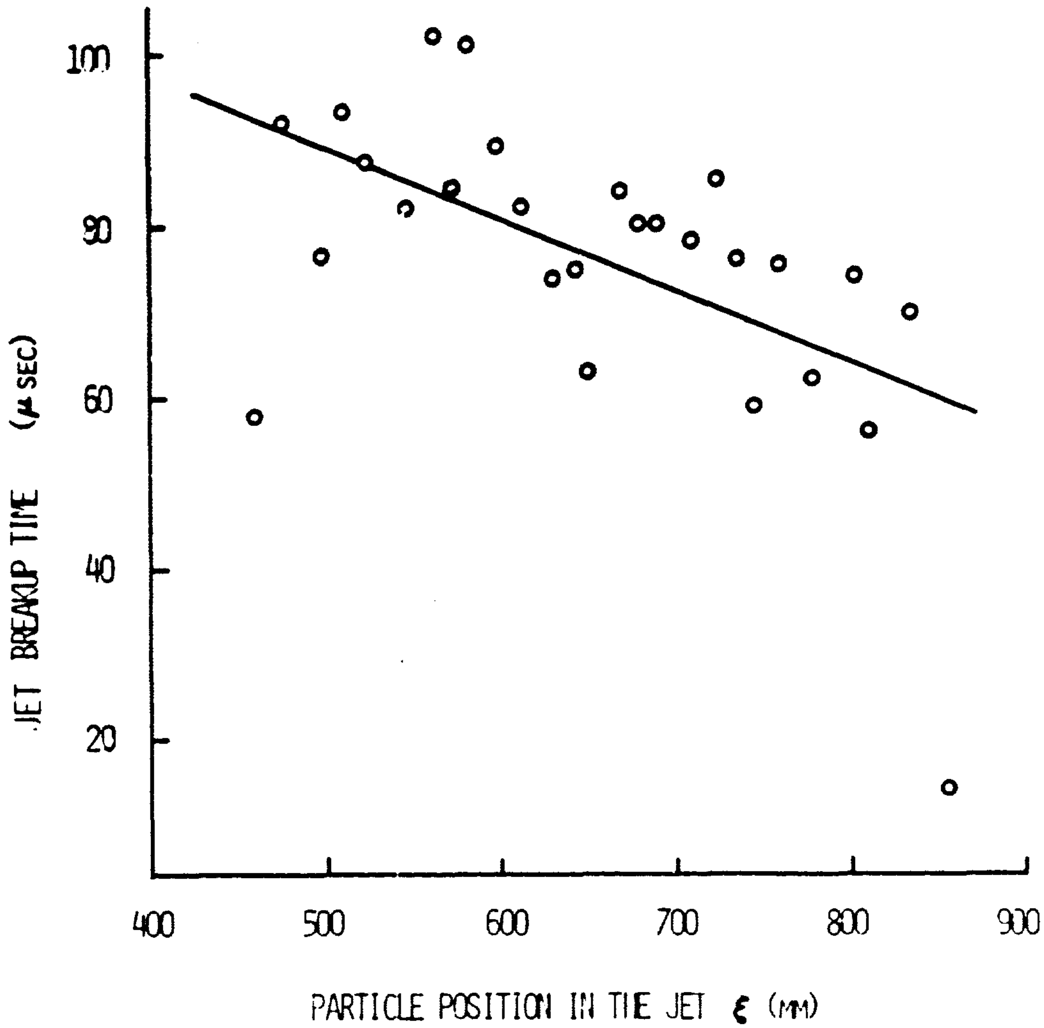

FIGURE B16. Jet breakup time vs. jet position at t=130.7 μsec for the 50.8 mm, 42°, 2.54 mm wall, copper lined charge (charge no. 7).

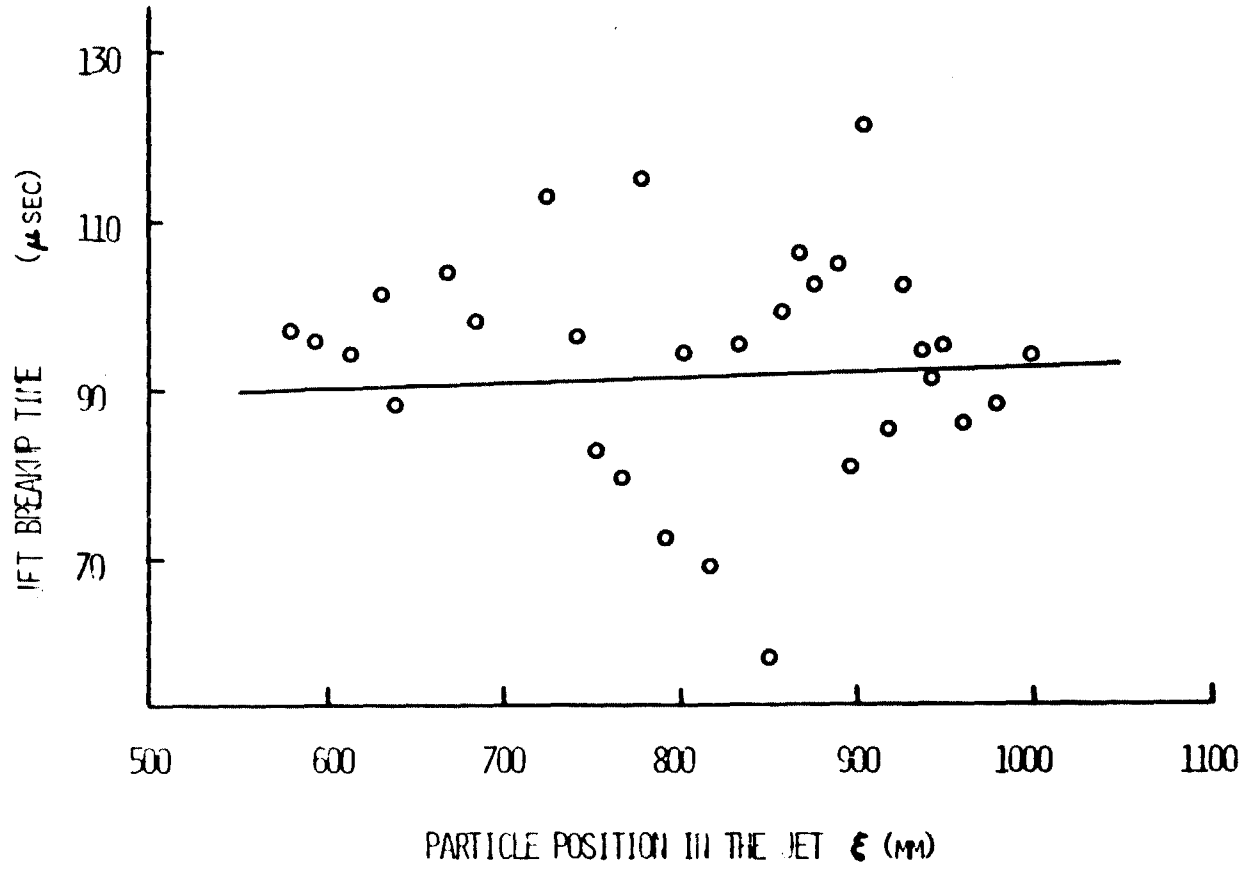

FIGURE B17. Jet breakup time vs. jet particle position at t=130.5 μsec for the 81.3 mm, 42°, tapered wall, copper lined charge (charge no. 5).

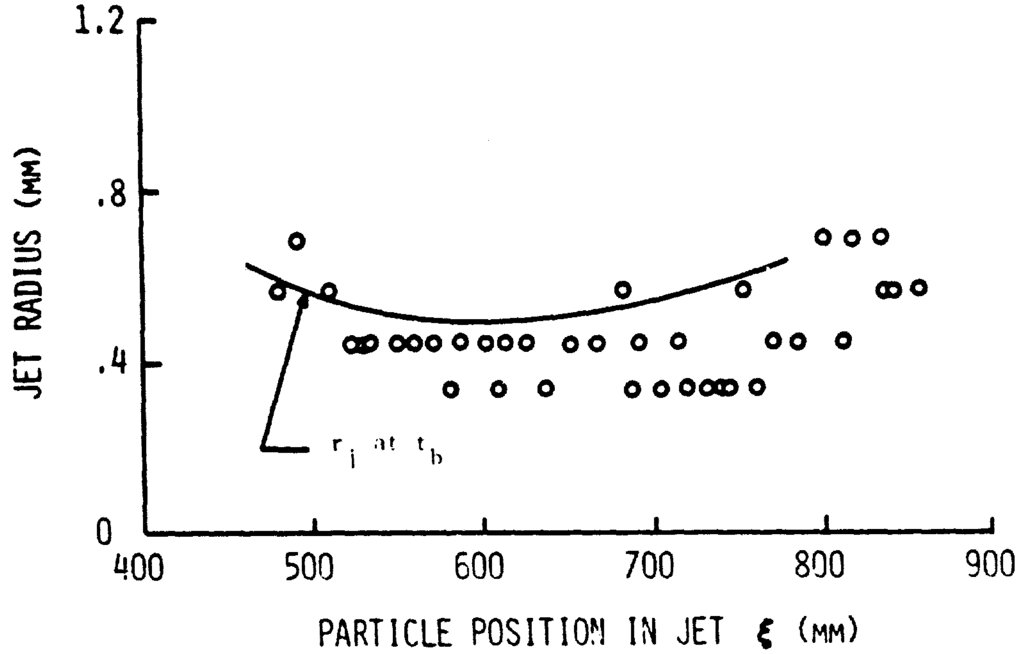

FIGURE B18. Theoretical and experimental jet radius vs. jet particle position at t=107.7 μsec for the 38.1 mm, 20°, 1.168 mm wall, copper lined charge (charge no. 1).

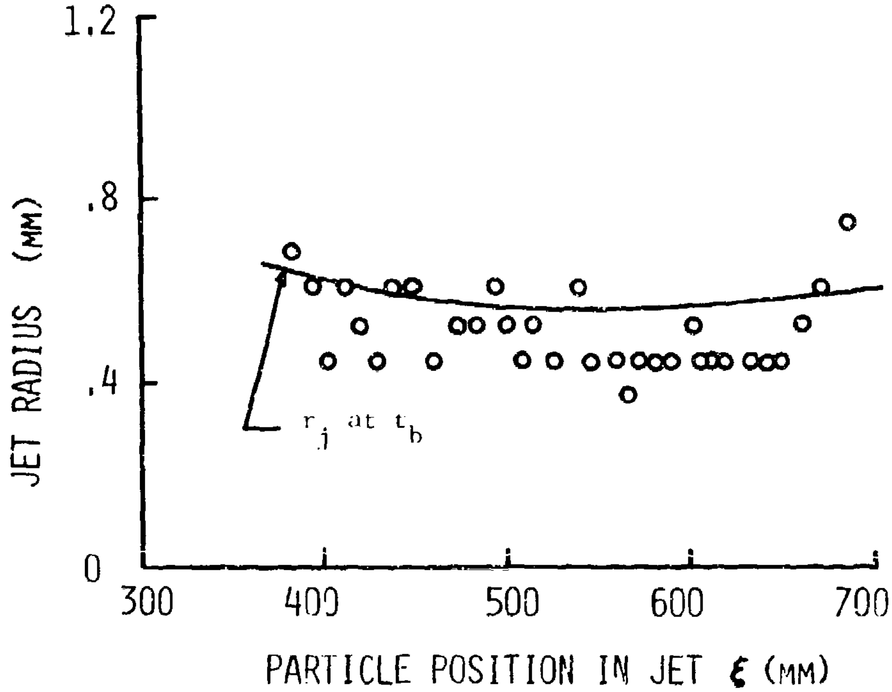

FIGURE B19. Theoretical and experimental jet radius vs. jet particle position at t=93.4 μsec for the 38.1 mm, 40°, 1.168 mm wall, copper lined charge (charge no. 2).

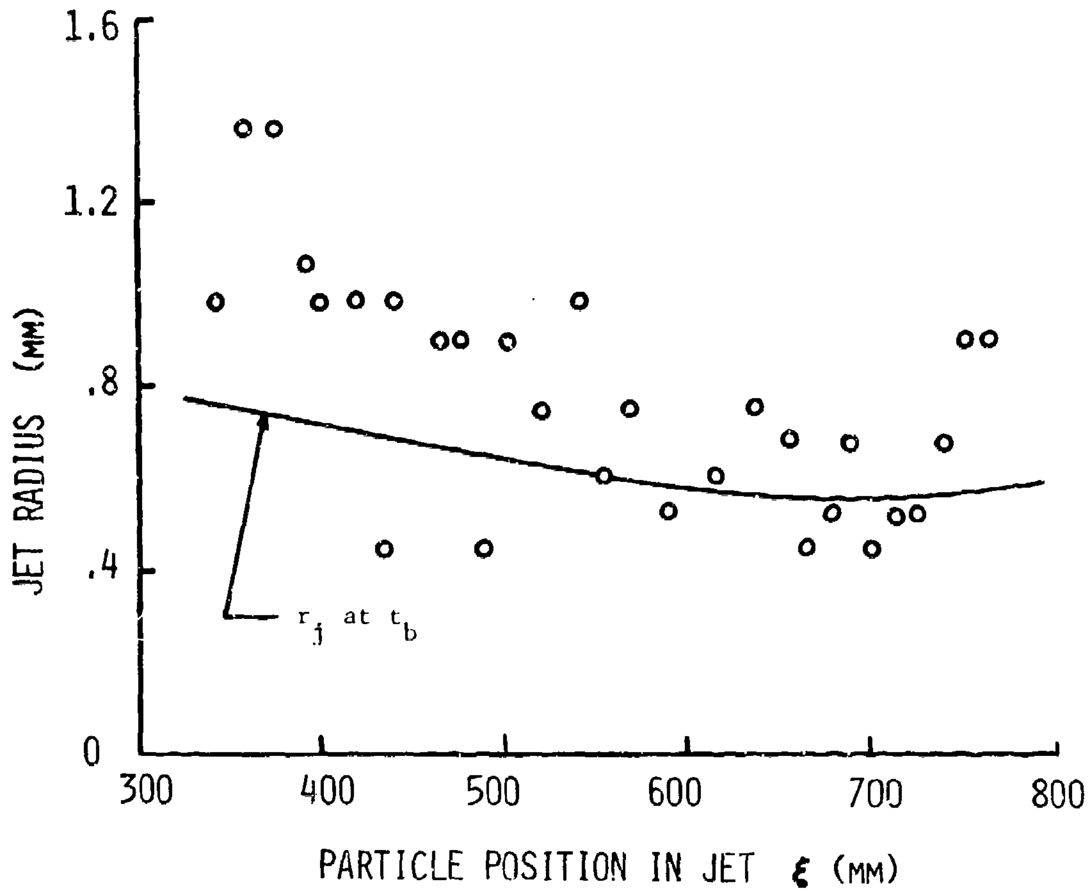

FIGURE B20. Theoretical and experimental jet radius vs. jet particle position at t=122.7 μsec for the 38.1 mm, 60°, 1.168 mm wall copper lined charge (charge no. 3).

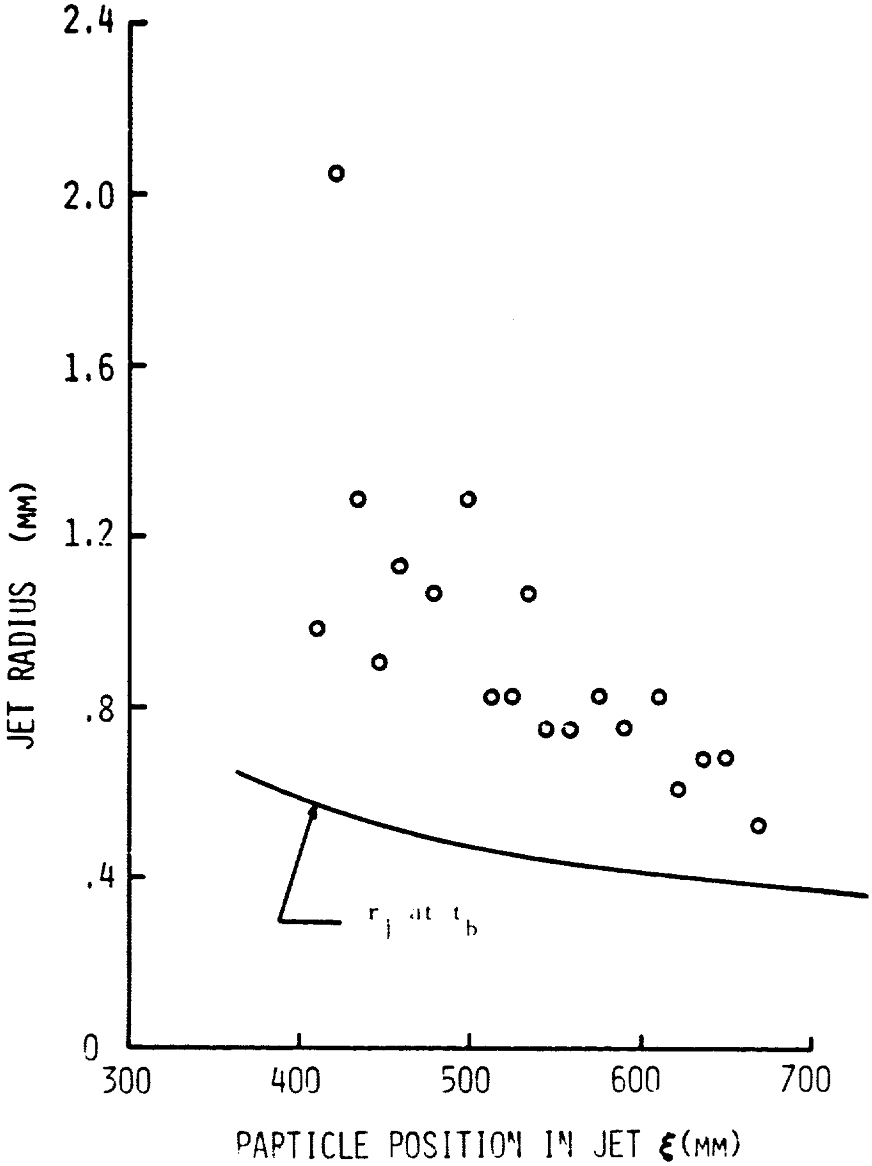

FIGURE B21. Theoretical and experimental jet radius vs. jet particle position at t=133.3 μsec for the 38.1 mm, 90°, 1.168 mm wall copper lined charge (charge no. 4).

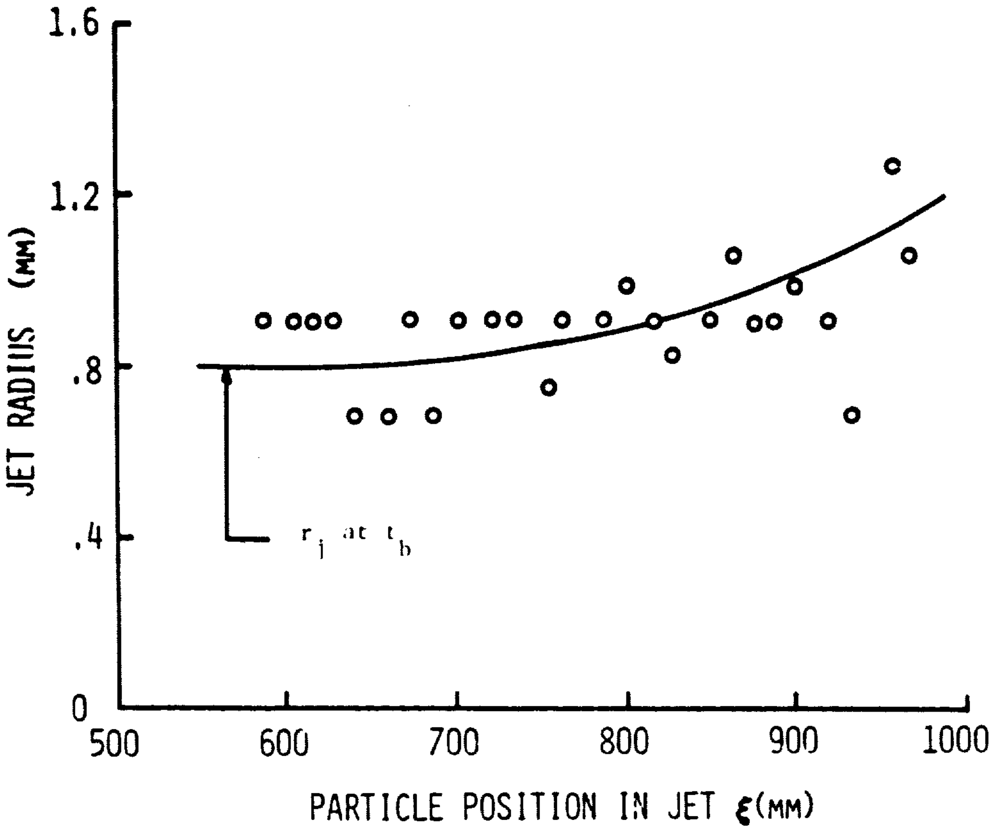

FIGURE B22. Theoretical and experimental jet radius vs. jet particle position at t=113.1 μsec for the 38.1 mm, 40°, 1.626 mm wall aluminum lined charge (charge no. 9).

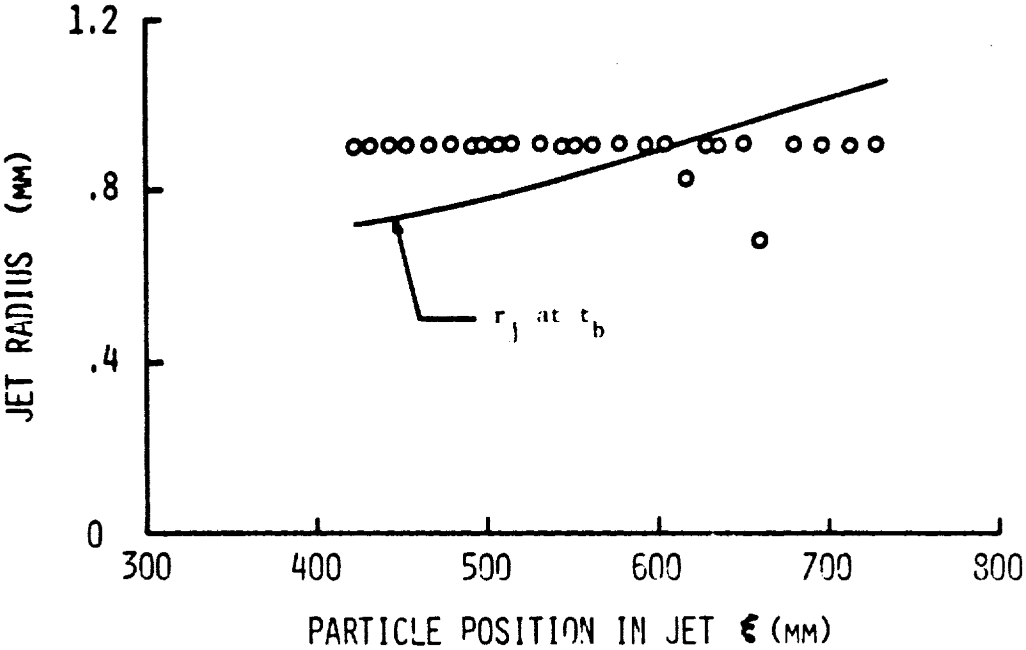

FIGURE B23. Theoretical and experimental jet radius vs. jet particle position at t=97.7 μsec for the 38.1 mm, 60°, 1.626 mm wall aluminum lined charge (charge no. 10).

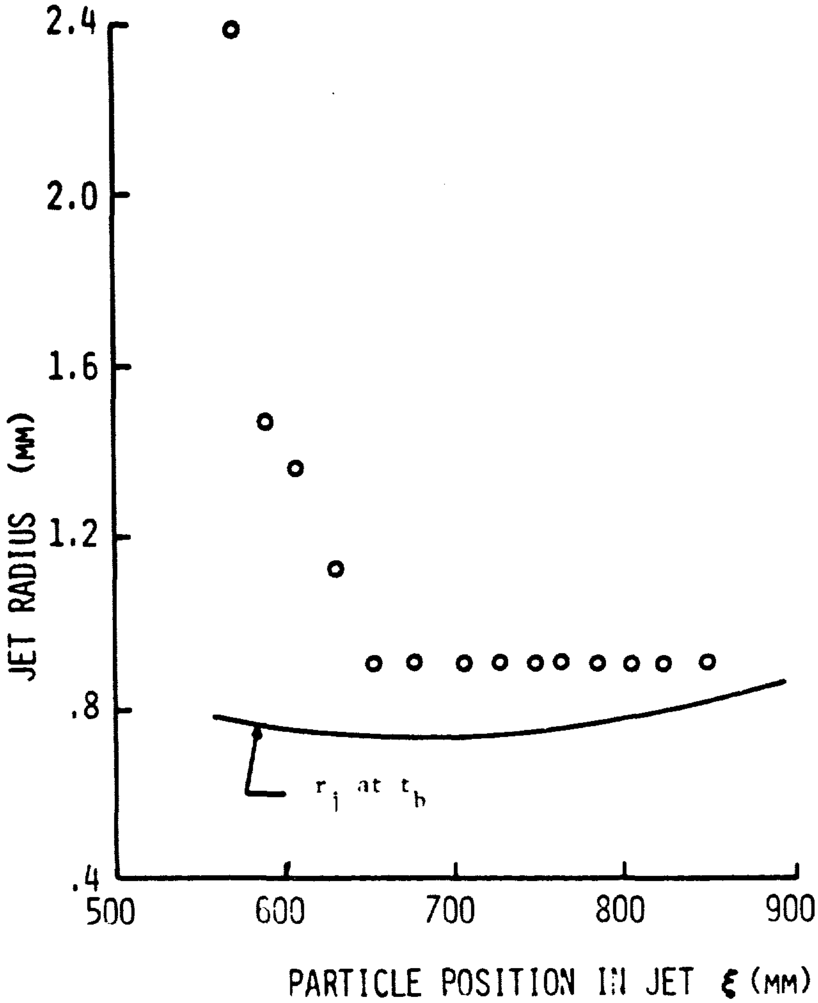

FIGURE B24. Theoretical and experimental jet radius vs. jet particle position at t=132.8 μsec for the 38.1 mm, 90°, 1.626 mm wall aluminum lined charge (charge no. 11).

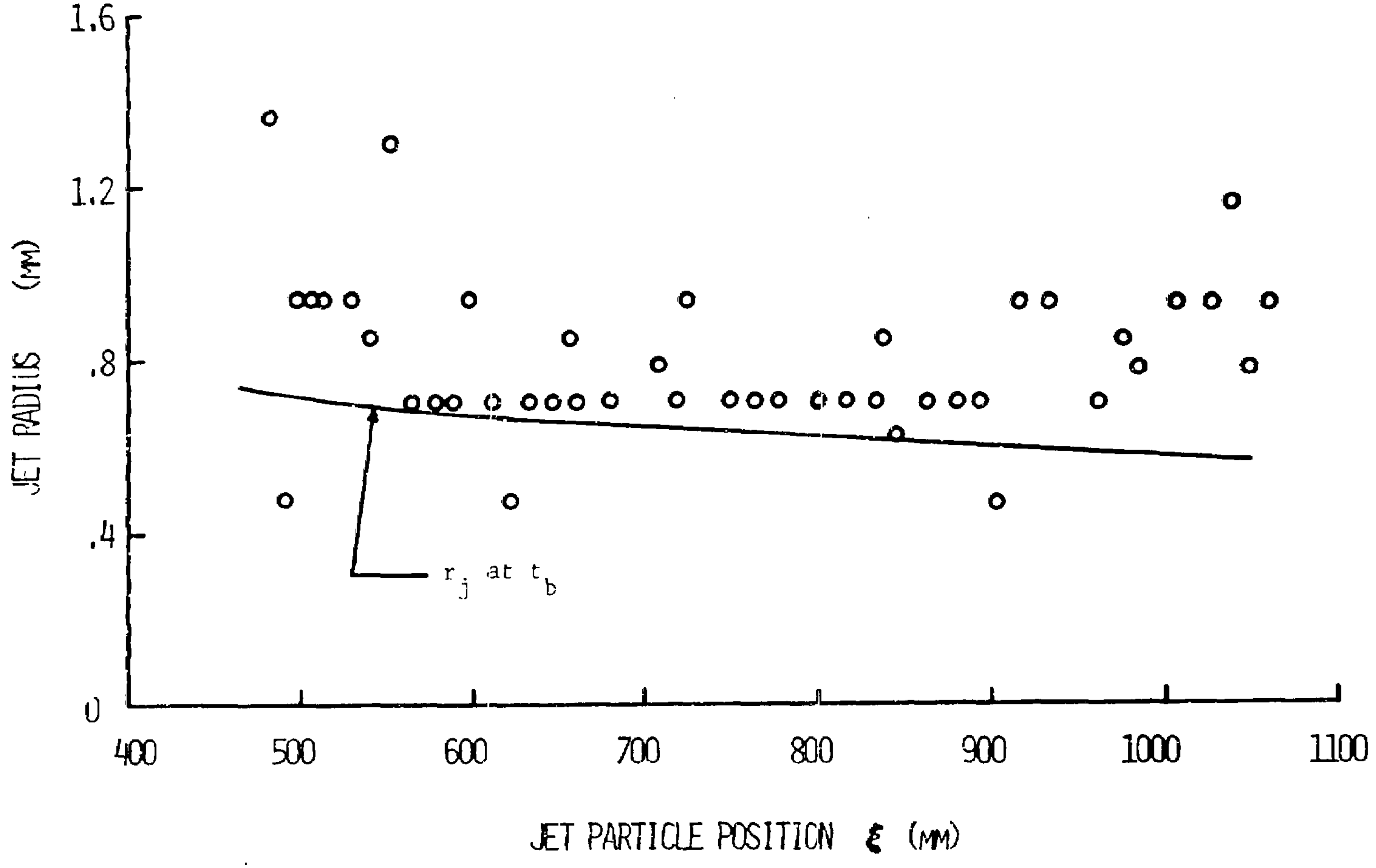

FIGURE B25. Theoretical and experimental jet radius vs. jet particle position at t=130.6 μsec for the 50.8 mm, 42°, 0.762 mm wall copper lined charge (charge no. 5).

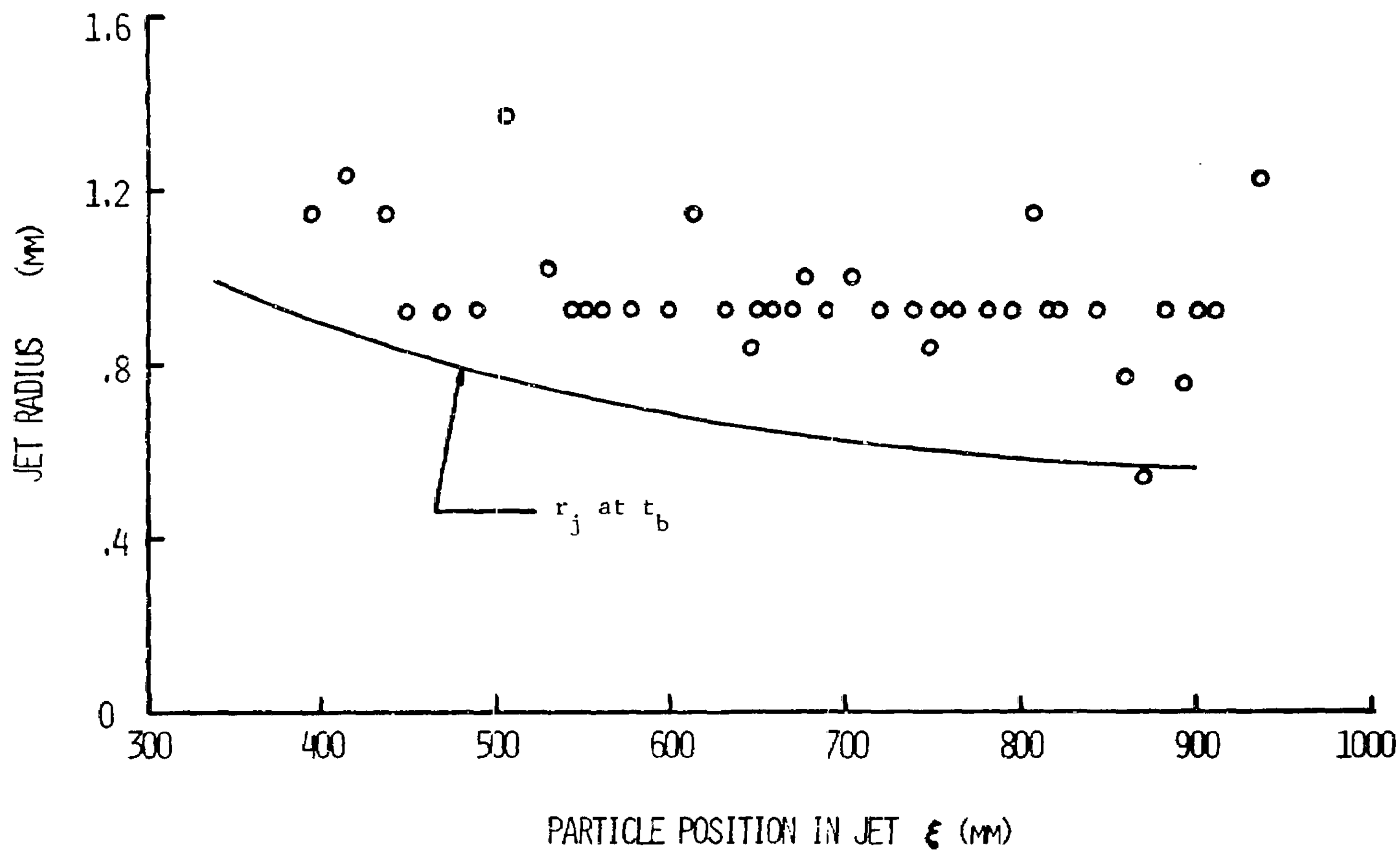

FIGURE B26. Theoretical and experimental jet radius vs. jet particle position at t=130.5 μsec for the 50.8 mm, 42°, 1.524 mm wall copper lined charge (charge no. 6).

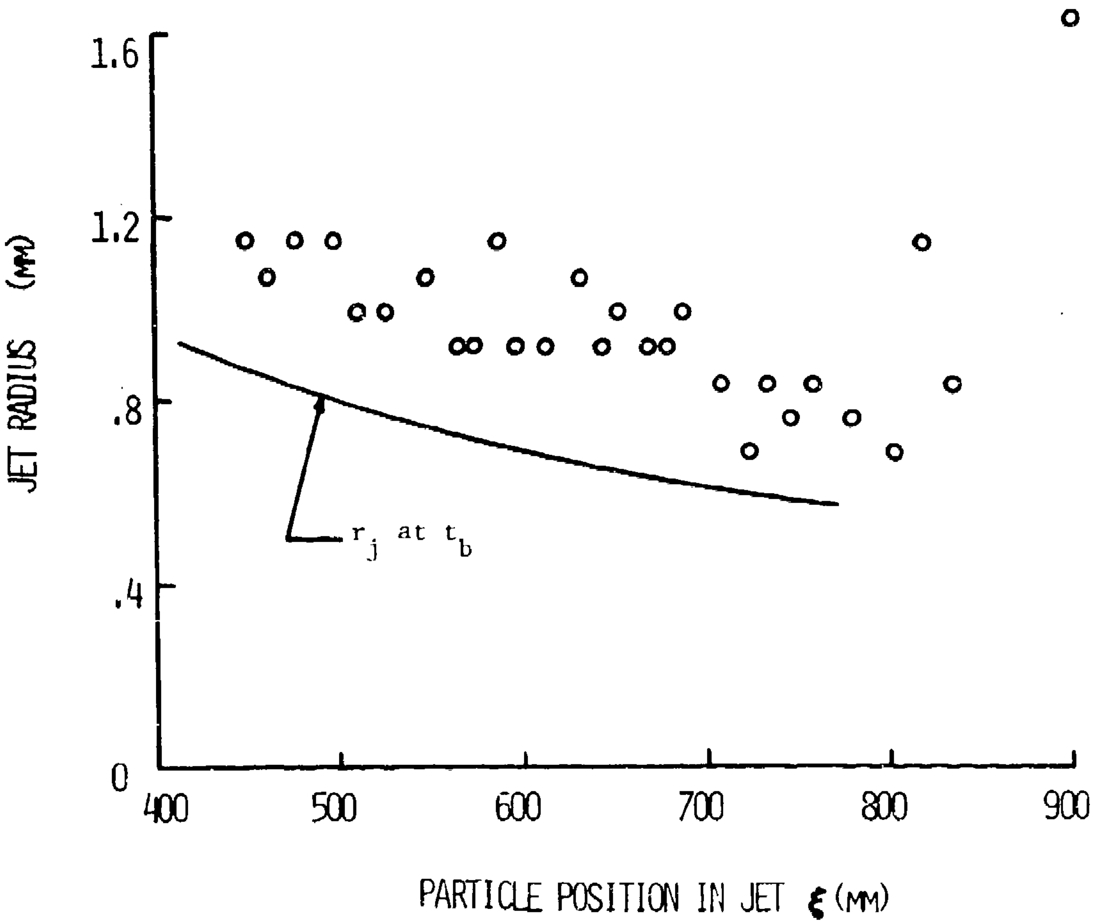

FIGURE B27. Theoretical and experimental jet radius vs. jet particle position at t=130.7 μsec for the 50.8 mm, 42°, 2.54 mm wall copper lined charge (charge no. 7).

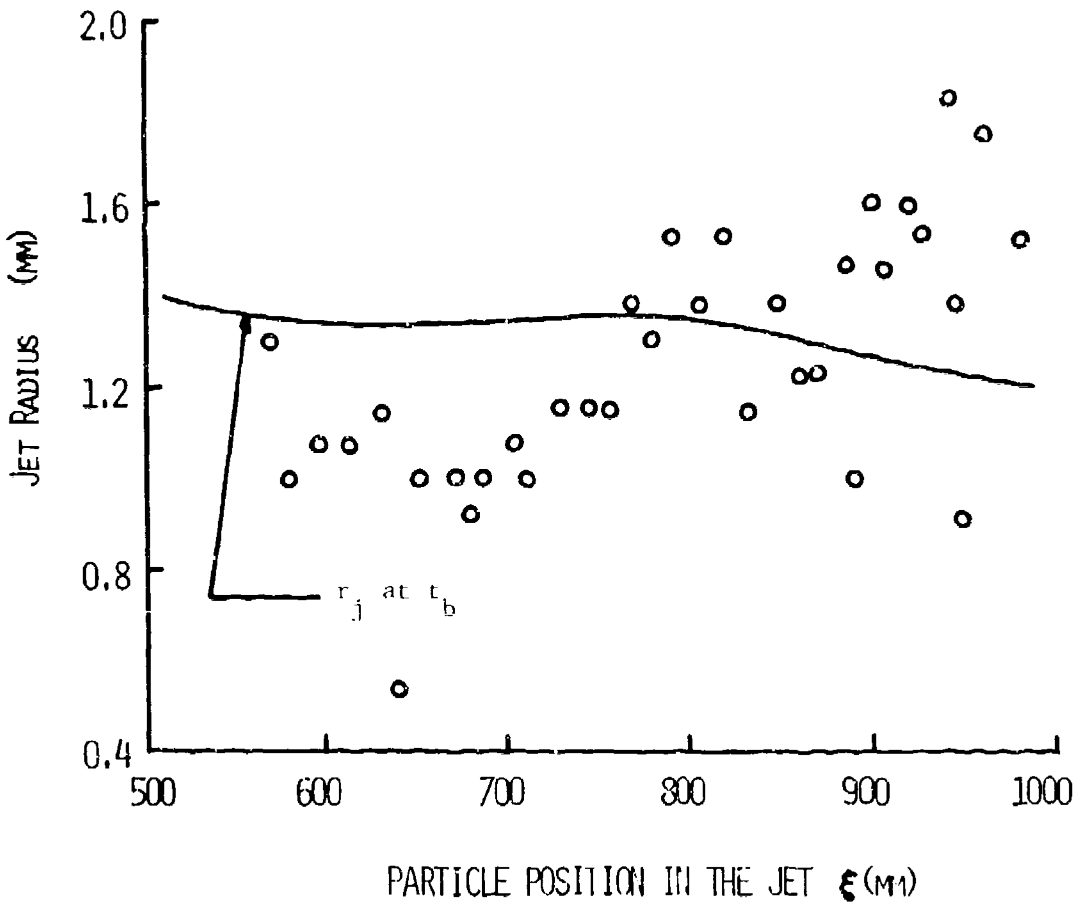

FIGURE B28. Theoretical and experimental jet radius vs. jet particle position at t=130.5 μsec for the 81.3 mm 42°, tapered wall copper lined charge (charge no. 8). (Note: The lead particle at 1003 mm in the jet has a radius of 4.6 mm and is not plotted here for convenience.)

Appendix C

This appendix contains tabulated data for the jet velocity, breakup time, length, diameter, radius, aspect ratio and ΔV_j of the jet segments as computed from radiograph measurements for the eleven charges studied in this report.

The breakup times in these tables are referred to t=0 when the charge is first initiated. Throughout the rest of the report, including the plots of appendix B, all times are referred to t=0 when the detonation wave first reaches the apex of the liner cone. The time it takes for the wave to travel from the point of initiation to the apex of the cone for charges 5,6 and 7 is 6.4μsec; for all other charges this time is 7.0μsec.

CHARGE NO. 1. 30.1 MM. 20 DEGREE. 1.168 MM WALL. COPPER LINER

ALL VALUES ARE THE AVERAGE FROM THREE RADIOGRAPHS

NO.	VELOCITY MM/MICROSEC	BU TIME MICROSEC.	LENGTH MM.	DIAMETER MM.	RADIUS MM.	L/D RATIO	VEL CHANGE
1	8.37018E 00	4.52740E 01	4.55000E 00	1.13750E 00	5.68750E-01	4.16667E 00	1.42544E-01
2	8.22763E 00	5.48500E 01	2.95750E 00	1.13750E 00	5.68750E-01	2.66667E 00	3.99123E-02
3	8.10772E 00	4.48750E 01	2.27500E 00	1.13750E 00	5.68750E-01	2.16667E 00	2.28070E-02
4	8.10491E 00	5.33722E 01	1.82000E 00	1.36500E 00	6.82500E-01	1.50000E 00	1.53947E-01
5	8.01098E 00	5.48500E 01	5.68750E 00	1.36500E 00	6.82500E-01	4.16667E 00	5.13155E-02
6	7.95965E 00	4.48750E 01	2.73000E 00	9.10000E-01	4.55000E-01	3.00000E 00	9.12281E-02
7	7.86042E 00	4.20820E 01	4.09500E 00	1.36500E 00	6.82500E-01	3.00000E 00	1.42544E-01
8	7.72588E 00	5.38250E 01	5.68750E 00	9.10000E-01	4.55000E-01	6.25000E 00	1.39649E-01
9	7.56623E 00	5.23024E 01	5.21250E 00	9.10000E-01	4.55000E-01	5.75000E 00	9.69298E-02
10	7.46930E 00	4.34500E 01	1.36500E 00	6.82500E-01	3.41250E-01	2.00000E 00	7.98246E-02
11	7.35947E 00	6.60700E 01	4.55000E 00	1.13750E 00	5.68750E-01	4.16667E 00	1.14035E-01
12	7.27544E 00	4.63750E 01	2.73000E 00	6.82500E-01	3.41250E-01	4.50000E 00	5.70175E-02
13	7.21342E 00	4.48750E 01	4.36500E 00	6.82500E-01	3.41250E-01	7.00000E 00	4.36140E-02
14	7.17251E 00	5.27500E 01	5.00500E 00	6.82500E-01	3.41250E-01	8.00000E 00	1.00311E-01
15	7.10447E 00	5.91500E 01	2.50250E 00	6.82500E-01	3.41250E-01	4.00000E 00	1.02612E-01
16	6.96194E 00	5.72000E 01	2.04750E 00	9.10000E-01	4.55000E-01	2.25000E 00	7.98246E-02
17	6.86222E 00	4.37067E 01	6.59750E 00	6.82500E-01	3.41250E-01	1.10000E 01	1.02612E-01
18	6.77734E 00	6.21345E 01	2.04750E 00	9.10000E-01	4.55000E-01	2.25000E 00	6.27193E-02
19	6.71567E 00	5.15000E 01	1.92000E 00	6.82500E-01	3.41250E-01	3.00000E 00	6.04211E-02
20	6.64325E 00	5.98400E 01	3.18500E 00	1.13750E 00	5.68750E-01	2.91667E 00	1.71053E-01
21	6.47719E 00	5.53845E 01	7.28000E 00	9.10000E-01	4.55000E-01	8.00000E 00	1.48246E-01
22	6.32095E 00	5.65125E 01	4.55000E 00	9.10000E-01	4.55000E-01	5.00000E 00	1.30842E-01
23	6.19211E 00	5.29500E 01	6.82500E 00	6.82500E-01	3.41250E-01	1.15000E 01	1.19737E-01
24	6.07237E 00	5.52597E 01	3.41250E 00	9.10000E-01	4.55000E-01	3.75000E 00	1.31140E-01
25	5.94123E 00	7.19500E 01	5.00500E 00	9.10000E-01	4.55000E-01	5.50000E 00	7.98246E-02
26	5.88140E 00	5.40500E 01	9.10000E-01	6.82500E-01	3.41250E-01	1.50000E 00	4.56140E-02
27	5.81579E 00	5.09455E 01	6.37000E 00	9.10000E-01	4.55000E-01	7.00000E 00	1.00155E-01
28	5.62753E 00	7.48000E 01	3.41250E 00	9.10000E-01	4.55000E-01	3.75000E 00	4.56140E-02
29	5.50202E 00	6.23333E 01	4.32250E 00	6.82500E-01	3.41250E-01	7.00000E 00	9.12281E-02
30	5.44979E 00	5.91500E 01	4.77750E 00	9.10000E-01	4.55000E-01	5.25000E 00	1.71053E-01
31	5.31974E 00	6.27333E 01	4.32250E 00	9.10000E-01	4.55000E-01	4.75000E 00	5.70175E-02
32	5.20272E 00	5.62192E 01	7.05250E 00	9.10000E-01	4.55000E-01	7.75000E 00	1.93860E-01
33	5.06866E 00	5.48500E 01	4.32250E 00	9.10000E-01	4.55000E-01	4.75000E 00	1.71053E-02
34	5.05175E 00	5.23333E 01	2.27500E 00	9.10000E-01	4.55000E-01	2.50000E 00	9.12281E-02
35	4.98053E 00	7.40011E 01	5.46000E 00	9.10000E-01	4.55000E-01	6.00000E 00	1.53947E-01
36	4.80650E 00	6.81500E 01	7.96250E 00	1.13750E 00	5.68750E-01	7.33333E 00	1.08158E-01
37	4.81942E 00	6.62500E 01	5.91500E 00	1.36500E 00	6.82500E-01	4.33333E 00	1.59649E-01
38	4.45077E 00	XXXXXXXXXXXX	4.09500E 00	1.13750E 00	5.68750E-01	3.66667E 00	XXXXXXXXXXXX
		************	************	************	************	************	************
AVERAGE =		5.74081E 01	4.11895E 00	9.39934E-01	4.69967E-01	4.68848E 00	1.05714E-01
					STANDARD DEVIATION	2.43538E 00	5.00975E-02
					COEFF. OF VARIATION	5.19670E-01	4.73899E-01

Preceding Page Blank

CHARGE NO. 2. 38.1 MM, 40 DEGREE, 1.168 MM WALL, COPPER LINER

ALL VALUES ARE THE AVERAGE FROM THREE RADIOGRAPHS

NO.	VELOCITY MM/MICROSEC	80 TIME MICROSEC.	LENGTH MM.	DIAMETER MM.	RADIUS MM.	L/D RATIO	VEL CHANGE
1	8.01237E 00	6.86936E 01	1.00167E 01	1.51667E 00	7.58333E-01	7.58333E 00	1.51496E-01
2	7.86087E 00	8.29701E 01	1.13750E 01	1.21333E 00	6.06667E-01	9.55556E 00	7.76299E-02
3	7.78324E 00	6.63635E 01	5.40000E 00	1.06167E 00	5.30833E-01	5.22222E 00	1.55260E-01
4	7.62798E 00	5.89881E 01	4.85333E 00	9.10000E-01	4.55000E-01	5.33333E 00	2.83950E-02
5	7.59959E 00	7.51071E 01	5.91500E 00	9.10000E-01	4.55000E-01	6.50000E 00	1.34448E-01
6	7.40514E 00	7.10273E 01	7.43167E 00	9.10000E-01	4.55000E-01	8.16667E 00	1.35375E-01
7	7.32976E 00	7.42636E 01	1.00100E 01	9.10000E-01	4.55000E-01	1.10000E 01	1.44840E-01
8	7.18492E 00	5.36885E 01	1.66833E 00	9.10000E-01	4.55000E-01	1.83333E 00	4.35616E-02
9	7.14136E 00	4.68166E 01	2.57833E 00	9.10000E-01	4.55000E-01	2.83333E 00	3.31416E-02
10	7.10822E 00	6.34329E 01	3.94333E 00	1.06167E 00	5.30833E-01	3.88889E 00	1.55260E-01
11	6.95296E 00	6.31281E 01	7.73500E 00	9.10000E-01	4.55000E-01	8.50000E 00	1.20236E-01
12	6.83273E 00	6.15591E 01	4.24667E 00	9.10000E-01	4.55000E-01	4.66667E 00	6.72099E-02
13	6.76552E 00	7.30251E 01	3.18500E 00	9.10000E-01	4.55000E-01	3.50000E 00	9.27966E-02
14	6.67272E 00	6.15144E 01	1.38500E 00	7.58333E-01	3.79167E-01	1.83333E 00	4.82799E-02
15	6.62444E 00	6.65535E 01	9.40333E 00	9.10000E-01	4.55000E-01	1.03333E 01	1.04725E-01
16	6.45971E 00	7.55164E 01	5.30833E 00	9.10000E-01	4.55000E-01	5.83333E 00	1.14563E-01
17	6.34515E 00	6.77465E 01	6.82500E 00	1.21333E 00	6.06667E-01	5.83333E 00	1.56215E-01
18	6.18894E 00	6.76602E 01	9.40333E 00	9.10000E-01	4.55000E-01	1.03333E 01	1.35375E-01
19	6.05356E 00	7.07308E 01	4.39833E 00	1.06167E 00	5.30833E-01	4.22222E 00	5.77449E-02
20	5.99582E 00	5.96791E 01	2.57833E 00	9.10000E-01	4.55000E-01	2.83333E 00	1.08861E-01
21	5.88695E 00	7.92378E 01	7.43167E 00	1.06167E 00	5.30833E-01	7.22222E 00	8.90049E-02
22	5.79795E 00	7.20510E 01	4.85333E 00	1.21333E 00	6.06667E-01	4.05556E 00	1.34448E-01
23	5.66350E 00	6.57557E 01	6.06667E 00	1.06167E 00	5.30833E-01	5.77778E 00	1.00352E-01
24	5.56315E 00	7.18748E 01	7.83667E 00	1.06167E 00	5.30833E-01	7.66667E 00	1.66635E-01
25	5.39652E 00	6.49634E 01	6.82500E 00	9.10000E-01	4.55000E-01	7.50000E 00	1.54305E-01
26	5.24221E 00	7.84110E 01	7.12833E 00	1.21333E 00	6.06667E-01	6.11111E 00	1.28775E-01
27	5.11344E 00	7.00338E 01	9.25167E 00	1.21333E 00	6.06667E-01	7.94444E 00	8.80499E-02
28	5.02539E 00	6.10935E 01	2.73000E 00	9.10000E-01	4.55000E-01	3.00000E 00	1.02262E-01
29	4.92312E 00	8.26067E 01	6.67333E 00	1.06167E 00	5.30833E-01	6.44444E 00	1.12653E-01
30	4.81047E 00	6.30417E 01	5.00167E 00	1.21333E 00	6.06667E-01	4.77778E 00	7.29116E-02
31	4.73756E 00	6.81429E 01	3.64000E 00	9.10000E-01	4.55000E-01	4.00000E 00	1.36358E-01
32	4.60120E 00	7.52378E 01	8.34167E 00	1.21333E 00	6.06667E-01	7.11111E 00	1.47705E-01
33	4.45350E 00	XXXXXXXXXXX	6.07333E 00	1.36500E 00	6.82500E-01	4.88889E 00	XXXXXXXXXXX
		************	************	************	************	************	************
AVERAGE =		6.85226E 01	6.10343E 00	1.03409E 00	5.17045E-01	5.94865E 00	1.11215E-01
					STANDARD DEVIATION	2.44723E 00	4.07664E-02
					COEFF. OF VARIATION	4.11392E-01	3.66556E-01

CHARGE NO. 3. 30.1 MM. 60 DEGREE. 1.100 MM WALL. COPPER LINER

ALL VALUES ARE THE AVERAGE FROM THREE RADIOGRAPHS

NO.	VELOCITY MM/MICROSEC	NO TIME MICROSEC.	LENGTH MM.	DIAMETER MM.	RADIUS MM.	L/D RATIO	VEL CHANGE
1	6.67001E 00	6.98778E 01	5.53833E 00	1.92000E 00	9.10000E-01	6.41667E 00	1.14093E-01
2	6.55593E 00	5.81154E 01	4.71167E 00	1.92000E 00	9.10000E-01	2.58333E 00	9.08731E-02
3	6.65700E 00	6.28223E 01	5.75333E 00	1.36500E 00	6.92500E-01	4.22222E 00	1.35916E-01
4	6.30148E 00	9.57295E 01	7.73500E 00	1.00167E 00	5.30833E-01	7.55556E 00	1.03619E-01
5	6.19753E 00	6.69557E 01	3.91500E 00	1.30167E 00	3.10833E-01	5.72222E 00	4.74619E-02
6	5.61000E 00	6.43423E 01	3.45000E 00	9.10000E-01	4.55000E-01	6.00000E 00	1.36908E-01
7	5.97316E 00	7.33017E 01	4.70167E 00	1.36500E 00	5.92500E-01	3.77778E 00	5.09398E-02
8	5.91422E 00	7.25374E 01	3.13557E 00	1.00167E 00	5.33833E-01	3.27778E 00	1.33095E-01
9	5.70813E 00	7.16203E 01	1.01617E 01	9.10000E-01	4.55000E-01	1.11667E 01	5.79949E-02
10	5.72313E 00	7.11979E 01	5.13333E 00	1.15500E 00	5.92500E-01	4.08559E 00	1.06371E-01
11	5.55670E 00	7.60905E 01	9.53333E 00	1.51667E 00	7.53333E-01	6.01111E 00	2.21500E-01
12	5.33325E 00	7.60452E 01	1.47117E 01	1.21333E 00	6.06667E-01	1.25556E 01	2.06337E-01
13	5.12095E 00	7.97423E 01	1.13733E 01	1.00167E 00	5.30833E-01	1.10556E 01	1.58016E-01
14	4.97496E 00	5.12732E 01	4.25167E 00	1.51667E 00	7.58333E-01	5.22222E 00	1.59711E-01
15	4.91523E 00	9.15352E 01	1.30100E 01	1.21333E 00	6.06667E-01	9.50000E 00	1.38114E-01
16	4.62709E 00	7.95173E 01	9.43333E 00	1.97167E 00	9.85833E-01	4.91667E 00	1.52112E-01
17	4.47493E 00	5.52311E 01	1.07683E 01	1.51667E 00	7.58333E-01	7.01667E 00	1.74935E-01
18	4.31004E 00	7.95233E 01	1.10717E 01	1.82000E 00	9.10000E-01	6.08333E 00	8.93079E-02
19	4.21000E 00	5.50217E 01	6.05567E 00	9.10000E-01	4.55000E-01	6.66667E 00	1.18041E-01
20	4.09101E 00	1.03009E 02	6.97567E 00	1.82000E 00	9.10000E-01	3.83333E 00	1.30814E-01
21	3.95500E 00	6.96477E 01	1.45533E 01	1.82000E 00	9.10000E-01	4.15667E 00	1.72175E-01
22	3.70202E 00	1.38753E 02	5.70333E 00	1.97167E 00	9.85833E-01	2.91667E 00	5.13253E-02
23	3.73150E 00	9.95744E 01	3.61157E 00	9.10000E-01	4.55000E-01	6.10667E 00	1.00173E-01
24	3.50332E 00	7.43974E 01	1.57733E 01	1.97167E 00	9.85833E-01	9.10000E 00	1.50091E-01
25	3.40443E 00	9.75091E 01	3.49333E 00	1.97167E 00	9.85833E-01	1.81667E 00	6.70294E-02
26	3.33700E 00	6.92597E 01	1.12233E 01	2.12333E 00	1.00167E 00	5.30000E 00	1.50880E-01
27	3.19012E 00	9.12491E 01	4.73667E 00	2.73000E 00	1.36500E 00	1.55556E 00	1.24069E-01
28	3.05943E 00	9.87878E 01	1.43833E 01	2.73000E 00	1.36500E 00	5.44444E 00	1.73098E-01
29	2.00033E 00	************	6.67333E 00	1.97167E 00	9.85333E-01	3.38333E 00	************
		************	************	************	************	************	************
AVERAGE =		6.09679E 01	8.57170E 00	1.56097E 00	7.80493E-01	5.91636E 00	1.35131E-01
					STANDARD DEVIATION	2.66179E 00	4.53310E-02
					COEFF. OF VARIATION	4.49659E-01	3.35456E-01

BEST AVAILABLE COPY

CHARGE NO. 4. 38.1 MM. 90 DEGREE. 1.160 MM WALL. COPPER LINER

ALL VALUES ARE THE AVERAGE FROM THREE RADIOGRAPHS

NO.	VELOCITY MM/MICROSEC	BO TIME MICROSEC.	LENGTH MM.	DIAMETER MM.	RADIUS MM.	L/D RATIO	VEL CHANGE
1	5.31053E 00	6.70678E 01	7.12833E 00	1.06167E 00	5.30833E-01	6.65884E 00	1.50834E-01
2	5.16012E 00	6.89259E 01	8.64500E 00	1.36500E 00	6.82500E-01	6.77778E 00	8.90668E-02
3	5.07026E 00	5.40732E 01	4.95333E 00	1.36500E 00	6.82500E-01	3.77778E 00	1.22024E-01
4	4.94823E 00	7.73673E 01	5.13067E 00	1.21333E 00	6.06667E-01	4.33333E 00	7.16935E-02
5	4.87634E 00	5.04927E 01	9.40333E 00	1.60833E 00	8.04167E-01	5.72222E 00	1.00812E-01
6	4.71553E 00	7.56961E 01	6.37000E 00	1.51667E 00	7.58333E-01	4.30556E 00	1.23925E-01
7	4.59160E 00	7.94251E 01	9.70667E 00	1.66833E 00	8.34167E-01	5.80889E 00	1.35268E-01
8	4.45633E 00	6.90333E 01	7.57333E 00	1.51667E 00	7.58333E-01	5.05556E 00	1.19187E-01
9	4.33715E 00	9.27576E 01	5.75333E 00	1.51667E 00	7.58333E-01	3.86111E 00	6.43275E-02
10	4.27252E 00	6.54235E 01	7.55333E 00	2.12333E 00	1.06167E 00	3.66667E 00	1.05943E-01
11	4.15638E 00	7.54457E 01	5.52500E 00	1.56833E 00	7.84167E-01	4.13889E 00	8.23004E-02
12	4.05450E 00	[illegible]	3.44333E 00	1.56833E 00	7.84167E-01	2.33333E 00	9.27035E-02
13	[illegible]	9.06702E 01	1.17917E 01	2.57833E 00	1.28917E 00	4.66667E 00	1.54190E-01
14	3.83755E 00	9.38100E 01	1.27400E	2.12333E 00	1.06167E 00	6.08333E 00	1.55402E-01
15	3.65228E 00	1.00057E 02	1.01617	2.27500E 00	1.13750E 00	4.53333E 00	8.79742E-02
16	3.50451E 00	9.75523E 01	.33567	1.62000E 00	8.10000E-01	4.33333E 00	1.39733E-01
17	3.45457E 00	8.81557E 01	4..55000E	2.57833E 00	1.28917E 00	1.61111E 00	6.33790E-02
18	3.39119E 00	1.21743E 02	1.47117E 01	4.09500E 00	2.04750E 00	3.52605E 00	5.10787E-02
19	2.34012E 00	XXXXXXXXXXXX	5.57333E 00	1.97167E 00	9.85833E-01	3.43333E 00	XXXXXXXXXXXX
		============	============	============	============	============	============
AVERAGE =		5.35951E 01	7.43245E 00	1.79386E 00	[illegible]	4.40571E 00	1.09467E-01
					STANDARD DEVIATION	1.35054E 00	3.76247E-02
					COEFF. OF VARIATION	3.01044E-01	3.43709E-01

CHARGE NO.5 50.8 MM. 42 DEGREE. 0.762 MM WALL. COPPER LINER

ALL VALUES ARE THE AVERAGE FROM THREE RADIOGRAPHS

NO.	VELOCITY MM/MICROSEC	90 TIME MICROSEC.	LENGTH MM.	DIAMETER MM.	RADIUS MM.	L/D RATIO	VEL CHANGE
1	8.47063E 00	1.02009E 02	9.20000E 00	1.84000E 00	9.20000E-01	5.00000E 00	7.71826E-02
2	8.39305E 00	2.52205E 01	6.84000E 00	1.53333E 00	7.66667E-01	4.27778E 00	5.55884E-02
3	8.33607E 00	4.32994E 01	6.13333E 00	2.30000E 00	1.15000E 00	2.66667E 00	4.42563E-02
4	8.29341E 00	4.60325E 01	8.55667E 00	1.84000E 00	9.20000E-01	4.66667E 00	1.20907E-01
5	8.17290E 00	6.21626E 01	8.55667E 00	1.84000E 00	9.20000E-01	4.66667E 00	1.49154E-01
6	7.97375E 00	7.96500E 01	5.52667E 00	1.53333E 00	7.66667E-01	3.83333E 00	5.50545E-02
7	7.91069E 00	6.50090E 01	6.13333E 00	1.66667E 00	8.43333E-01	3.66667E 00	1.22533E-01
8	7.79619E 00	5.12751E 01	7.03333E 00	1.38000E 00	6.90000E-01	5.11111E 00	2.10484E-01
9	7.50571E 00	6.41972E 01	7.60667E 00	1.84000E 00	9.20000E-01	4.16667E 00	1.21439E-01
10	7.40427E 00	7.71405E 01	8.57667E 00	1.84000E 00	9.20000E-01	4.66667E 00	1.80030E-01
11	7.30424E 00	6.91477E 01	1.99333E 00	9.20000E-01	4.60000E-01	2.16667E 00	7.79855E-02
12	7.22626E 00	6.66527E 01	3.53333E 00	1.27000E 00	6.90000E-01	2.77778E 00	9.25817E-02
13	7.14305E 00	5.03494E 01	1.17600E 01	1.38000E 00	6.90000E-01	8.66667E 00	1.44365E-01
14	6.99931E 00	7.21633E 01	7.52000E 00	1.38000E 00	6.90000E-01	5.66667E 00	1.05429E-01
15	6.83395E 00	3.55633E 01	2.75000E 00	1.22667E 00	6.13333E-01	2.33333E 00	3.20003E-02
16	6.80122E 00	4.50557E 01	6.90000E 00	1.68667E 00	8.43333E-01	4.15994E 00	2.93251E-02
17	6.77290E 00	7.31949E 01	4.60000E 00	1.38000E 00	6.90000E-01	3.33333E 00	1.01893E-01
18	6.59100E 00	7.17763E 01	5.52000E 00	1.38000E 00	6.90000E-01	4.00000E 00	1.21439E-01
19	6.45976E 00	7.75008E 01	1.07333E 01	1.38000E 00	6.90000E-01	7.77778E 00	2.10494E-01
20	6.23908E 00	3.41412E 01	9.53667E 00	1.38000E 00	6.90000E-01	6.88889E 00	8.92667E-02
21	6.17093E 00	5.15414E 01	7.51333E 00	1.38000E 00	6.90000E-01	5.44444E 00	1.55148E-01
22	6.01567E 00	3.25243E 01	5.92667E 00	1.38133E 00	6.90000E-01	4.22222E 00	1.06511E-01
23	5.95104E 00	1.09750E 02	6.13333E 00	1.84000E 00	9.20000E-01	3.33333E 00	4.47603E-02
24	5.90625E 00	6.90432E 01	2.75000E 00	1.38000E 00	6.90000E-01	2.00000E 00	8.90480E-02
25	5.71721E 00	6.59449E 01	9.20000E 00	1.53333E 00	7.66667E-01	6.05556E 00	2.50208E-02
26	5.60300E 00	6.99149E 01	1.16533E 01	1.38000E 00	6.90000E-01	8.44444E 00	1.53833E-01
27	5.33917E 00	4.99459E 01	3.99667E 00	1.38000E 00	6.90000E-01	2.88889E 00	4.45223E-02
28	5.20494E 00	5.81317E 01	2.91333E 00	1.66667E 00	8.43333E-01	1.75000E 00	8.02467E-02
29	5.17040E 00	5.16492E 01	6.74667E 00	1.38000E 00	6.90000E-01	4.88889E 00	1.17310E-01
30	5.05924E 00	5.30249E 01	7.51333E 00	1.38000E 00	6.90000E-01	5.44444E 00	1.10841E-01
31	4.94005E 00	4.23213E 01	1.99333E 00	9.20000E-01	4.60000E-01	2.16667E 00	4.39117E-02
32	4.85047E 00	7.08931E 01	1.07333E 01	1.38000E 00	6.90000E-01	7.77778E 00	9.79802E-02
33	4.76707E 00	5.74904E 01	3.98667E 00	1.84000E 00	9.20000E-01	2.16667E 00	7.82465E-02
34	4.60051E 00	7.76841E 01	4.29667E 00	1.38000E 00	6.90000E-01	1.55556E 00	8.79800E-02
35	4.60053E 00	7.52880E 01	4.60000E 00	1.38000E 00	6.90000E-01	3.33333E 00	1.08946E-01
36	4.45157E 00	5.60452E 01	4.44667E 00	1.38000E 00	6.90000E-01	3.22222E 00	4.05223E-02
37	4.40706E 00	4.70516E 01	5.59667E 00	2.60667E 00	1.30333E 00	2.20000E 00	1.20572E-01
38	4.20047E 00	1.01440E 02	7.66667E 00	1.66667E 00	8.43333E-01	4.60000E 00	1.04444E-01
39	4.17603E 00	6.78594E 01	5.52667E 00	1.84000E 00	9.20000E-01	3.16667E 00	1.00562E-01
40	4.01547E 00	4.20578E 01	5.21333E 00	1.84000E 00	9.20000E-01	2.83333E 00	2.00592E-02
41	3.98743E 00	6.08459E 01	6.20667E 00	1.84000E 00	9.20000E-01	3.81667E 00	4.99210E-02
42	3.93748E 00	8.33682E 01	4.75333E 00	1.84000E 00	9.20000E-01	2.58333E 00	4.47748E-02
43	3.88871E 00	7.96500E 01	3.37333E 00	9.20000E-01	4.60000E-01	3.66667E 00	1.10109E-01
44	3.73000E 00	************	8.50667E 00	2.76000E 00	1.38000E 00	3.11111E 00	************
		************	************	************	************	************	************
AVERAGE =		7.38612E 01	6.47653E 00	1.57844E 00	7.89318E-01	4.17495E 00	1.14052E-01
					STANDARD DEVIATION	1.72308E 00	5.47307E-02
					COEFF. OF VARIATION	4.12765E-01	4.79317E-01

CHARGE NO. 6, 50.8 MM, 42 DEGREES, 1.524 MM WALL, COPPER LINER

ALL VALUES ARE THE AVERAGE FROM THREE RADIOGRAPHS

NO.	VELOCITY MM/MICROSEC.	BU TIME MICROSEC.	LENGTH MM.	DIAMETER MM.	RADIUS MM.	L/D RATIO	VEL CHANGE
1	7.60390E 00	5.29513E 01	1.21133E 01	2.45333E 00	1.22667E 00	5.11111E 00	1.36325E-01
2	7.46757E 00	6.49062E 01	9.01333E 00	1.86000E 00	9.20000E-01	5.33333E 00	5.59389E-02
3	7.39163E 00	6.07713E 01	6.75333E 00	1.84000E 00	9.20000E-01	2.50133E 00	7.01627E-02
4	7.31347E 00	6.19071E 01	7.05333E 00	1.53333E 00	7.66667E-01	6.00067E 00	6.09966E-02
5	7.24667E 00	7.65234E 01	6.46667E 00	1.84000E 00	9.20000E-01	7.01667E 00	1.28240E-01
6	7.11023E 00	5.59053E 01	2.41333E 00	1.07333E 00	5.36667E-01	2.77778E 00	8.46916E-02
7	7.02656E 00	5.66023E 01	1.01200E 01	1.53333E 00	7.66667E-01	6.75000E 00	1.45269E-01
8	6.88727E 00	6.55631E 01	1.07333E 01	1.94000E 00	9.70000E-01	5.03333E 00	1.09932E-01
9	6.69943E 00	7.25693E 01	9.12667E 00	1.92667E 00	9.20000E-01	5.03333E 00	1.09932E-01
10	6.60049E 00	4.21557E 01	2.41333E 00	1.54000E 00	9.20000E-01	6.01667E 00	1.06049E-02
11	6.61306E 00	4.30410E 01	6.59333E 00	2.43333E 00	1.15000E 00	1.59333E 00	7.20507E-02
12	6.46314E 00	7.54957E 01	5.53667E 00	1.84000E 00	9.20000E-01	2.46667E 00	1.30255E-01
13	6.38674E 00	5.92652E 01	8.12667E 00	1.84000E 00	9.20000E-01	6.00667E 00	7.05946E-02
14	6.21350E 00	4.73572E 01	4.13333E 00	1.94000E 00	9.20000E-01	4.41667E 00	1.72912E-01
15	6.09667E 00	4.81708E 01	5.52000E 00	1.54000E 00	9.20000E-01	5.08333E 00	1.17637E-01
16	6.05766E 00	5.87561E 01	3.49667E 00	1.63667E 00	8.43333E-01	1.00000E 00	3.80130E-02
17	6.02464E 00	3.64170E 01	7.92000E 00	1.54000E 00	9.20000E-01	2.38389E 00	2.74645E-02
18	5.89403E 00	7.49502E 01	1.07333E 01	1.94000E 00	9.20000E-01	6.25000E 00	1.31658E-01
19	5.76756E 00	6.76647E 01	7.92000E 00	1.49333E 00	7.46667E-01	5.08333E 00	1.20666E-01
20	5.62251E 00	4.12114E 01	9.50667E 00	1.84000E 00	9.20000E-01	3.96667E 00	1.05051E-01
21	5.49474E 00	5.42747E 01	6.46667E 00	1.49333E 00	7.46667E-01	5.16667E 00	1.42719E-01
22	5.49949E 00	1.02750E 02	5.52000E 00	1.54000E 00	9.20000E-01	2.25000E 00	5.43017E-02
23	5.34059E 00	1.02612E 02	7.47333E 00	1.94000E 00	9.20000E-01	3.00000E 00	1.04083E-01
24	5.32042E 00	4.16473E 01	5.52667E 00	1.84000E 00	9.20000E-01	4.33333E 00	2.74645E-02
25	5.29243E 00	4.67633E 01	2.76000E 00	1.68667E 00	8.43333E-01	3.16667E 00	2.74645E-02
26	5.13030E 00	4.16473E 01	1.35667E 01	1.84000E 00	9.20000E-01	1.66667E 00	1.50651E-01
27	4.94035E 00	1.30139E 02	9.68000E 00	2.30000E 00	1.15000E 00	7.01667E 00	1.45786E-01
28	4.87361E 00	4.12561E 01	9.50667E 00	1.94000E 00	9.20000E-01	4.20000E 00	6.71050E-02
29	4.68946E 00	1.00722E 02	1.27267E 01	1.94000E 00	9.20000E-01	5.16667E 00	1.03970E-01
30	4.51100E 00	1.00309E 02	9.53667E 00	1.84000E 00	9.20000E-01	6.91667E 00	1.76641E-01
31	4.44359E 00	1.18137E 02	6.44000E 00	1.84000E 00	9.20000E-01	5.16667E 00	6.71050E-02
32	4.39936E 00	5.08732E 01	6.76667E 00	1.84000E 00	9.20000E-01	3.50000E 00	6.45560E-02
33	4.29312E 00	5.87361E 01	1.01200E 01	2.14667E 00	1.07333E 00	3.66667E 00	1.56217E-01
34	4.04224E 00	1.15127E 02	1.41367E 01	2.76000E 00	1.38000E 00	4.76667E 00	2.40081E-01
35	3.90216E 00	1.03542E 02	1.56400E 01	1.84000E 00	9.20000E-01	5.11111E 00	1.30132E-01
36	3.76300E 00	9.06113E 01	1.04267E 01	1.84000E 00	9.20000E-01	8.50000E 00	1.45051E-01
37	3.55057E 00	1.16137E 02	1.13867E 01	1.84000E 00	9.20000E-01	5.66667E 00	2.40519E-01
38	3.51179E 00	9.56375E 01	9.04667E 00	2.30000E 00	1.15000E 00	6.16667E 00	6.07720E-02
39	3.27100E 00	1.00350E 02	1.73267E 01	2.45333E 00	1.22667E 00	3.93333E 00	2.39009E-01
40	3.12603E 00	************	9.66000E 00	2.30000E 00	1.15000E 00	7.11111E 00	1.45051E-01
		************	************	************	************	************	************
AVERAGE =		9.06050E 01	8.58667E 00	1.91283E 00	9.56417E-01	4.47542E 00	1.14797E-01
					STANDARD DEVIATION	1.61666E 00	5.90800E-02
					COEFF. OF VARIATION	3.60029E-01	5.21626E-01

CHARGE NO.7 50.8 MM, 42 DEGREE, 2.540 MM WALL, COPPER LINER

ALL VALUES ARE THE AVERAGE FROM THREE RADIOGRAPHS

NO.	VELOCITY MM/MICROSEC	80 TIME MICROSEC.	LENGTH MM.	DIAMETER MM.	RADIUS MM.	L/D RATIO	VEL CHANGE
1	6.76620E 00	1.97059E 01	1.06667E 01	3.22000E 00	1.61000E 00	3.38095E 00	1.00852E-01
2	6.65934E 00	7.40151E 01	7.05333E 00	1.66667E 00	8.33333E-01	4.25000E 00	7.23519E-02
3	6.50699E 00	6.18412E 01	1.06667E 01	2.30000E 00	1.15000E 00	4.73913E 00	1.12302E-01
4	6.47469E 00	7.92473E 01	6.50000E 00	1.30000E 00	6.50000E-01	5.00000E 00	2.39150E-01
5	6.23553E 00	6.60341E 01	1.11933E 01	1.53333E 00	7.66667E-01	7.30869E 00	1.23502E-01
6	6.11233E 00	7.99972E 01	1.11933E 01	1.68667E 00	8.43333E-01	6.75000E 00	1.28653E-01
7	5.90330E 00	6.83739E 01	6.74667E 00	1.53333E 00	7.66667E-01	4.47222E 00	9.60012E-02
8	5.92730E 00	6.11532E 01	2.60667E 00	1.66667E 00	8.33333E-01	1.55556E 00	1.00502E-01
9	5.82668E 00	6.95649E 01	5.52667E 00	1.30000E 00	6.50000E-01	4.22222E 00	9.35521E-02
10	5.74332E 00	6.33196E 01	1.27267E 01	1.66667E 00	8.33333E-01	7.69444E 00	1.96650E-01
11	5.54667E 00	5.80265E 01	5.90000E 00	1.99333E 00	9.96667E-01	3.01667E 00	7.01019E-02
12	5.40077E 00	5.40265E 01	6.90000E 00	1.84000E 00	9.20000E-01	3.75000E 00	7.01019E-02
13	5.39067E 00	6.91377E 01	8.74000E 00	1.84000E 00	9.20000E-01	4.75000E 00	1.00303E-01
14	5.22230E 00	6.80035E 01	8.43333E 00	1.99333E 00	9.96667E-01	4.25000E 00	2.24005E-02
15	5.19990E 00	7.99258E 01	5.52000E 00	1.84000E 00	9.20000E-01	3.00000E 00	1.18652E-01
16	5.00133E 00	7.87043E 01	5.82667E 00	2.14667E 00	1.07333E 00	2.73333E 00	1.04950E-01
17	4.89630E 00	6.67545E 01	1.04267E 01	1.84000E 00	9.20000E-01	5.66667E 00	1.08252E-01
18	4.79010E 00	9.44110E 01	7.36000E 00	1.84000E 00	9.20000E-01	4.00000E 00	1.45903E-01
19	4.68442E 00	1.05713E 02	7.97333E 00	2.30000E 00	1.15000E 00	3.46667E 00	8.29520E-02
20	4.50125E 00	6.92765E 01	6.59333E 00	1.84000E 00	9.20000E-01	3.58333E 00	7.87014E-02
21	4.48255E 00	1.06709E 02	6.74667E 00	1.84000E 00	9.20000E-01	3.66667E 00	1.45004E-01
22	4.33754E 00	6.71869E 01	1.73267E 01	2.14667E 00	1.07333E 00	8.15000E 00	1.78900E-01
23	4.15064E 00	9.10629E 01	8.69333E 00	1.99333E 00	9.96667E-01	4.40333E 00	1.00502E-01
24	4.05014E 00	9.75670E 01	8.12667E 00	1.99333E 00	9.96667E-01	4.11667E 00	1.17752E-01
25	3.94039E 00	6.11032E 01	1.07333E 01	2.30000E 00	1.15000E 00	4.66667E 00	2.01005E-01
26	3.73930E 00	9.69544E 01	9.35333E 00	2.30000E 00	1.15000E 00	4.06667E 00	1.57103E-01
27	3.58720E 00	6.29006E 01	1.04267E 01	2.14667E 00	1.07333E 00	4.90000E 00	2.27002E-02
28	3.57950E 00	************	8.43333E 00	2.30000E 00	1.15000E 00	3.66667E 00	************
		************	************	************	************	************	************
AVERAGE =		8.10132E 01	8.56476E 00	1.94952E 00	9.74762E-01	4.47789E 00	1.10764E-01
					STANDARD DEVIATION	1.50281E 00	5.32810E-02
					COEFF. OF VARIATION	3.35607E-01	4.80631E-01

CHARGE NO. 8, 81.3 MM, 42 DEGREE, TAPERED WALL, COPPER LINER

ALL VALUES ARE THE AVERAGE FROM THREE RADIOGRAPHS

NO.	VELOCITY MM/MICROSEC	80 TIME MICROSEC.	LENGTH MM.	DIAMETER MM.	RADIUS MM.	L/D RATIO	VEL CHANGE
1	8.32517E 00	9.96025E 01	2.80600E 01	9.20000E 00	4.60000E 00	3.05000E 00	6.60568E-02
2	8.25911E 00	9.37165E 01	1.21133E 01	3.06667E 00	1.53333E 00	3.96032E 00	1.89517E-01
3	8.06959E 00	9.17222E 01	1.22667E 01	3.52667E 00	1.76333E 00	3.49405E 00	2.79164E-02
4	8.04168E 00	1.00950E 02	2.60667E 00	1.84000E 00	9.20000E-01	1.41667E 00	6.76276E-02
5	7.97405E 00	9.71185E 01	2.14667E 00	2.76000E 00	1.38000E 00	8.22222E-01	4.56087E-02
6	7.92844E 00	9.98589E 01	8.58667E 00	3.68000E 00	1.84000E 00	2.34325E 00	9.55440E-02
7	7.83290E 00	1.09013E 02	5.82667E 00	3.06667E 00	1.53333E 00	1.91270E 00	1.00918E-01
8	7.73198E 00	8.73770E 01	8.12667E 00	3.22000E 00	1.61000E 00	2.62963E 00	1.00394E-01
9	7.63159E 00	1.25614E 02	7.82000E 00	2.91333E 00	1.45667E 00	2.68254E 00	6.22538E-02
10	7.56933E 00	7.65480E 01	5.06000E 00	3.22000E 00	1.61000E 00	1.57738E 00	3.97112E-02
11	7.52962E 00	1.15993E 02	3.98667E 00	1.99333E 00	9.96667E-01	2.00000E 00	7.73281E-02
12	7.45229E 00	1.08008E 02	1.02733E 01	2.91333E 00	1.45667E 00	3.60952E 00	1.01965E-01
13	7.35033E 00	1.11346E 02	6.44000E 00	2.45333E 00	1.22667E 00	2.69444E 00	9.60676E-02
14	7.25426E 00	1.05266E 02	8.43333E 00	2.45333E 00	1.22667E 00	3.58333E 00	1.28834E-01
15	7.12543E 00	8.50641E 01	9.81333E 00	2.76000E 00	1.38000E 00	3.55556E 00	7.78517E-02
16	7.04757E 00	1.01053E 02	7.20667E 00	2.30000E 00	1.15000E 00	3.21111E 00	1.68022E-01
17	6.87955E 00	7.55762E 01	1.11933E 01	3.06667E 00	1.53333E 00	3.79643E 00	5.79272E-02
18	6.82162E 00	1.00323E 02	8.25000E 00	2.76000E 00	1.38000E 00	3.02381E 00	1.55180E-01
19	6.66645E 00	7.88531E 01	3.98667E 00	3.06667E 00	1.53333E 00	1.30952E 00	1.30405E-01
20	6.53604E 00	1.19702E 02	8.12667E 00	2.60667E 00	1.30333E 00	3.14444E 00	1.53639E-01
21	6.38243E 00	8.57643E 01	6.59333E 00	2.76000E 00	1.38000E 00	2.38889E 00	9.17410E-02
22	6.29069E 00	8.91175E 01	7.36000E 00	2.30000E 00	1.15000E 00	3.20889E 00	1.18610E-01
23	6.17208E 00	9.88837E 01	7.05333E 00	2.30000E 00	1.15000E 00	3.13333E 00	1.51377E-01
24	6.02070E 00	1.04985E 02	1.15000E 01	2.30000E 00	1.15000E 00	5.00000E 00	1.82482E-01
25	5.83722E 00	1.13206E 02	1.20000E 01	1.99333E 00	9.96667E-01	6.55000E 00	7.24778E-02
26	5.76474E 00	8.75209E 01	4.60000E 00	2.14667E 00	1.07333E 00	2.10667E 00	1.46526E-01
27	5.61022E 00	1.03897E 02	7.05333E 00	1.99333E 00	9.96667E-01	3.56667E 00	9.98706E-02
28	5.51035E 00	1.29100E 02	3.37333E 00	1.84000E 00	9.20000E-01	1.83333E 00	1.01215E-02
29	5.50223E 00	1.06790E 02	8.58667E 00	1.99333E 00	9.96667E-01	4.31667E 00	2.77455E-01
30	5.22477E 00	3.05455E 01	1.25733E 01	1.99333E 00	9.96667E-01	6.40333E 00	2.91014E-02
31	5.19567E 00	9.43807E 01	3.22000E 00	1.07333E 00	5.36667E-01	3.11111E 00	7.99461E-02
32	5.11572E 00	1.06879E 02	9.98667E 00	2.30000E 00	1.15000E 00	4.46667E 00	1.78246E-01
33	4.93748E 00	1.00096E 02	1.27267E 01	2.14667E 00	1.07333E 00	6.00000E 00	1.51900E-01
34	4.78550E 00	1.01299E 02	1.04267E 01	2.14667E 00	1.07333E 00	4.90000E 00	1.52429E-01
35	4.63315E 00	1.02628E 02	9.50667E 00	1.99333E 00	9.96667E-01	5.06667E 00	7.24778E-02
36	4.58067E 00	XXXXXXXXXXXX	7.82000E 00	2.60667E 00	1.30333E 00	3.17857E 00	XXXXXXXXXXXX
		************	************	************	************	************	************
AVERAGE =		9.76503E 01	8.48870E 00	2.68759E 00	1.34380E 00	3.31299E 00	1.07557E-01
					STANDARD DEVIATION	1.38189E 00	5.57745E-02
					COEFF. OF VARIATION	4.17111E-01	5.18558E-01

CHARGE NO.9 50.8 MM. 40 DEGREE, 1.626 MM WALL. ALUMINUM LINER

ALL VALUES ARE THE AVERAGE FROM THREE RADIOGRAPHS

NO.	VELOCITY MM/MICROSEC	BU TIME MICROSEC.	LENGTH MM.	DIAMETER MM.	RADIUS, MM.	L/D RATIO	VEL CHANGE
1	9.03215E 00	5.64109E 01	1.00100E 01	2.12333E 00	1.06167E 00	4.76667E 00	1.28526E-01
2	8.90363E 00	5.28352E 01	8.79667E 00	2.73000E 00	1.36500E 00	3.22222E 00	1.66770E-01
3	8.73086E 00	7.22991E 01	6.82500E 00	1.36500E 00	6.82500E-01	5.00000E 00	1.17315E-01
4	8.61954E 00	6.52375E 01	1.04650E 01	1.82000E 00	9.10000E-01	5.75000E 00	2.04448E-01
5	8.81309E 00	2.52638E 01	5.30833E 00	1.97167E 00	9.85833E-01	2.71667E 00	7.19409E-02
6	8.34315E 00	5.82899E 01	3.79167E 00	1.82000E 00	9.10000E-01	2.08333E 00	1.32431E-01
7	8.21072E 00	5.10243E 01	3.48833E 00	1.82000E 00	9.10000E-01	1.91667E 00	1.51427E-01
8	8.05929E 00	5.62573E 01	3.40833E 00	2.12333E 00	1.06167E 00	1.66667E 00	1.21094E-01
9	7.93620E 00	5.10729E 01	8.34167E 00	1.82000E 00	9.10000E-01	4.58333E 00	2.19614E-01
10	7.71859E 00	2.65928E 01	3.98333E 00	1.66833E 00	8.34167E-01	2.38889E 00	7.94486E-02
11	7.63914E 00	4.76262E 01	4.09500E 00	1.82000E 00	9.10000E-01	2.25000E 00	1.58973E-01
12	7.40016E 00	6.18767E 01	4.55000E 00	1.97167E 00	9.85833E-01	2.33333E 00	1.66619E-01
13	7.31355E 00	5.70539E 01	9.55500E 00	1.82000E 00	9.10000E-01	5.25000E 00	2.04372E-01
14	7.10917E 00	5.58167E 01	6.97667E 00	1.82000E 00	9.10000E-01	3.83333E 00	4.92161E-02
15	7.05996E 00	7.05553E 01	4.70167E 00	1.51667E 00	7.58333E-01	3.13889E 00	2.23318E-01
16	6.83664E 00	7.20615E 01	1.36500E 01	1.82000E 00	9.10000E-01	7.50000E 00	7.57200E-02
17	6.76492E 00	5.93178E 01	3.33667E 00	1.82000E 00	9.10000E-01	1.83333E 00	2.04498E-01
18	6.55042E 00	7.30008E 01	7.88667E 00	1.82000E 00	9.10000E-01	4.33333E 00	1.93073E-01
19	6.36335E 00	6.06357E 00	6.67333E 00	1.36500E 00	6.82500E-01	4.88889E 00	6.43198E-02
20	6.29903E 00	7.33742E 01	4.39833E 00	1.82000E 00	9.10000E-01	2.41667E 00	1.58935E-01
21	6.14009E 00	8.10455E 01	1.10717E 01	1.36500E 00	6.82500E-01	8.11111E 00	1.59086E-01
22	5.98101E 00	6.95096E 01	9.10000E 00	1.36500E 00	6.82500E-01	6.66667E 00	1.43808E-01
23	5.83720E 00	7.65544E 01	5.00500E 00	1.82000E 00	9.10000E-01	2.75000E 00	8.70068E-02
24	5.75019E 00	6.21225E 01	6.52167E 00	1.82000E 00	9.10000E-01	3.58333E 00	1.09807E-01
25	5.60039E 00	7.43570E 01	6.37000E 00	1.82000E 00	9.10000E-01	3.50000E 00	1.65540E-01
26	5.45403E 00	XXXXXXXXXXXX	8.49333E 00	1.82000E 00	9.10000E-01	4.66667E 00	XXXXXXXXXXXX
		============	============	============	============	============	============
AVERAGE =		5.82089E 01	6.80167E 00	1.80250E 00	9.01250E-01	3.89038E 00	1.43092E-01
					STANDARD DEVIATION	1.76580E 00	5.17296E-02
					COEFF. OF VARIATION	4.53869E-01	3.61512E-01

CHARGE NO.10 50.8 MM. 60 DEGREE, 1.626 MM WALL. ALUMINUM LINER

ALL VALUES ARE THE AVERAGE FROM THREE RADIOGRAPHS

NO.	VELOCITY MM/MICROSEC	GO TIME MICROSEC.	LENGTH MM.	DIAMETER MM.	RADIUS MM.	L/D RATIO	VEL CHANGE
1	7.90543E 00	5.80358E 01	1.74417E 01	1.82000E 00	9.10000E-01	9.58333E 00	3.03438E-02
2	7.86709E 00	6.26390E 01	7.66667E 00	1.82000E 00	9.10000E-01	4.33333E 00	2.10140E-01
3	7.6[illegible]95E 00	7.23113E 01	1.42567E 01	1.82000E 00	9.10000E-01	7.83333E 00	1.91819E-01
4	7.46513E 00	4.49574E 01	7.88667E 00	1.82000E 00	9.10000E-01	4.33333E 00	2.20852E-01
5	7.24420E 00	8.77573E 01	6.67333E 00	1.36500E 00	6.82500E-01	4.88889E 00	7.10812E-02
6	7.17320E 00	6.62696E 01	7.20000E 00	1.82000E 00	9.10000E-01	4.00000E 00	1.98627E-01
7	6.97457E 00	7.28737E 01	7.12833E 00	1.82000E 00	9.10000E-01	3.91667E 00	9.78110E-02
8	6.87676E 00	6.20460E 01	2.12333E 00	1.82000E 00	9.10000E-01	1.16667E 00	9.40074E-02
9	6.78275E 00	8.18424E 01	1.03133E 01	1.66833E 00	8.34167E-01	6.27778E 00	1.17735E-01
10	6.60502E 00	6.49454E 01	9.25167E 00	1.82000E 00	9.10000E-01	5.08333E 00	1.11527E-01
11	6.55349E 00	7.14630E 01	6.08667E 00	1.82000E 00	9.10000E-01	3.33333E 00	2.30844E-01
12	6.32263E 00	5.49035E 01	7.58333E 00	1.82000E 00	9.10000E-01	4.16667E 00	1.28447E-01
13	6.19410E 00	8.69523E 01	1.27400E 01	1.82000E 00	9.10000E-01	7.00000E 00	1.26044E-01
14	6.06014E 00	7.36848E 01	3.33667E 00	1.82000E 00	9.10000E-01	1.83333E 00	1.19236E-01
15	5.98890E 00	9.61478E 01	6.52167E 00	1.82000E 00	9.10000E-01	3.58333E 00	1.21439E-01
16	5.82746E 00	7.63533E 01	1.36500E 01	1.82000E 00	9.10000E-01	7.50000E 00	2.17849E-01
17	5.60961E 00	6.53533E 01	5.30833E 00	1.82000E 00	9.10000E-01	2.91667E 00	5.80664E-02
18	5.55154E 00	6.27050E 01	7.43167E 00	1.82000E 00	9.10000E-01	4.08333E 00	9.09039E-02
19	5.46064E 00	9.02794E 01	5.46000E 00	1.82000E 00	9.10000E-01	3.00000E 00	6.26710E-02
20	5.39797E 00	9.67329E 01	5.46000E 00	1.82000E 00	9.10000E-01	3.00000E 00	1.88015E-01
21	5.20995E 00	1.07497E 02	1.51667E 01	1.82000E 00	9.10000E-01	8.33333E 00	5.41619E-02
22	5.15579E 00	9.71808E 01	1.07683E 01	1.82000E 00	9.10000E-01	5.91667E 00	2.58996E-01
23	4.59600E 00	1.09318E 02	1.27400E 01	1.82000E 00	9.10000E-01	7.00000E 00	1.57480E-01
24	4.73932E 00	9.15924E 01	9.55500E 00	1.82000E 00	9.10000E-01	5.25000E 00	1.53175E-02
25	4.72400E 00	1.08305E 02	1.09200E 01	1.82000E 00	9.10000E-01	6.00000E 00	5.66640E-02
26	4.66733E 00	XXXXXXXXXXXX	6.37000E 00	1.82000E 00	9.10000E-01	3.50000E 00	XXXXXXXXXXXX
		============	============	============	============	============	============
AVERAGE =		7.96058E 01	8.82000E 00	1.79667E 00	8.98333E-01	4.91667E 00	1.29524E-01
					STANDARD DEVIATION	2.06363E 00	6.83966E-02
					COEFF. OF VARIATION	4.19722E-01	5.28061E-01

CHARGE NO. 11 50.8 MM. 90 DEGREE. 1.626 MM WALL. ALUMINUM LINER

ALL VALUES ARE THE AVERAGE FROM THREE RADIOGRAPHS

NO.	VELOCITY MM/MICROSEC	90 TIME MICROSEC.	LENGTH MM.	DIAMETER MM.	RADIUS MM.	L/D RATIO	VEL CHANGE
1	6.58152E 00	9.35909E 01	1.95650E 01	1.82000E 00	9.10000E-01	1.07500E 01	1.67391E-01
2	6.41413E 00	1.05524E 02	1.59250E 01	1.82000E 00	9.10000E-01	8.75000E 00	1.55978E-01
3	6.25815E 00	8.90395E 01	1.16025E 01	1.82000E 00	9.10000E-01	6.37500E 00	1.63587E-01
4	6.09457E 00	1.00390E 02	1.31950E 01	1.82000E 00	9.10000E-01	7.25000E 00	1.67391E-01
5	5.92717E 00	1.15176E 02	1.27400E 01	1.82000E 00	9.10000E-01	7.00000E 00	1.29348E-01
6	5.79703E 00	1.05524E 02	1.50150E 01	1.82000E 00	9.10000E-01	8.25000E 00	1.55978E-01
7	5.64105E 00	1.16935E 02	1.56975E 01	1.82000E 00	9.10000E-01	8.62500E 00	1.98022E-01
8	5.48703E 00	1.18759E 02	1.63800E 01	1.82000E 00	9.10000E-01	9.00000E 00	2.05435E-01
9	5.24239E 00	1.31162E 02	1.93375E 01	1.82000E 00	9.10000E-01	1.06250E 01	1.71196E-01
10	5.07120E 00	1.30647E 02	1.20575E 01	1.82000E 00	9.10000E-01	6.62500E 00	1.06613E-01
11	4.80478E 00	1.33156E 02	2.73000E 01	2.27500E 00	1.13750E 00	1.20000E 01	1.30957E-01
12	4.74783E 00	1.17616E 02	1.63800E 01	2.73000E 00	1.36500E 00	6.00000E 00	1.17935E-01
13	4.62909E 00	1.09900E 02	1.29675E 01	2.95750E 00	1.47875E 00	4.41667E 00	1.52174E-01
14	4.47772E 00	XXXXXXXXXXXX	1.97925E 01	4.77750E 00	2.38875E 00	4.15000E 00	XXXXXXXXXXXX
		************	************	************	************	************	************
AVERAGE =		1.12878E 02	1.72737E 01	2.21000E 00	1.10500E 00	8.30869E 00	1.61031E-01
					STANDARD DEVIATION	3.57044E 00	2.49282E-02
					COEFF. OF VARIATION	4.26341E-01	1.54803E-01